Preliminary design of reusable future space access vehicles

PhD Thesis

Federico Toso

Department of Mechanical and Aerospace Engineering

University of Strathclyde, Glasgow

February 19, 2023

This thesis is the result of the author's original research. It has been composed by the author and has not been previously submitted for examination which has led to the award of a degree.

Signed: Federico Toso

Date: February 19, 2023

Acknowledgements

Completing this document has been a struggle. Writing has never been my strong suit, and as a curious person I always move to the next area to explore, digest, understand, never stopping the process of learning. Backtracking to stop and report my discoveries is a time I always dread.

I would have never been able to complete this thesis without the extraordinary support of friends and family, always pushing me towards the end goal, each in their own way, and for this, I thank you all, you've collectively put more energy than I did.

Most of all I need to thank Viola. We gambled a lot when, as a young couple, we changed country, jobs and started living (and working!) together for the first time. But I cannot think of a higher reward than having you in my life, you have supported me every single day, we have been through a lot of changes and our love has only endured and grown. Thank you for everything, wife!

Even though the PhD experience has been one of my most harrowing experiences to date, I will gladly do it again with no hesitation, and the main reason would be all the cFASTT team. You are a group of friends I never expected to find, I hope to continue keeping in contact with all of you even though we got scattered all around the world, and I hope this diaspora can enrich our exploration of culinary traditions. Rob, I don't understand how it is possible that I was so lucky to meet a person with whom I share so much, remember that you have 5 years of advantage, use them well, then, when you are done, let's get bald talking about rockets and tech. Javi, you are an amazing and inexhaustible source of knowledge in so many fields and areas, thank you for teaching me so much, in front of the screen and on the climbing wall. JJ, you pushed the envelope so hard that you crushed some of us, but without it, we would

have had a fraction of the fun, thanks bloodhound. Master, the wisdom granted to you by the aeons of time enlightened all of us, you have been the Polaris of our group, we strive to follow your path in our future. Daniel... we don't talk about people on the other side of the corridor. And you lost the game, again.

Thanks to all the people met in Strathclyde and Glasgow, the list is too long for this document, it would risk overtaking most chapters by length, but you made that city my favourite place on Earth. Thanks Emma, Aine, Ciara, Tom, Maddalena, Lorenzo, and all those that do not fit here, I hope I enriched your life just a fraction of what you did to mine.

Thanks to Giorgio, Marco, Deme, Rudy and all the other gamers that shared many nights across long distances, it's incredible how much time we have passed physically distant, and how negligible it has been on our friendship. We cheered and suffered together in digital worlds and it is great to be able to finally see you more frequently in the real one, I did not notice how much I missed you guys!

Last but not least, thanks to all my family, I am sorry I got further away, I know I have been a grumpy, complaining brother/son/etc living far away, but I intend to fix it in the next years by being a grumpy, complaining brother/son/etc living close-by. Your continuous support from the start of my education to this point has been fundamental, I cannot express how thankful I am to have such wonderful parents that have nurtured and fostered my curiosity for all my life. Mario, one of my regrets is having stretched a bit our connection, we've spent most of our life under the same roof, until I left for Scotland, but I am very happy we got closer again as this document is being completed. I am proud of the man you've become.

Abstract

The space economy can only thrive if reliable, responsive and economical access to space is granted by the launch industry. The competitive spur at the turn of the millennium has started numerous endeavours attempting to capture shares of the launch market, providing alternative solutions with different value propositions.

These new, innovative, launch vehicles, deviating from the more classical architectures and CONOPS, require complicated, multidisciplinary evaluations of their performances to enable analyses and trade-offs from the early design phases to guide the development. These added complexities are even more pronounced for reusable, lifting body vehicles with multiple or combined-cycle engine types, where the aerodynamics, propulsion, and trajectory influence each others.

This work provides a methodology to perform mission analysis from the concept of a project onwards, integrating a flexible simulator structure in a trajectory optimisation framework with MDO capabilities suitable for the early phase vehicle sizing. The whole stack is designed to be readable, modular, and flexible, accepting the different levels of fidelity available at each milestone of the project time-line. A direct, multiple shooting transcription enables the use of discontinuous datasets with rapid model integration. The breakdown of the trajectory in multiple sub-arcs, and the multi start approach provide a stable framework able to converge and identify solutions from wide search-spaces, even when the analyst cannot provide an initial guess.

The approach presented is validated with a suite of standardised trajectory optimisation test cases, and applied to a range of problems exploring all the different phases that a reusable lifting body vehicle might encounter during nominal and off-nominal operations. The methodology can be employed from the analysis of the commercial

viability of a concept to the trajectory design for mission and safety analysis required for regulatory framework compliance.

Keywords: Space launch vehicle design, trajectory optimisation, mission analysis

Contents

List of Figures

List of Tables

List of symbols

a	:	semi-major axis, m
acc	:	acceleration, $\mathrm{m\,s^{-2}}$
A_e	:	nozzle exit area, $\mathrm{m^2}$
$\mathcal{B}$	:	body-relative reference frame
c_L	:	lift coefficient
c_D	:	drag coefficient
D	:	aerodynamic drag force, N
e	:	eccentricity
$\mathcal{F}$	:	geocentric rotating reference frame
F_T	:	thrust, N
g	:	gravitational acceleration, $\mathrm{m\,s^{-2}}$
h	:	altitude, m
H_W	:	enthalpy on the wall, J
H_{ST}	:	static enthalpy of the incoming flow, J
i	:	inclination, rad
I_{sp}	:	specific impulse, s
K	:	empirical constant (equation 4.6)
L	:	aerodynamic lift force, N
M	:	Mach number
m	:	vehicle mass, kg
m_0	:	initial mass, kg
m_f	:	final mass, kg

m_{gtow}	:	gross take off mass, kg
n_c	:	number of control points
n_e	:	number of shooting arcs
n_{eng}	:	number of engines
n_p	:	number of flight phases
p	:	atmospheric pressure, Pa
$\dot{q}_{conv}$	:	convective heat flux, $\mathrm{W\,m^{-2}}$
$\dot{q}_{dyn}$	:	dynamic pressure, Pa
R^2	:	coefficient of determination
r_C	:	local radius of curvature, m
r_E	:	Earth's radius, m
S	:	Surface area, $\mathrm{m^2}$
T	:	Thrust, N
t	:	time, s
t_{orbit}	:	orbit period, s
tof	:	time of flight, s
Tol	:	tolerance
T	:	temperature, K
T_W	:	wall temperature, K
u	:	control variables
v	:	velocity, $\mathrm{m\,s^{-1}}$
v_e	:	exit velocity $\mathrm{m\,s^{-1}}$
x	:	state variables
α	:	angle of attack, rad
γ	:	flight path angle, rad
θ_{sw}	:	wing sweep angle, rad
ε	:	thrust offset angle, rad
ϵ_T	:	emissivity of the body
ϵ	:	specific orbital energy, $\mathrm{m^2\,s^{-2}}$

θ	:	longitude coordinates, rad
λ	:	latitude coordinates, rad
μ	:	bank angle, rad
μ_E	:	Earth's standard gravitational parameter, $\mathrm{m}^3\,\mathrm{s}^{-2}$
ρ	:	atmospheric density, $\mathrm{kg}\,\mathrm{m}^{-3}$
σ	:	Stefan-Boltzmann constant, $\mathrm{W}\,\mathrm{m}^{-2}\,\mathrm{K}^{-4}$
τ	:	throttle
χ	:	heading angle, rad
ω_E	:	Earth's angular rate, $\mathrm{rad}\,\mathrm{s}^{-1}$

0	:	initial
f	:	final
hs	:	hypersonic regime
p	:	propellants
ref	:	reference
ss	:	sub- and super- sonic regime
SL	:	sea level
tgt	:	target
x	:	x-axis
y	:	y-axis
z	:	z-axis

List of acronyms

AAO	:	All At Once
AIAA	:	American Institute of Aeronautics and Astronautics
AoA	:	Angle of Attack
AoB	:	Angle of Bank
ASTOS	:	AeroSpace Trajectory Optimisation Software
CAMTOS	:	Collocation And Multiple Shooting Trajectory Optimization Software
cFASTT	:	Centre for Future Air-Space Transportation Technologies
CFD	:	Computational Fluid Dynamics
CONOPS	:	Concept of Operations
CSG	:	Centre Spatial Guyanais
DLR	:	Deutsches Zentrum für Luft- und Raumfahrt
DNA	:	Deoxyribonucleic acid
DoF	:	Degrees of Freedom
DSMC	:	Direct Simulation Monte Carlo
ECEF	:	Earth Centered Earth Fixed
ECI	:	Earth Centered Inertial
ESA	:	European Space Agency
FPA	:	Flight Path Angle
GEO	:	Geostationary Earth Orbit
GNC	:	Guidance, Navigation and Control
GPOPS	:	General Purpose OPtimal Control Software

GUI	:	Graphical User Interface
HOTOL	:	Horizontal Take-Off and Landing
HTHL	:	Horizontal Take-off and Horizontal Landing
HWM14	:	Horizontal Wind Model 2014
IAC	:	International Astronautical Congress
ISA	:	International Standard Atmosphere
IAU	:	International Astronomical Union
ITAR	:	International Traffic in Arms Regulations
KKT	:	Karush–Kuhn–Tucker
LEO	:	Low Earth Orbit
LHS	:	Latin Hypercube Sampling
LV	:	Launch Vehicle
MDO	:	Multidisciplinary Design Optimisation
MECO	:	Main Engine Cut-Off
MEO	:	Medium Earth Orbit
MSGRA	:	Multiple Sequential Gradient Restoration Algorithm
NLP	:	Non-Linear Programming
ODE	:	Ordinary Differential Equation
OTIS4	:	Optimal Trajectories by Implicit Simulations 4
POST2	:	Program to Optimize Simulated Trajectories II
RTLS	:	Return To Launch Site
SABRE	:	Synergetic Air Breathing Rocket Engine
SQP	:	Sequential Quadratic Programming
SGRA	:	Sequential Gradient Restoration Algorithm
SSTO	:	Single Stage To Orbit
TROPICO	:	TRajectory OPtimisation, Integration and COntrol
TSTO	:	Two Stage To Orbit
WGS 84	:	World Geodetic System 84

List of conference proceedings and papers

- F Toso, A Riccardi, E Minisci, and CA Maddock. Optimisation of ascent and descent trajectories for lifting body space access vehicles. In 66th International Astronautical Congress, 2015.
- LA Ricciardi, M Vasile, F Toso, and CA Maddock. Multi-objective optimal control of the ascent trajectories of launch vehicles. In AIAA/AAS Astrodynamics Specialist Conference, 2016.
- F Toso, and CA Maddock. Deployed payload analysis for a single stage to orbit spaceplane. In 67th International Astronautical Congress, 2016.
- RJ Garner, F Toso, and CA Maddock. Comparison of the emissions of current expendable launch vehicles and future spaceplanes. In 67th International Astronautical Congress, 2016.
- S McIntyre, T Fawcett, T Dickinson, CA Maddock, A Mogavero, LA Ricciardi, F Toso, M West, K Kontis, KH Lo, S Rengarajan, D Evans, A Milne, and S Feast. How to launch small payloads? Evaluation of current and future small payload launch systems. In 14th Reinventing Space Conference, 2016.
- S McIntyre, T Fawcett, T Dickinson, M West, CA Maddock, A Mogavero, LA Ricciardi, F Toso, K Kontis, KH Lo, S Rengarajan, D Evans, A Milne, and S Feast. A commercially driven design approach to UK future small payload launch systems. In 14th Reinventing Space Conference, 2016.

- F Toso, and CA Maddock. Launch abort trajectory optimisation for reusable launch vehicles. In 21st AIAA International Space Planes and Hypersonics Technologies Conference, 2017.

- CA Maddock, F Toso, LA Ricciardi, A Mogavero, KH Lo, S Rengarajan, K Kontis, A Milne, J Merrifield, D Evans, M West, and S McIntyre. Vehicle and mission design of a future small payload launcher. In 21st AIAA International Space Planes and Hypersonics Technologies Conference, 2017.

- F Toso, and CA Maddock. Initial guess generation strategies for spaceplane trajectory optimisation. In Transactions of the Japan Society for Aeronautical and Space Sciences, 2017.

- CA Maddock, F Toso, M West, J West, K Kontis, S Rengarajan, D Evans, A Milne, and S McIntyre. Conceptual design analysis for a two-stage-to-orbit semi-reusable launch system for small satellites. In Acta Astronautica 152, August 2018.

- CA Maddock, LA Ricciardi, F Toso, and M Vasile. Multidisciplinary design analysis of a semi-reusable two-stage-to-orbit small payload launch system. In 70th International Astronautical Congress, 2019.

Chapter 1

Introduction

Space has historically been a hostile environment that provides an exceptional location to perform science, communication and observation missions, but at a very high entry cost. While space is hazily defined as anything above the Karman Line at approximately 100 km, the majority economical value [1] of commercial activities lies between low Earth orbits (LEO, with an orbital altitude lower than approximately 2 000 km above the Earth's surface) and geostationary orbits (GEO, 35 786 km above the equator).

The reason for the high cost of sending a payload to orbit is well described by the Tsiolkovsky rocket equation (1.1), and its impact is referred to as "the tyranny of the rocket equation [2]".

$$\Delta V = v_e \ln \frac{m_0}{m_f} \tag{1.1}$$

This fundamental equation of rocketry expresses the change of velocity ΔV as a product of an engine efficiency metric v_e and the logarithm of a term related to the amount of available propellant by the initial (wet) m_0 and final (dry) m_f masses of the vehicle.

To accelerate the spacecraft to orbital velocity, the ascent vehicle has to produce a ΔV of about $10\,\mathrm{km\,s^{-1}}$, while carrying along the launcher inert structure, the payload and, most importantly, the propellant itself leading to an exponential increase of the required masses.

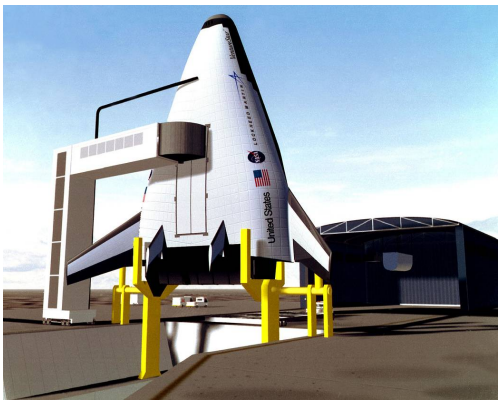

(a) VentureStar on its launch pad. Credit: NASA.

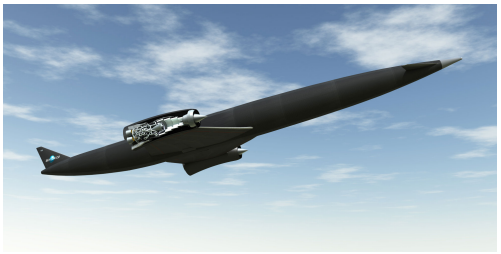

(b) Skylon spaceplane with cutout of the engine. Credit: ESA.

Figure 1.1: Artist's rendition of SSTO concepts.

In addition to the tight mass margins, the launch environment is one the most extreme a man-made machine has to endure, on the same level of stresses as the re-entry, with extreme changes of pressure, temperature and high levels of accelerations and vibrations, further increasing the required structural mass of the launch system producing enormous amounts of energy through chemical reactions.

As of today, even with state of the art technologies, all these compounded issues prevent the orbital delivery of mass in excess of the inert structure and systems required for a single stage launcher. Therefore, no Single Stage To Orbit (SSTO) vehicle to date has ever succeeded in its mission of achieving Earth's orbit, even with the most efficient propellant combinations. Some of the proposed configurations that showed most promise, but have been abandoned over the years, were the Lockheed Martin X-33 VentureStar [3], depicted in Figure 1.1a, and the Reaction Engines Skylon [4], in Figure 1.1b.

All ascent vehicles that have achieved orbit to date, relied on multiple stages that mitigate the aforementioned limitations, splitting the exponential mass ratio requirements of the rocket equation between multiple stages and, consequently, the required ΔV. This approach has allowed the delivery of payloads weighting up to tens of metric tons to Earth's orbit.

1.1 Objectives of the thesis and contribution to the field

The objective of the approach herein presented is to provide information for the mission analysis activities and to assess the viability in general of a launcher, in particular for reusable, lifting body vehicles. This is achieved through the formulation and implementation of an open-source, computationally affordable framework to support in the decision making process for the definition of a business case, early design choices and configuration trade-offs of future space access vehicles. The same process can also be used to refine the project further in more advanced stages, performing mission and flight safety analyses. This approach needs to be able to answer a multitude of questions from different fields, ultimately leading to *"can the vehicle perform the mission, and at what cost?"*, where cost is not necessarily an economical measure. The approach must leverage flexibility, modularity and multidisciplinarity in a manner that can provide more benefit than hurdles to the analyst.

The activity can be separated in the following objectives:

1. Devise a modular methodology to address a wide ranging multitude of cases, drawing from past research, methods and applications in the field, with a forward looking approach to the trend of future computational capabilities.

2. Develop a modular trajectory optimisation framework to be used for launch vehicle analysis, with particular attention to multidisciplinarity, computational efficiency and accessibility.

3. Demonstrate its application in a multitude of scenarios proving the capabilities for the missions and vehicles under consideration, verifying in the process that the results obtained do respect the expectations.

1.2 Thesis organization

The thesis is organised in the following chapters:

Chapter 2 - Background This chapter presents the high level overview of the field of trajectory optimisation. The first section provides a snapshot of the approaches that have been developed and used to find solutions to the problem. The second section presents some of the most successful implementations. In its entirety it provides context and background for the chapters that follows.

Chapter 3 - Methodology and validation This chapter describes the novel methodology implemented in this work, the reasons behind the choices from the options presented in the overview, and how to break down the trajectory optimisation problem in its fundamental parts to solve it. The approach is verified though the use of standard test-cases.

Chapter 4 - Ascent and descent of a SSTO vehicle This chapter offers the first practical implementation of the methodology to model, simulate and optimise a predefined vehicle, optimise its trajectory and evaluate the performances in a scenario characterised by constraints that would be encountered in a real world application.

Chapter 5 - Vehicle sizing and performance analysis This chapter expands the analysis to the estimation of the performances of a vehicle, introducing multidisciplinary design optimisation to determine the size of the vehicle. The optimised configuration is then tested targeting orbits at different altitudes and inclinations, analysing the impact on the deliverable payload mass.

Chapter 6 - Ascent abort scenario analysis This chapter presents the study of the performances of a lifting body vehicle in case of an abort occurring during ascent, analysing the approaches that yield the maximum down- and cross- range capabilities to target emergency landing locations.

Chapter 7 - Conclusions and future work This chapter concludes the thesis summarising the approach and results presented in the thesis, mentioning the results obtained in commercial applications and outlining topics of interest for future work.

Chapter 2

Background

This chapter describes the current market landscape for launch vehicles, identifying the factors driving the design of new vehicles as they strive to capture market share or a niche to exploit with economically viable solutions. Trajectory optimization is introduced as a tool to assist in the development of new concepts, incorporating advancements in computational modelling and technology research. A state of the art review is provided, outlining the methodological background and current techniques, with real-word examples of their application.

The space launch market is constantly evolving [5], driven by a range of factors including the increasing demand for satellite launches [6], the competition among launch providers, and the desire to reduce the cost of access to orbit. Promising approaches to achieving this goal are the development of reusable lifting body (RLV) and single stage to orbit (SSTO) vehicles, which have the potential to lower the overall cost of launches.

However, the design and performance of such vehicles is highly complex and requires careful evaluation and trade-off analysis. This is where trajectory optimization comes in, as it allows engineers and researchers to analyse and compare different design concepts and assess their feasibility and potential performance. In fact, understanding the optimal trajectory for a launch vehicle is crucial for maximizing its efficiency and minimizing its cost.

Therefore, in this chapter, the optimal control problem will be explored, which forms the basis for trajectory optimization in the context of reusable launch vehicles. Various approaches to solving this problem will be discussed and the state of the art in this field will be reviewed. A high level overview of the field of trajectory optimisation is provided, closing with some of the most relevant applications, both as case studies, and programs developed to analyse the problem. Chapter 3 will motivate the choices of methods and approaches selected among the ones presented, with a more specific introduction of the disciplines governing trans-atmospheric flight for the application to reusable lifting body space access vehicles.

2.1 Current drivers of orbital launch vehicle design

The space sector is currently experiencing a commercial inflation thanks to the miniaturization of satellite components [6], the advancements in computing power density and the increase of exploitation capabilities and awareness regarding the possibilities offered by in-orbit science [7]. Commercial activities are growing in the satellite market in both absolute and relative share compared to governmental sector. From smallsats to cubesats, the production rate of companies is increasing [6]. Recent proposals for commercial broadband satellite communication constellations in development by companies such as Oneweb [8] (720 satellites planned in Low Earth Orbit (LEO) and 1280 in Medium Earth Orbit (MEO)) and SpaceX [9] (4408 satellites in LEO) has further increased the demand for launch capacity by orders of magnitude compared to past decades [5].

Smaller satellites in the order of 100 kg have now the majority share of the current market thanks to the initial deployments of the aforementioned constellations [10]. Ride-sharing missions are now routinely part of the launch manifesto of medium lift vehicles such as ISRO PSLV [11], SpaceX Falcon9 [12] and AVIO VEGA [13], with multiple payloads arranged within the fairing as shown in Figure 2.1.

The increased demand for launch of small-(< 500 kg) and micro-(< 100 kg) satellites is enabling new LSPs to enter the market with smaller, cheaper vehicles, requiring reduced initial expenditures, and allow the contribution of venture capital firm invest-

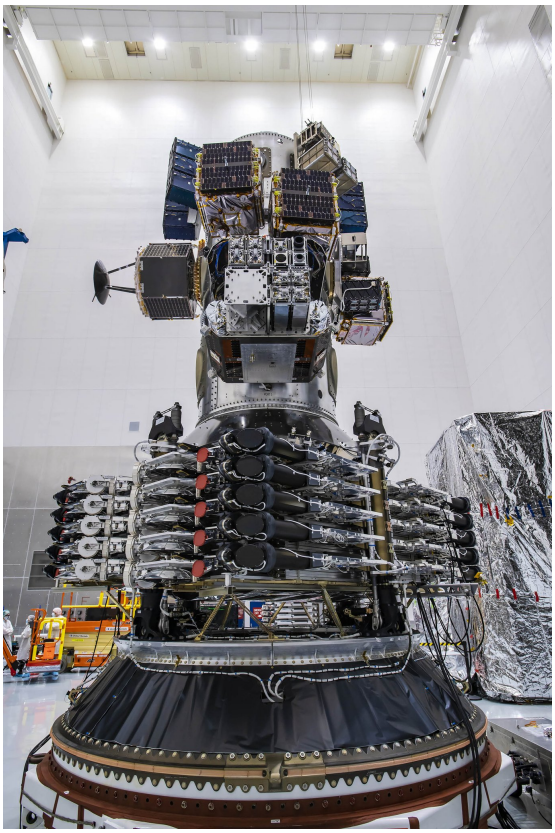

Figure 2.1: Payload stack of the Transporter-1 mission, photographed in the clean room before encapsulation in the fairing. Credit: SpaceX.

ments. Drawn by the increased demand for launch capacity, new players are entering the market at a faster rate than ever before. Hundreds of new launcher vehicles are in various status of development at the start of the 2020s [14], leveraging some of the same technological advancements that sparked the recent commercial satellite growth [15].

The commercial orbital launch success of the RocketLab Electron in 2018 [16], with continuous operations since, are clear demonstrations of new capabilities developed by commercial companies from nations that do not possess launch vehicle heritage. Even though it could be argued that this specific example benefited from US knowledge exchanges, similar initiatives are distributed worldwide, with some of them in advanced status of design, on track to fly in the first half of the 2020s [14]. Commercial launch activities are also planned from the United Kingdom for the first time in history, thanks

Figure 2.2: First successful recovery of the Falcon 9 first stage on the 22nd December 2015 after the ORBCOMM-2 mission. Credit: SpaceX.

to the governmental support and push towards a local commercial launch capability and connected regulations [17] [18].

In parallel to the initiative from small launchers, SpaceX demonstrated in 2014 the capability to land the first stage of a medium lift vehicle [19], the Falcon 9. The first landmark successful recovery of the first stage during an operational flight happened in 2015, shown in Figure 2.2. In 2021, they achieved the milestones of flying 10 missions with the same booster stage, within a timespan of 27 months [20]. This capability, once dismissed by the major players of the launch industry, is now in the plans of future operations of RocketLab testing parachute recovery [21], the China Academy of Launch Vehicle Technology company that started incorporating gridfins [22] in their Long March vehicles, and the European funded initiatives such as RETALT [23] and THEMIS [24].

Reusable launchers are a particularly appealing concept for two main reasons: cost savings and launch capacity. The former is a consequence of the fact that while about 9/10 of the vehicle by mass is fuel, it is also the cheaper part. Recovering engines, tanks, avionics and any other components has the potential to dramatically reduce the cost of a launch when refurbishment is more convenient than production from scratch. The

Figure 2.3: Relativity Space's Stargate metal 3D printer manufacturing a cylindrical rocket section. Credit: Relativity Space.

second advantage comes from the logistics of manufacturing: whenever the factories producing rockets and the commercial suppliers are running at full capacity, refurbishment for reuse presents an opportunity to increase launch capacity supply without increasing manufacturing throughput. One of the limiting factors of the launch availability supply is the production rate of complex components, with engines and large carbon wrapped tanks manufacturing cadence being a limiting factor. Alternative efforts in overcoming the production rate limits of rocket factories are currently undergone by Relativity Space, attempting to streamline and automatize the majority of the rocket production rate [25], with the possibility of scaling the production linearly with the number of machines; the first prototype printer is depicted in Figure 2.3. While the use of the additive manufacturing for complex launcher components is an ever increasing trend across the whole industry [26], it is unclear the degree of success that can be reached by complete manufacturing automation.

All these commercial initiatives that started in the last decades, often referred to as *NewSpace*, separated from the traditional governmental ones by presenting innovative approaches to space access. This expansion and new talent provides a fertile ground

for the development of new concepts, reigniting the interest in reusable lifting body vehicles [14].

The first orbital reusable launch system with a lifting body was the Space Shuttle System, with the Orbiter upper stage and solid rocket booster casings reflown on multiple missions after refurbishment (Figure 2.4a). The high cost associated with those maintenance activities and the public reaction to the accidents ultimately halted the program in 2011. Many concepts such as the Horizontal Take-Off and Landing vehicle [27] (HOTOL, Figure 2.4b), its iteration Skylon (Figure 1.1b), the X-33 (Figure 1.1a), and others have been cancelled in the recent decades, leaving the SNC Dream Chaser [28] (Figure 2.4c) as the most promising commercial reusable lifting body vehicle under development. The US military branches have flown multiple times the X-37B [29] (Figure 2.4d), an unmanned, controllable, reusable upper stage characterised by a lifting body and employed for secret orbital missions lasting multiple months.

2.2 Trajectory design for mission analysis

The work presented in this document provides an approach to evaluate the performances of different configurations of lifting body vehicles in diverse scenarios, with the focus on reusable orbital access vehicles. The benefits of having such capability can span the whole launch industry from the venture capital firms reducing the risk associated with investments by rapidly evaluating new concepts, to the performance analysis in the early phases of the design definition, until the mission trajectory design for compliance with either regulatory or insurance safety requirements. Early phases are the most important on a cost basis, since architectural decisions taken at the beginning of the project have long-lasting impacts that are hard to recover from [30].

In the field of launcher mission analysis, optimisation is a tool that can be used do design trajectories to solve scenarios like the maximisation of payload [31], the minimisation of risk to overflown populations [32], or the minimisation of the loads and stresses generated during flight [33]. Each of those problems has an associated optimal trajectory that is fully dependent on the setup of the case under analysis. Trajectory optimisation is a fundamental step where all technical disciplines coalesce into the study

(a) Space Shuttle on the launch pad. The orbiter and the 2 solid rocket boosters were refurbished between flights. The orange external tank was demised, and not recovered. Credit: NASA.

(b) Artist impression of the BAe HOTOL. Credit: Reaction Engines.

(c) SNC Dream Chaser during landing after drop test. Credit: SNC.

(d) X-37B Orbital Test Vehicle during taxi on the flightline in June 2009 at Vandenberg AFB, California. Credit: US Air Force.

Figure 2.4: Spaceplane designs.

of the vehicle performances, driving technical trade-off and providing feedback on the project evolution. The coupling of multiple disciplines generates solutions that improve on a specific metric when compared to optimal solutions found by analysing a single field or topic, but it introduces additional complexity and increases the computational time required to solve the problem [31].

When optimisation is performed to find a solution to a specific problem, the algorithms require thousands, millions or more evaluations before halting. While the available processing power follows an exponential trend thanks to technological deflation, new modelling techniques adapt on accessible resources; analyses such as chemical or fluid dynamic simulations will increase their complexity and their accuracy over time. This implies that using coupled high fidelity simulations to find optimal solutions is a computationally intensive problem that can take excessive time to be solved. This limitation can be circumvented by using low order models, less accurate but fast enough to be used in a problem requiring optimisation [34].

It is suggested by Betts that the needs of the aerospace community have been one of the drivers for the development of the necessary numerical methods for trajectory optimisation [35]. Mathematical optimisation is a continuously growing field that has been dramatically changing multiple engineering and science domains, and it is a fundamental building block of many emergent fields such as machine learning [36] and real time navigation algorithms [37].

2.3 Optimal control

The optimal control problem's [38] purpose is to determine the evolution of a dynamic system through control $\mathbf{u}$ to minimise the performance index [39] J of equation 2.1.

$$J = \phi[t_f, \mathbf{y}(t_f), \mathbf{u}(t_f)] + \int_{t_0}^{t_f} L[t, \mathbf{y}(t), \mathbf{u}(t)]\, dt \tag{2.1}$$

The optimal control problem is thus formulated in the Bolza form; it is a Lagrange problem if the first addendum ϕ is zero, while it is a Mayer problem when the integral

L is null. The problem is subject to the dynamic constraints, path constraints and boundary conditions of the system 2.2.

The system evolution is usually defined by a set of ordinary differential equations $\dot{\mathbf{y}}$ function of the states $\mathbf{y}$, controls $\mathbf{u}$, parameters $\mathbf{p}$ and an independent variable, commonly time t. Boundary constraints $\mathbf{b}$ and path constraints $\mathbf{c}$ are also included.

$$\begin{cases} \dot{\mathbf{y}} = f[t, \mathbf{y}(t), \mathbf{u}(t)] \\ \mathbf{b}[t_j, \mathbf{y}(t_j), \mathbf{u}(t_j)] = 0 \\ \mathbf{c}[t, \mathbf{y}(t), \mathbf{u}(t)] \leq \mathbf{0} \end{cases} \tag{2.2}$$

In the scenarios presented in this work:

- the state constraints are determined by the dynamic of the systems describing the evolution of position and velocity vectors,
- the boundary constraints set the state, control and time limits at the boundaries between flight phases, including the initial and final flight conditions,
- and the path constraints are computed and applied along continuous sections of the trajectory.

The problem is defined as multi-objective if there are multiple cost functions. It is usually constrained by inequality and equality constraints, determining if the values of a performance metric violates its threshold or achieves the desired target.

Examples of real word equivalents to the mathematical formulations are thermo-structural limitations of the airframe as inequality path constraints, where specific load limits must never be exceeded during flight. The matching of the final conditions with predefined target states are equality boundary constraints. Ascent trajectories might terminate at specific orbital parameters while descent flights might require precise targeting of the landing zone.

2.4 Indirect and direct methods

Optimal control seeks the control laws for a given system that minimizes a cost functional subject to initial and final states as well as path constraints. This is an infinite dimensional optimization problem, for which usually it is not possible to find the exact analytic solution, hence the need of a numerical method for approximating its solution. Numerical methods are divided into indirect and direct methods [40].

2.4.1 Indirect methods

Indirect methods attempt to find the root of a function or set of functions that describe the problem, computing the slope of the merit function and determining when it is close to zero. To find the root of the necessary condition, it is required to derive the adjoint equations, gradients, control equations, and transversal conditions. This calls for a high degree of knowledge from the mission analyst, creating a high barrier of entry, it is time consuming, and it makes the approach unsuitable for fast evolving, mutable problems and requirements which characterise the early phases of a vehicle design [39]. Indirect methods are generally not robust, presenting issues when the initial guess is not known or far from the solution [40]. It is an approach more suitable for the study of well consolidated vehicles and scenarios, with fixed problem setup, known initial guess, and marginal changes between iterations, providing better solutions compared to direct methods in such problems [41].

2.4.2 Direct methods

Direct methods discretise the states and controls of the trajectory, transcribing the case to a non-linear programming (NLP) problem, where the constraint or cost function are not linear. In this approach, the dynamic system can be a black box, interacting with the solver only by providing the merit function and constraints, not requiring explicit derivation of the equations used in indirect methods. They are extremely sensitive to variables at the beginning of the trajectory, and this issue is usually mitigated through the use of multiple shooting [35]. Direct methods are usually more robust than indirect

ones, and can recover from a wider range of initial guesses if the optimisation algorithm has the capability [39].

2.5 Transcription

While the behaviour of the dynamic systems considered in this work are described by a set of ordinary differential equations ODE presented in the following chapter, the problem for optimisation must be formulated, or transcribed, with a finite set of variables to be solved through the algorithms of choice. Transcription methods fall into two categories: shooting and collocation methods [40].

2.5.1 Single shooting

The simplest problem of trajectory optimisation is the selection of the angle of throw of a projectile to a target [42]. A single shooting algorithm is the least complicated approach to solve the problem [35], where the only control variables are the initial states. The miss distance from the target location, or defect, is reduced by changing the angle of throw, until the trajectory ends in the bull's eye. This approach works fine for the simple projectile problem but it presents stability issues when the time of flight is long, where small changes in the initial conditions produce large effect in the final ones [35].

Transcription by the single shooting approach results in a non-linear programming (NLP) problem with a relatively small number of independent design variables, but dynamical systems which are subject to instability for certain values of their control parameters (as is often the case) are difficult to treat with this method [35].

2.5.2 Collocation

A second category of transcription approaches is represented by the collocation methods, approximating the trajectory states, controls, constraints and objectives with curve fits (i.e. polynomials and splines) where the boundary conditions are satisfied at each node of the grid. These methods are more stable than single shooting and provide

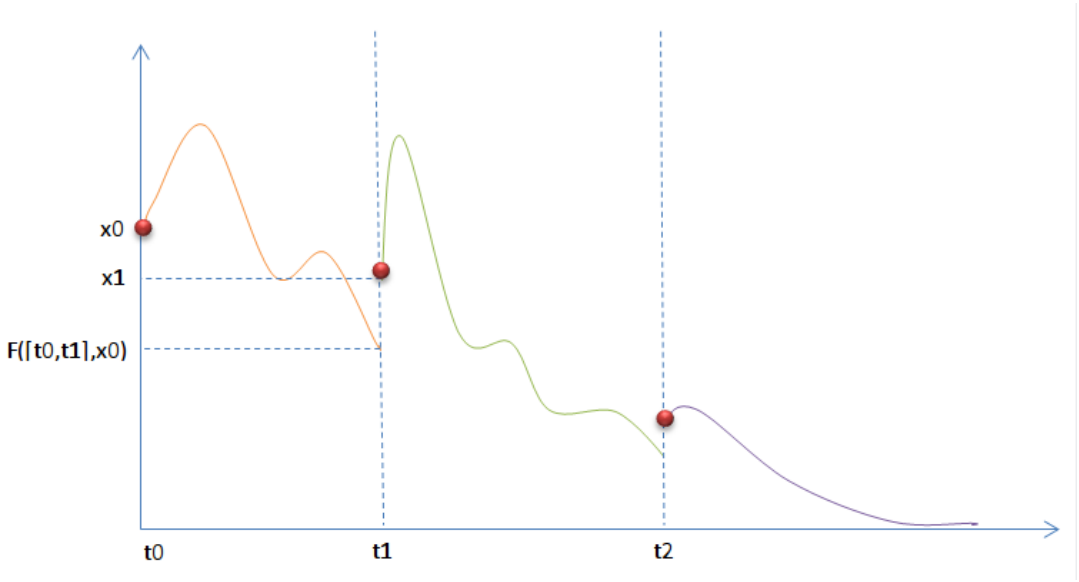

Figure 2.5: Multiple shooting discretisation

a low accuracy, fast result, that can be further refined by increasing the number of grid-points. The solution accuracy must be verified with a single shooting integration since the solver interfaces directly only with the polynomials and not with the dynamic equations. In case of unacceptable discrepancies, the problem must be analysed with a denser grid. They are suited for long duration arcs, ballistic or low thrust flight, where shooting methods are limited by the speed of the numerical integration [39].

2.5.3 Multiple shooting

Multiple shooting subdivides the trajectory in multiple single shooting sub-arcs (Figure 2.5) that need to match states when one ends and the other begins. The midpoints between trajectory segments require extra variables to be added to the problem, and the mismatch, or defect, at the boundary is treated as an equality constraints. This additional complexity provides further stability to the problem and effectively produces a sparse Jacobian matrix, with sparsity increasing with the number of intervals, efficiently handled by a multitude of NLP solvers. A further advantage is provided by the fact that each sub-arc can be simulated independently from the others, providing the possibility of parallel computation of the simulation.

2.6 Nonlinear Optimisation Methods

Optimisation algorithms can be broadly divided in 2 macro categories, stochastic and deterministic [40].

The two classes have complementary characteristics and some algorithms combine aspect from both to strike a balance between search-space exploration, exploitation and computational time.

The algorithms iterate by changing the optimisation variables until a specific stopping criteria is met. The final coordinates found correspond to a cost, which is desirable to be a minimum. The value of a cost function is a local minimum when it is the smallest value within a given range. It is a global minimum if such range spans the entire search-space domain of the optimisation variables.

The selection of algorithm examples, listed in the following two subsections, have been selected by the author based on the familiarity accrued during the research for this thesis's work.

2.6.1 Deterministic methods

Deterministic methods compute the slope of the merit function at each step and move towards the local minimum, with limited exploration capabilities, but more efficiently moving towards the local optimum [40].

Examples of commonly used algorithms include:

- *Newton's Method* [43], where the decision vector is updated iteratively by moving towards the root of the cost function through second order derivation.
- *Sequential Quadratic Programming (SQP)* [44] is similar to Newton's Method, but allows inclusion of equality and inequality constraints through the use of Lagrange multipliers and the application of the Karush–Kuhn–Tucker (KKT) conditions.
- *Pattern Search* [45], a derivative free approach that explores each dimension separately and moves toward the lowest value found, iteratively reducing the search-step any time no improvement is found. It can handle discontinuous functions.

The first two are the basis on which many of the local optimisation software libraries build upon, with notable examples used in the field being WORHP [46] and SNOPT [47].

2.6.2 Stochastic methods

Stochastic methods uses a mix of approaches that exploit random parameters to provide good exploration of the search-space [40]. They generally do not require computation of the problem gradient, and cannot guarantee that a minimum has been found.

Examples of commonly used algorithms include:

- *Genetic Algorithm* [48], where the optimisation vector is treated similarly to a population characterised by DNAs undergoing evolution with random mutations, selection driven by the cost function and crossover among multiple competing candidates.

- *Particle Swarm Optimisation* [49], characterised by a population of individuals moving in the search-space toward areas of improved cost, driven by momentum and knowledge of the best candidate location found individually or shared by connected neighbours.

- *Simulated Annealing* [50], mimicking the process of cooling materials, with repeated random tentative improvements of the solution within a decreasing exploration area, proportional with the energy of the system.

- *Differential Evolution* [51], similar to the Genetic Algorithm, it differs by generating a trial vector from mutation and crossover of the existing population, and direct selection by comparison with the target vector.

Memetic Algorithms are a class of algorithms that provides an extension to evolutionary approaches such as the Genetic Algorithms, with additional capability to perform local improvements [52]. The purpose of this combination is to leverage the strengths of the two approaches: exploration with the evolving population, and exploitation through local search techniques.

Stochastic methods are widely used in designing interplanetary trajectories, but rarely in the launch vehicle design and mission analysis [53]. Castellini and Lavagna have postulated that they could be a viable alternative that merits further exploration.

2.7 Initial guess strategies

Optimisation problems can be provided with an initial guess, an approximate solution that speeds up the convergence by identifying promising areas of the problem search-space. The benefit is logically more pronounced when combined with local optimisation algorithms, characterised by limited exploration capabilities.

If the initial guess is not provided, most scientific computing libraries generate a randomised starting vector, and the algorithm solving the problem does not receive any benefit. An experienced analyst can manually generate an initial guess based on empirical expertise accrued on similar problems, but the process can be time intensive and subject to personal bias.

Alternatively, the initial guess can be obtained as a solution of a simplified problem: neglecting forces or removing constraints [54], simplifying the dynamics, reducing the optimisation problem dimensions. These approaches have in common the requirement to re-formulate the problem in the desired simplified form.

To prevent duplicating or modifying the problem, exploratory algorithms can be employed to identify candidate guesses [55], solving the problem with global methods to find the initial guess, and local exploitation to refine the final solution. The ascent scenario presented in chapter 4 applies such approach.

All the other scenarios presented in this work employ a multi-start approach: multiple initial guesses are analysed separately with a short optimisation, and the best one (i.e. lowest constraint violation norm) is selected for the final optimisation. Further details are provided in the individual application cases.

The author of this work has explored the trade-off between multi-start strategies [56], using randomised vectors generated with Latin Hypercube Sampling (LHS) and Mersenne Twister [57]. The use of LHS is further explored in combination with altering the weighting of the constraints relative to the objective function, changing the

integration time-step and introducing white noise into the first guess vectors for runs that failed to converge. The performances are analysed for computational run time, convergence rate and violation level of the constraints. A focus is also put on methods that reduce the dependency on the expertise of the user to produce a problem-specific first guess.

The post-processing of results by relaxing the constraints and the introduction of white noise showed marginal improvement on the convergence rate, but the small population size and the single problem analysed prevent from selecting the best approach on absolute terms, as presented in section 5 of the trade-off analysis of the aforementioned paper [56].

2.8 Trajectory optimisation programs

The tight margins available in space launch activities have spurred the continuous research of approaches to squeeze as much performance as possible from the launchers. Many companies and institutions have developed their own in-house solutions with source-codes kept secret and closely guarded, and some endeavours have gained widespread recognition and became a product on their own.

A selection of some of those software packages is listed in alphabetical order to provide a general overview of the field, based on relevance to this thesis, and frequently used in similar applications.

2.8.1 ASTOS

AeroSpace Trajectory Optimisation Software, or ASTOS [58], is a commercial suite of tools initially developed by DLR before being spun off, that assists the design of ascent, orbital and entry vehicles. It includes a multitude of modules that can be used to address specific questions in different disciplines. It also provides the users with a preloaded set of models that can be used for simulation. The combination of simulation, optimisation and modelling capabilities provides a versatile software that contains all the building blocks to assess the performances of a space vehicle and design reference

trajectories with optimisation methods. It provides a high degree of flexibility, with building blocks for system design, 3-DoF or 6-DoF simulations, and the Collocation and Multiple Shooting Trajectory Optimization Software (CAMTOS [59]) optimiser allowing the use of direct, indirect and collocation methods.

2.8.2 GPOPS2 and DIDO

The General Purpose OPtimal Control Software 2 [60] is a MATLAB proprietary software developed by Patterson and Rao. It can solve multiple-phase optimal control problems using variable-order Gaussian quadrature collocation methods. It is notable in this list due to its application not only in aerospace applications [61] [62], but also in other fields of study [63] [64].

Similar general purpose software [65] using direct collocation methods include SOCS [39], DIDO [66], DIRCOL [67], and the predecessor GPOPS [68]. DIDO is of particular relevance within the scope of this thesis due to its recent application in the study of a multi-stage partially reusable launch system with rocket and air-breathing propulsion [69].

2.8.3 OTIS4

The Optimal Trajectories by Implicit Simulations [70] is developed by NASA Glenn Research Center, subject to ITAR restrictions and uses direct collocation to generate trajectories. It includes the possibility of using multiple shooting and performing parametric vehicle design. Detailed information of its implementation are scarce, but it seems a tool more focused on the general optimal control problem, where for the trajectory optimisation needs, POST2 is preferred.

2.8.4 POST2

The first iteration of Program to Optimize Simulated Trajectories II (POST2) was created by Martin Marietta for NASA Langley Research Center to support the Space Shuttle and following programs [71]. The second, current, version is continuously developed by NASA, can handle point mass simulations with different DoF, multiple bodies

and multiple manoeuvres, making it well suited for NASA's requirements of design of launch, entry and interplanetary missions. Its usage restricted under the ITAR regulations and optimisation is performed with NPSOL [72], a SQP solver developed in Fortran.

2.8.5 SGRA

The Sequential Gradient Restoration Algorithm, in its single arc (SSGRA) and multiple arc (MSGRA) [73] variants has been developed by Miele [74] from the late 1960s onward. It is an indirect method and, as the name suggests, it iterates repeating 2 steps: the first one is a gradient phase to improve the merit function, and a second one to force constraint satisfaction. It has a high barrier of entry regarding user knowledge, but its open implementation favoured it for the application in multiple aerospace programs, including recent developments of ESA's Intermediate eXperimental Vehicle IXV [75].

2.9 State of the art on spaceplane trajectory design

As anticipated in chapter 1, mission analysis for ascent and re-entry vehicles has drawn considerable attention over the past decades; trajectory design for space missions is one of the aspect that is optimised to increase margins and reduce mass of the vehicles in ascent and re-entry. Spaceplanes combine the constraints of both directions of the flight, providing an interesting test case for research groups interested in transatmospheric flight, with multiple disciplines required to solve the emerging multidisciplinary problems.

As mentioned in the introduction, the field is closely linked with the space shuttle program, given its record of the first spaceplane succesfully operated for multiple decades. In 1974, 7 years before the first flight, Brusch [76] presented a direct method with sub-arc subdivision to solve ascent and abort scenarios for the Space Shuttle. The study highlights the trade-off between direct and indirect methods, concluding with the same remarks on the computational time vs analyst time explained in section 2.4.

The paper presents an unconstrained optimisation algorithm that solves a constrained problem by adding a penalty factor calculated from on constraint violations.

The Shuttle program evolved over time, computational speed improved following Moore's law [77], increasing the achievable level of fidelity and capabilities. This capacity culminated into day-of-launch analysis, generating a trajectory lowering the vehicle stresses (loads, controls, performances) by adapting to the most up to date atmospheric measurements, used up to the last launch in 2011. Harrington's paper [78] details such rigorous process and the data flow within NASA and all the teams involved in the launch operations.

The initial trajectory optimisation is performed with angle of attack, bank and throttle control, similarly to the application cases of chapter 4, 5, and 6. This first step of the Space Shuttle ascent trajectory design is simulated in 3dof, with the objective minimising the loads on the vehicle, while satisfying the constraints, incorporating the day of launch measurements.

A second analysis, at higher fidelity, is then performed to further reduce the loads, simulated in 6 degrees of freedom, with GNC models in the loop, obtaining a guidance law based on flight Mach as the independent variable. While not explicitly defined due to ITAR restrictions, it is likely that the optimisation were performed out with OTIS (see section 2.8).

The source offers an insight in the final operations of a long running program, reminding that the processes are more important than the methods, especially when lives are at stake, and safety is a fundamental requirement, without which space operations could not be licensed to operate.

The impact of the Space Shuttle program is evident in literature, with important books such as Betts's book [39] on optimal control, continues to be referenced in recent studies [79], and it has inspired the generation of multiple concepts of reusable vehicles. A comprehensive comparative is provided by Bayer [80], but some of the lifting body SSTO concepts that have shaped the research for this work are listed below in chronological order.

NASA has supported studies for a fully reusable SSTO replacement of the Space Shuttle primarily to reduce the cost to access space, and improve the turnaround times [81]. The VentureStar program [82], with its X-33 subscale demonstrator, consisted of a vehicle capable of vertical take-off and flight to orbit with its aerospike engine [83], able to perform efficiently on a wide range of altitudes. The vehicle would be recovered with horizontal landing on a runway, shielded from the re-entry conditions by a metallic TPS, with lower maintenance cost when compared to the Shuttle's [84]. The nominal trajectories have been generated in 3-dof [85] with POST [71] and OTIS [70].

SGRA [74] has been successfully employed by its creator, Miele, for the trajectory optimisation of a SSTO vehicle inspired by VentureStar [86], in 2-dof on a spherical non-rotating Earth.

One of the most important SSTO concepts for this thesis is the british HOTOL [27] of the 1980s. This initial attempt was an important stepping stone for the future development of the SABRE engine [87], at the core of the Skylon [4] SSTO vehicle concept of the early 2000s. The engine would transition from rocket to pre-cooled ramjet depending on the flight regime to maximise the efficiency through the use of atmospheric oxygen.

The interest into the Skylon concept sparked collaborations between industry and academia, such as the one with the cFASTT research group [88]. This group used the cFASTT-1 [89] concept vehicle inspired by Skylon as a starting point to develop multidisciplinary analysis capabilities [90], thermal protection system (TPS) design [91], aerothermodynamics [92] [93], propulsion [94] [95], and environmental impact [96]. The author of this document contributed to the research group with the development of methodologies for trajectory design and mission analysis.

Lazarus [97] is a concept originated in the Georgia Institute of Technology for a SSTO with multiple methods of propulsion. The vehicle would be accelerated until take-off with an electrically powered sled on a rail up to $M = 0.7$; then it would ignite a rocket based combined cycle (RBCC) engine until $M = 3$, switch to ramjet propulsion until $M = 6$, scramjet until $M = 10$, and gradually transition to rocket mode until orbit insertion. The analysis of the vehicle design could benefit from many

ITAR-restricted tools, such as CBAERO [98] for the aerodynamics, SCCREAM [99] fro the propulsion, and POST for the trajectory design. This tool had been already in use in the research group since the 1990s, starting from the trajectory design of the Lazarus predecessors: a generalised SSTO with rocket-based combined cycle engines [100], followed by Hyperion [101] and Stargazer [102].

This work aims at bridging the gap between simplified problem formulations and high fidelity proprietary tools to solve the SSTO trajectory problems, with a flexible methodology described in the next chapter.

2.10 Summary of the chapter

This section of the thesis has presented an overview of the theoretical and technical fundamentals that constitute the basis of trajectory optimisation, starting from a description of the optimal control problem, to the applications. The different methods have been presented and compared for capabilities, and practical consequences.

This background chapter has provided the mathematical formulation, with methodologies to transform the optimal control problem into something that can be solved by the chosen algorithms. Practical cases follow the theoretical section, with description of notable applications of the methodologies as software implementations, and as application on existing or theoretical spaceplanes.

The next chapter will delve into the implementation of the methodology developed during the research, motivating the choices made, with frequent references to the content of this background chapter.

Chapter 3

Development of Methods for Trajectory Optimisation

Optimisation is a tool often used in mission analysis for launch vehicles due to its versatility in analysing multidisciplinary hierarchies of interconnected systems that are too complex to study analytically as a whole. Various approaches can be employed to evaluate the behaviour of a vehicle in the environment it is expected to fly through, but they all aim to find the most effective way to achieve an objective while satisfying constraints that define the mission or the problem, as anticipated in chapter 2.

Mission analysis for space access vehicle is an complex topic, requiring a high degree of multidisciplinary knowledge to identify errors or knowledge gaps from the results. The inputs cover the entirety of the launcher and the environment, the data is often presented with subsystem-specific levels of complexity that vary across the whole system, and most, if not all, optimisation algorithms can exploit any weakness which include modelling limitations and mistakes occurring in the set-up of the problem, potentially leading to infeasible solutions or catastrophic scenarios, if the issues are not identified and corrected [39].

This chapter presents the approach in the adaptation and integration of methodologies used in the applications of this thesis, with the objective of providing first and foremost a logical, modular structure that is easy to understand, develop, maintain, evolve over time and that can tackle a wide variety of cases, possibly sacrificing com-

putational speed for ease of use and reduced time to set up. The logic behind this choice is that computational time is relatively cheaper than the time of the analyst. The following sections also describe the methodology from the combination of forces, representing physical phenomena and models at subsystem levels that influence the physics of flight, to the optimisation algorithms used to define the guidance required.

3.1 Approach

TROPICO [103] (TRajectory OPtimisation, Integration and COntrol) is an open-source software[1] developed by the author of this document to carry out the computational activities required for the solution of the problems presented. The software has been structured from the ground up to address specific questions related to the mission analysis for space access vehicles, in particular reusable ones, with continuous interfacing with industrial partners to integrate their needs and requirements.

The approach described in this thesis has been built in a layered structure, keeping disciplines separate and modular as much as possible. This breakdown allows the integration with unit testing or validation and verification of the single modules used. The structure can be conceptualised with Figure 3.1 or described from the innermost core to the outermost shell:

- the subsystem models of the vehicle and the environment
- the simulation of flight through the dynamic equations
- the control law definition
- the integrator
- the optimisation
- the pre- and post-processors interfacing with the user

The code is written in MATLAB, the software with the largest user-base within the cFASTT research group at the beginning of the development of the methodology. The

[1] *https://github.com/federico-toso/TROPICO*. Accessed: 2022-09-01

input file, storing the problem set-up as either variables or function handles, is used to define the investigated scenarios and it is the most frequently accessed file, in the continuously iterative process of mission analysis.

The modular components from Figure 3.1, further described in this chapter are:

- the first guess generation methods
- the optimisation algorithm
- the objective of the cost function
- the constraints applied on the full trajectory, on specific points, or on a per-phase basis.
- the equations of motion
- the discipline-specific functions, for both the environment and the vehicle performances.

The latter item is the most important of the list, as the disciplinary models are the fundamental elements that determine the evolution of flight for the studied scenario.

The modules are specified in the input file with a string selecting among different options commented within the code, function handles pointing to files from the library, or pointing directly to MATLAB functions. For example, in a classical re-entry scenario, it is likely that the propulsion modelling is not required and thus disabled, and a higher fidelity thermal function customized on the specific vehicle could be required; on the other hand, an ascent trajectory might place more emphasis on the propulsion and use a low fidelity thermal estimation only for fairing release. The users can code their own functions with the approach that is most suitable for their own case. As any analysis is different from the others, it is expected that the user has a customised set of requirements for their scenario, and has some basic familiarity with MATLAB to write the application-specific functions, using the provided scripts as templates. The library of modules that are publicly available in the on-line repository is limited to the ones used in this dissertation, or for the published research results listed before the introduction, but only when not covered by non-disclosure agreements.

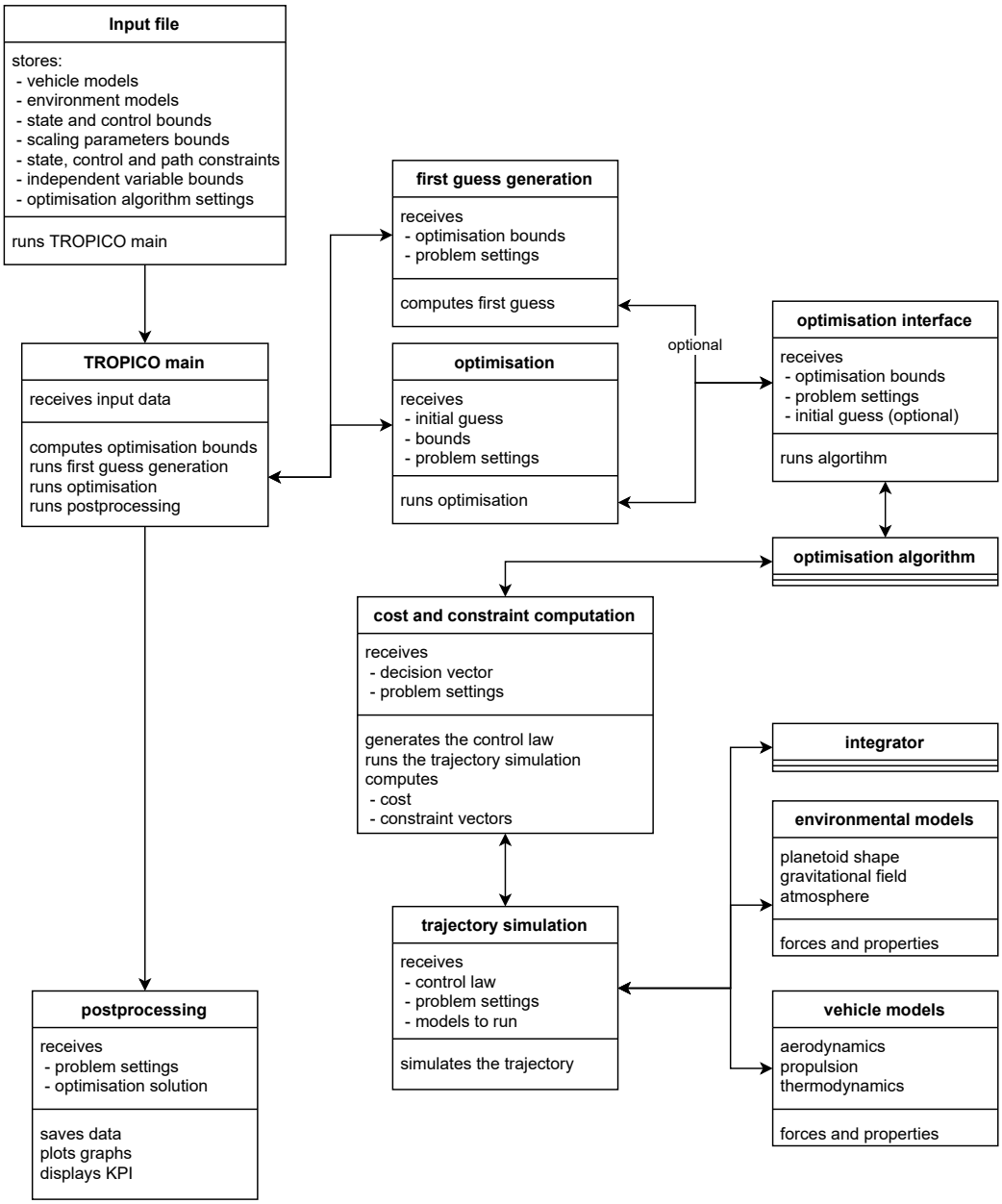

Figure 3.1: Visualisation of the information flow in TROPICO

3.2 Modelling of space access vehicles

One of the most important tasks in the simulation of the behaviour of the studied vehicle for the purpose of trajectory optimisation is the compromise between accuracy of the results and computational time driven by the complexity of the models used to generate them. The equations of motion and the subsystem routines are not only evaluated millions of times in each optimisation run, but also require different models for the various phases of flight and stages in a launcher. The balance of these factor directly influences the level of fidelity of the simulation and the run time of the optimisation, limited by the available computational power.

3.2.1 Dynamics - the governing equations

All the application cases presented in this study model the vehicles as point masses on an Earth Centered Earth Fixed reference frame with 3 degrees of freedom.

The validation cases, at the end of this chapter, are the only exception to this choice. Those scenarios use an exact copy of the simplified reference frame and system of dynamic equations provided by the original authors, detailed in the relevant section.

The dynamic equations 3.1 for the transatmospheric flight are presented as a set of Ordinary Differential Equations (ODE) that can be integrated by initial value problem solvers, and are the same for ascent or descent. Within this model, the vehicle is considered as a point with a time-varying mass centred on the Centre-of-Mass of the vehicle. The set of equations of motion are calculated within a geocentric rotating reference frame using spherical coordinates, denoted by $\mathcal{F}$.

The state vector $\mathbf{x} = [h, \lambda, \theta, v, \gamma, \chi]$ contains the 6 variables for position and velocity, with altitude h (the radial distance is $r = h + R_E$), and velocity v relative to the reference frame. The flight path angle γ is measured from the local horizon, the heading angle χ is defined clockwise from the local North, and they are illustrated in Figure 3.2. λ and θ are the latitude and longitude coordinates on the Earth. The equations of motion are given by [104],

$$\dot{h} = \dot{r} = v \sin\gamma \tag{3.1a}$$

$$\dot{\lambda} = \frac{v \cos\gamma \sin\chi}{r} \tag{3.1b}$$

$$\dot{\theta} = \frac{v \cos\gamma \cos\chi}{r \cos\lambda} \tag{3.1c}$$

$$\begin{aligned}\dot{v} = {} & \frac{F_T \cos(\alpha + \varepsilon) - D}{m} - g \sin\gamma \\ & + \omega_E^2 r \cos\lambda \left(\sin\gamma \cos\lambda - \cos\gamma \sin\chi \sin\lambda\right)\end{aligned} \tag{3.1d}$$

$$\begin{aligned}\dot{\gamma} = {} & \frac{F_T \sin(\alpha + \varepsilon) + L}{mv} \cos\mu - \left(\frac{g}{v} - \frac{v}{r}\right) \cos\gamma \\ & + 2\omega_E \cos\chi \cos\lambda \\ & + \omega_E^2 \left(\frac{r}{v}\right) \cos\lambda \left(\sin\chi \sin\gamma \sin\lambda + \cos\gamma \cos\lambda\right)\end{aligned} \tag{3.1e}$$

$$\begin{aligned}\dot{\chi} = {} & \frac{L}{mv \cos\gamma} \sin\mu - \left(\frac{v}{r}\right) \cos\gamma \cos\chi \tan\lambda \\ & + 2\omega_E \left(\sin\chi \cos\lambda \tan\gamma - \sin\lambda\right) \\ & - \omega_E^2 \left(\frac{r}{v \cos\gamma}\right) \cos\lambda \sin\gamma \cos\chi\end{aligned} \tag{3.1f}$$

where α is the angle of attack, and μ is the bank angle, as visualised in Figure 3.3. ω_E is the angular rate of the planet, m is the mass of the vehicle, ε is the pitch offset angle between the direction of thrust F_T and the longitudinal plane of the vehicle, g is the gravitational acceleration, and L and D are the aerodynamic lift and drag forces, respectively. All the terms are time-varying, with the exception of ε in cases without thrust vectoring.

Looking at a standard aircraft body-relative reference frame $\mathcal{B}$, $+x^{\mathcal{B}}$ is towards the nose along the longitudinal axis of the spaceplane, $+y^{\mathcal{B}}$ is outwards along the starboard wing, and $+z^{\mathcal{B}}$ points downwards towards the Earth normal to the plane of symmetry given by $x^{\mathcal{B}}$-$y^{\mathcal{B}}$. The flight path angle is the angle between the local horizon (defined by as the plane tangent to the radial vector) and the velocity vector, while the flight heading angle is the angle between North (or the $x^{\mathcal{F}}$-axis) and the horizontal component of the velocity vector.

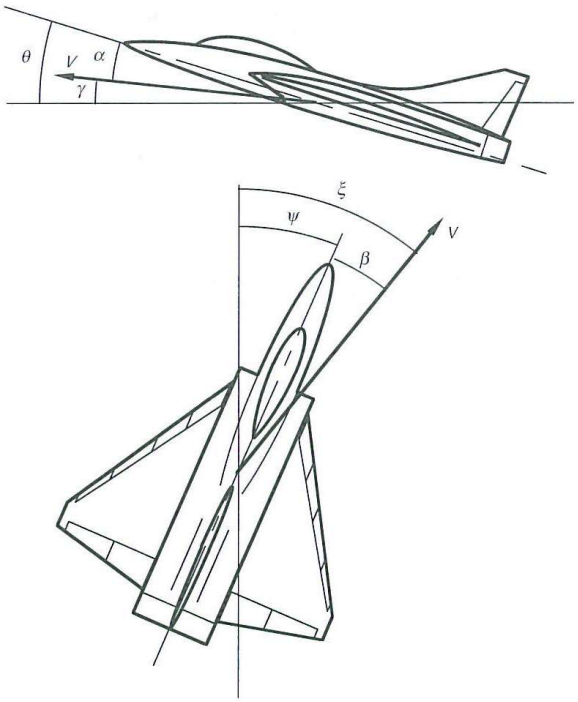

Fig. 2.2-9. Relationship among flight path, aerodynamic, and body-attitude angles with level wing tips.

Figure 3.2: Visualisation of the angle of attack α, flight path angle γ and heading ($\xi == \chi$), from Stengel [105]

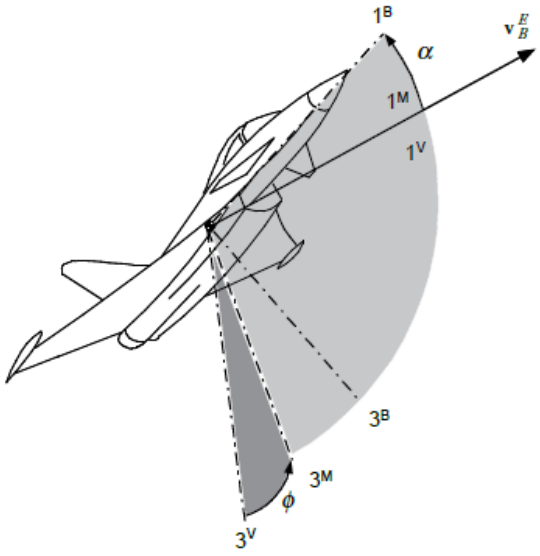

Fig. 8.7 Load factor plane of aircraft.

Figure 3.3: Visualisation of the angle of attack α and bank ($\phi == \mu$), from Zipfel [106]

The use of this set of equations introduces more freedom compared to a planar 2DoF, allowing for out-of-plane manoeuvres that can be exploited for complex cases (e.g. first stage re-entries on spaceports that do not lie on the target orbit plane) without the complications of a complete 6DoF simulation that would dramatically increase the requirements on the modelling of the problem. Nevertheless, the modular approach employed enables the use of different reference frames, as long as the inputs and outputs are provided in a consistent format. The implementation in MATLAB also allows for easy integration with Simulink, a toolbox that is often employed in the industry [107] for the simulation of complex aerospace systems, allowing the inclusion of GNC models or hardware in the loop simulators.

This reference frame is particularly useful when the flight modelling has direct consequences connected to geographical locations considered such as landing locations, launch-sites and any aspect related to safety, generally mapped on the location of residing populations overflown.

The state vector $\mathbf{x}^{\mathcal{F}}$ can be transformed into the ECI reference frame via the Earth Centered Earth Fixed (ECEF) frame using the conversions defined by the IAU Resolutions [108]. The ECI frame allows straightforward computation of the orbital parameters, which are often used as constraints on the final conditions for ascent trajectories.

3.2.2 Trajectory guidance and control law

Rocket powered vehicles are particularly unstable objects. The high fuel consumption continuously moves the center of gravity and they, not only traverse multiple flight regimes that drastically change aerodynamical properties such as the sound barrier, but they also change geometry due to staging and component jettison. A complete model of a vehicle should therefore include the guidance, navigation and control (GNC) systems that govern its flight. All orbital class launchers rely on robust autonomous systems to react to disturbances and manage the instabilities during flight [109].

The models of the GNC system are usually dependent on hardware and software that is available in the later stages of a launcher development program. The algorithms

are also heavily guarded trade secrets, with implication on international security, due to the possible military application.

This study does not include the modelling of a fully functional GNC, it instead uses a discretisation of the attitude profile that governs the flight. The vehicle is assumed to perfectly follow the open loop guidance with ideal navigation and control in all examples presented, with no deviation from the planned trajectory and no losses or delays associated to the activation of controls. While unrealistic, it is a first approximation that is commonly used in literature [33].

The vehicle's attitude is obtained by a guidance law, in turn this is provided as input for the subsystems generating the forces acting on the center of mass of the vehicle. In 3DoF there are 3 angles that determine the vehicle's orientation; the most important for launch ascent trajectories is the pitch angle, or the angle of attack lying in the plane of the trajectory, for the reference frame detailed in the previous section. The angle of sideslip or bank are used when out of plane manoeuvres are performed, such as a dog-leg in ascent or banked flight in return scenarios for either energy management or heading changes.

3.2.3 Vehicle Models

The attitude determined following the control law defines the orientation of the vehicle's body in space, consequently affecting the directions of the forces generated impacting the flight evolution and the loads affecting the vehicle. Those can be divided in two overlapping categories: the forces that directly affect the dynamics of flight, and the loads limitations set in the requirements of the payload and the launcher.

Propulsion

Arguably, the most important element for the ascent of a space access vehicle is the propulsive capability of its engine. All of the energy that is transferred to the payload from the ground to orbit comes from the propulsion systems.

The engines can also aid in the recovery of reusable stages. Notable flying examples include the return to base flight of the carrier aircraft after the release of the Pegasus

air launched rocket [110], and, more recently, the engine burns that the Falcon 9 and Falcon 9 Heavy main stages perform after separation until controlled propulsive landing on downrange barges or Return To Launch Site (RTLS).

The propellant mass flow rate, the thrust generated and its direction are the minimum set of elements necessary to simulate the flight, providing the instantaneous mass of the vehicle and thrust vector.

Aerothermodynamics

Conventional launchers are negatively affected during ascent by aerodynamic forces, introducing unwanted drag losses and structural stresses. For such reasons the bodies of orbital launchers are characterised by slender shapes. The same thing cannot be said of the ascent stage of the Apollo Lunar Module, with its distinct polygonal geometry, effectively providing the same functionality in an environment with no significant atmosphere.

Lifting body vehicles can offset part of the losses within the atmosphere by using aerodynamically efficient bodies. The lift generated counteracts the gravitational losses, the launcher climbs towards higher altitudes with lower pitch. While this approach is not an efficient ascent approach for conventional rocket propulsion, it opens up the possibility of using air-breathing engines for the early phases of flight, with one order of magnitude decrease in specific fuel consumption [111].

The simulation of the cases presented in this study takes into account the lift and drag forces for the simulation of flight dynamics, while additional performance parameters are tracked for the fulfilment of the constraints.

Other effects of the aerodynamic outside of the scope of this study include the flying qualities of the vehicle or movable surface deflections, which might be of interest in higher fidelity simulations.

Other aspects

Additional properties coming from the vehicle and environmental models must be computed and stored during the trajectory simulation to assist in the evaluation of the constraints.

Some of the most important factors during ascent, listed in contemporary LV payload user guides [110] [25], and included in the trajectories analysed in this work are:

- Acceleration load limits for the payload,
- Dynamic pressure and dynamic pressure multiplied by the angle of attack for the structural limitations of the launcher,
- Aerothermodynamic heat flux for the release of the fairing.

The same limitations are also applied to the return or re-entry missions, which could additionaly require the computation of

- Heat load for the Thermal Protection System.

The methodologies used to compute the aerothermodynamic parameters can vary in complexity from simple radiative-convective-conductive heat balances to higher fidelity TPS ablation models. As all the other vehicle models, the choice for most of the results presented in this study falls on engineering models that can rapidly be integrated and developed, leaving open the possibility of including more complex simulations in subsequent phases.

3.2.4 Environmental Models

The environment in which the vehicle moves affects the flight performance with directly contributing forces, and local effects that favour some launch sites over others. The contributions accounted for in the modelling included in this work are briefly summarised in this subsection.

The effect of the Earth's rotation can change the required energy to access LEO by about 5% when comparing high latitude or quasi-equatorial spaceports, with different results depending on the desired orbit inclination. The rotation of the planet at

an angular rate of $\omega_E = 7.292\,115 \times 10^{-5}\,\mathrm{rad\,s^{-1}}$, introduces a Eastward component of velocity reaching a maximum values of $v = 465.10\,\mathrm{m\,s^{-1}}$ at the Equator. The induced velocity is a free addition to the ΔV budget required for low inclination orbits, launching from the equator seems an obvious choice to increase the payload capacity of the launcher. The scenario is reversed when looking at retrograde or high inclination orbits, such as the often commercially used Sun-Synchronous Orbits. Launches into SSO need to cancel out the eastward velocity component and consequently benefit from spaceports located towards the poles.

The geometry of the planet introduces two other contributions, linked to the uneven distribution of matter: the local gravity field and ellipsoid. The World Geodetic System 84 (WGS 84) is currently used universally [112] and implemented in all the simulations presented in this work for the parameters defining the ellipsoid. The spherical harmonics up to order 4 are included in the implemented geopotential model, with the J2 coefficient being almost 4 orders of magnitude higher than the following ones. The radial and tangential components of the gravitational pull are computed from the local radius r_E, the vehicle's height above surface h and the latitude λ.

Above the surface, a major contribution to the flight of the vehicles is determined by the atmosphere, affecting the performances of the propulsion and the aerothermodynamics. The International Standard Atmosphere with no winds, similar to the US76 atmospheric model, is implemented in the cases presented due to their preliminary nature. Simulations for more advanced scenarios can employ higher fidelity models like the NRLMSISE-00 [113] for the atmospheric properties and the Horizontal Wind Model HWM14 [114] or NOAA's implementation to determine the statistical distribution of winds. These datasets use historical samples and correlation with factors such as date, geographical location and solar flux to predict the atmosphere characteristics. They are used for early safety or mission assurance analysis weeks or months before a launch, when the updated weather condition and forecast are not available [115].

3.3 The optimal control problem

The problem can be further extended beyond the design of the optimal trajectory by incorporating subsystem design variables in the optimisation. This approach is used in some of the scenarios presented in this thesis by scaling the size of the vehicle, the propellant load, the reference aerodynamic surface and the engine thrust. While these are some high level parameters, more suitable for the architectural definition of a novel launcher configuration, the methodology is applicable at later stages of design consolidation, when trade-off of engineering solution can be compared assessing their impact on the performance under scrutiny.

The choice of how to treat the optimal control problem must take into account all these elements, to identify the most suitable approach. The following sections detail the reasons behind the decisions among the possible methods presented in the introductory chapter.

3.3.1 Method

Direct methods have been the preferred choice for this work.

While indirect methods provide many advantages on a theoretical level, such as improved cost function values (estimated about 1% better by Von Stryk and Bulirsch [41]) and good convergence speed once a good initial guess is provided, they are more suitable for the repeated analysis of the same launch vehicle over missions with small changes, less so for the evaluation of new concepts or architectural trade-offs where the trajectory parameters are largely unknown. Indirect methods also pose a barrier of entry due to the steep learning curve necessary to work with them, and the customisability of a problem cannot be performed by an engineer without advanced trajectory optimisation training.

The decision to use direct techniques is due to their advantages in their modularity and flexibility, possibility of accessing different optimisation algorithms and handle discontinuities, often found in problems with multiple stages, morphing configurations or functional modes. The ease of use and possibility to recover from unknown or

erroneous initial guesses are additional benefits that ensure the generation of rapid results.

3.3.2 Transcription

The transcription method chosen is the multiple shooting.

Multiple shooting overcomes some shortcoming of the single shooting method, notably the sensitivity to the initial control variables for long duration flights, where small changes in the early phases of the trajectory affect disproportionally the end states [39].

The collocation methods have been excluded since the computational speed advantage is counterbalanced by the curve fitting approximation, that would not satisfy any regulator wanting to verify and validate the trajectory modelling and simulation.

3.3.3 NLP solvers

Direct methods can interchangeably interface with many suites of optimisation algorithms, as long as the features required by the problem are supported (e.g. constrained optimisation, single/multi objective). This provides flexibility and access to widely used and documented libraries such as SciPy, Pygmo, MATLAB's optimisation toolbox or any other equivalent option. The cases presented in this work have all been implemented in MATLAB, the software with the largest user-base within the author's research group at the beginning of the development of the methodology.

The preferred algorithm used in this study is MATLAB's `fmincon` with Sequential Quadratic Programming (SQP) [116], a gradient based method for exploitation supplemented by a multi-start strategy to improve the exploration capabilities.

3.4 Multidisciplinary Design Optimisation

Multidisciplinary Design Optimisation (MDO) is a technique used in the field of launcher design to perform system level optimisation, achieving a better results than studying each subsystem separately, through accounting for the interaction of the disciplines [117]. The process involves the iterative change of design parameters to identify the

configuration most suitable to perform the reference mission, and it is often used as a tool to size space transportation systems [118]. In the early phases of vehicle design, when the design is not finalised, it is possible to adjust variables that drive the performances of the complete launch system.

A basic MDO framework has been included to address the necessity of initial subsystems sizing, following the All At Once (AAO) method [117]. In this approach, the design parameters are fed to the subsystems at each iteration, performing the analysis of the updated vehicle configuration and trajectory at the same time.

The applications presented in the following chapters focus on 3 macro areas that most influence the flight of launchers, and in particular reusable lifting bodies. Those disciplines can be deducted from the vehicle contribution to the system of equations 3.1, and are: mass/structure, aerodynamics, and propulsion. Examples include respectively: the required propellant mass loading, the reference surface/length, and the engine sizing parameters.

The extra design variables are appended to the optimisation vector, and, during the execution, the variables are passed to the subsystem models that output the updated vehicle performance parameters.

3.5 Optimisation in TROPICO

TROPICO is a modular framework developed for mission analysis of future space access vehicles for the support of activities in project Phases from 0 onward.

The structure is based on 3 major components: the human interface, the optimisation framework and the simulation core. The first one is used to set up the user-inputs required for the case under analysis, translating the problem from a human readable structure to an optimisation problem, and presenting the solution after computation. The second one handles the interfacing between the optimisation algorithm and the simulation of the physical problem. This is done by translating the decision vector into simulation setup and post-processing of the simulation results to compute the values of the cost function and constraints. This information is used to iterate until optimisation

convergence. The simulation core is a user customisable environment that propagates the trajectory of a vehicle given a control law to follow from the initial states.

The task of optimising the ascent and descent trajectory is an optimal control problem. As stated in the previews sections, optimal control seeks the control laws for a given system that minimizes a cost functional subject to initial and final states as well as path constraints. This is an infinite dimensional optimization problem, for which usually it is not possible to find the exact analytic solution, hence the need of a numerical method for approximating its solution.

Direct methods are a robust methodology to solve optimal control problems. The main idea of the techniques is to discretise the control and state functions, and transform the infinite dimensional optimal control problem into a finite dimensional NLP problem.

A multiple shooting method instead divides the time in multiple shooting segments $[t_0, t_1, ..., t_M]$, as shown in Figure 2.5, where the trajectory is integrated numerically within the interval $[t_i, t_{i+1}]$ with initial conditions x_i, for all $i = 0, ..., M-1$. The state vector is given by,

$$\dot{x}(t) = f(x(t), u(t)), \quad x(t_i) = x_i \;\; t \in [t_i, t_{i+1}] \tag{3.2}$$

With each interval $[t_i, t_{i+1}]$, the control is further discretised in n_c control nodes: $\{u_0^i, ..., u_{n_c}^i\}$ for $i = 0, ..., M-1$ (see Figure 2.5). Boundary constraints on the control and states need to be imposed for $i = 1, ..., M-1$,

$$x_i = F([t_{i-1}, t_i], x_{i-1}), \quad u_{n_c}^{i-1} = u_0^i \tag{3.3}$$

where $F([t_{i-1}, t_i], x_{i-1})$ is the final state of the numerical integration on the interval $[t_{i-1}, t_i]$ with initial conditions x_{i-1}. This has the benefit of reducing integration errors often present over long integration times, and more importantly, can deal with discontinuities by aligning the transition between phases with any mathematical discontinuities within the models or the problem (e.g. separations, jettisons or changes in the aero-

dynamic regimes). The trade-off is the steep increase in the number of optimisation variables.

The decision vector of the optimization problem therefore has the following variables:

- The state vector at the start of each shooting phase $\mathbf{x}_i$, for $i = 0, ..., M-1$,
- The control nodes $\{\mathbf{u}_0^i, ..., \mathbf{u}_{n_c}^i\}$, for $i = 0, ..., M-1$,
- The time of flight for each shooting phase t_i, for $i = 1, ..., M$,

Additional variables are added to the vector in cases requiring multidisciplinary optimisation.

Path constraints on maximum temperatures, accelerations loads and dynamic pressure have also been included in the optimization problem formulation for the cases presented in this dissertation. Equality constraints are imposed on the final orbital elements in the case of ascent trajectories, while return ones can be characterised by final landing locations or conditions.

The method herein described is validated in the following section using scenarios from literature.

3.6 Validation

Betts's collection [119] of tests provides an extensive set of optimal control problems, complete with all the information required to reproduce the cases and cross-validate the methodology described in this chapter.

Among all available test cases, 4 bear higher similarity to the scenarios that this thesis investigates. The Space Shuttle re-entry problems, identified by the ID of *traj09*, *traj21*, *traj22* and *traj36* of increasing complexity, explore the controlled re-entry of a lifting body vehicle.

To implement these cases, we take advantage of the modular approach described in the previous sections of this chapter, setting up the test cases by specifying the required models, control limits and boundary conditions.

The equations of motion 3.4 are expressed in this case in a simplified form, neglecting the Coriolis force due to the rotation of the Earth.

$$\dot{h} = v \sin\gamma \tag{3.4a}$$

$$\dot{\theta} = \frac{v}{r} \cos\gamma \sin\chi / \cos\lambda \tag{3.4b}$$

$$\dot{\lambda} = \frac{v}{r} \cos\gamma \cos\chi \tag{3.4c}$$

$$\dot{v} = -\frac{D}{m} - g \sin\gamma \tag{3.4d}$$

$$\dot{\gamma} = \frac{L}{mv} \cos\beta + \cos\gamma \left(\frac{v}{r} - \frac{g}{v} \right) \tag{3.4e}$$

$$\dot{\chi} = \frac{1}{mv \cos\gamma} L \sin\beta + \frac{v}{r \cos\lambda} \cos\gamma \sin\chi \sin\lambda \tag{3.4f}$$

The aerodynamic forces lift L and drag D are expressed as polynomial curves dependent on angle of attack, while the thermal flux q is also a function of density ρ and velocity v. The parameters used provided by the original authors are listed in Table 3.1.

Table 3.1: Shuttle re-entry validation cases parameters.

$q = q_a q_r$	$m = \omega / g_0$
$D = \frac{1}{2} c_D S \rho v^2$	$a_0 = -0.20704$
$L = \frac{1}{2} c_L S \rho v^2$	$a_1 = 0.029244$
$g = \mu / r^2$	$\mu = 0.14076539\text{e}17$
$r = R_e + h$	$b_0 = 0.07854$
$\rho = \rho_0 exp[-h/h_r]$	$b_1 = -0.61592\text{e-}2$
$\rho_0 = 0.002378$	$b_2 = 0.621408\text{e-}3$
$h_r = 23800$	$q_r = 17700\sqrt{\rho}(0.0001v)^{3.07}$
$c_L = a_0 + a_1 \hat{\alpha}$	$q_a = c_0 + c_1 \hat{\alpha} + c_2 \hat{\alpha}^2 + c_3 \hat{\alpha}^3$
$c_D = b_0 + b_1 \hat{\alpha} + b_2 \hat{\alpha}^2$	$c_0 = 1.0672181$
$\hat{\alpha} = (180/\pi)\alpha$	$c_1 = -0.19213774\text{e-}1$
$R_e = 20902900$	$c_2 = 0.21286289\text{e-}3$
$S = 2690$	$c_3 = -0.10117249\text{e-}5$
$\omega = 203000$	$g_0 = 32.174$

All the validation cases are set up with 2 elements of 10 linearly spaced control nodes each, with a piecewise cubic interpolation. The final conditions and the matching between phases constitute the equality constraints of the problem.

3.6.1 Shuttle Maximum Downrange (traj09)

The first case is a planar trajectory from the atmospheric interface until a lower energy state, with initial and final conditions listed in Table 3.2. The same table lists the bounds set for the optimisation variables of the problem. Since the vehicle is initially placed at the crossing of the Equator and the Greenwich meridian and is flying on an equatorial orbit, the cost function 3.5 aims to maximise the final longitude, measured in radians.

$$max\theta(t_f) \tag{3.5}$$

The state variables with assigned final value listed in Table 3.2, are set with equality constraints 3.6.

$$x(t_f) = x_f \tag{3.6}$$

The inconsistencies in the units of measure are derived from the source material.

Table 3.2: *betts09* Test case setup

Variable			Initial value	Bounds	Final value
Altitude	h	ft	260000	[0, 260000]	80000
Velocity	v	ft/s	25600	[1, 25600]	2500
FPA	γ	deg	-1	[-89, 89]	-5
Latitude	λ	deg	0	[-pi/2, pi/2]	
Longitude	θ	deg	0	[-pi, pi]	
AoA	α	deg		[-90, 90]	
Duration	t	s	0	[0, 4000]	

The time history plots of the control variable AoA, and altitude for the solution found matching the final conditions are shown in Figure 3.4. The oscillation of the altitude profile in Figure 3.4b, similar to a phugoid effect, is a phenomenon that is often recurring in the results of this study and present in the results by Betts [39]. Chern et al. [120] explain the phenomena as an exchange between kinetic and potential energy, where a skip trajectory near vacuum significantly increases range.

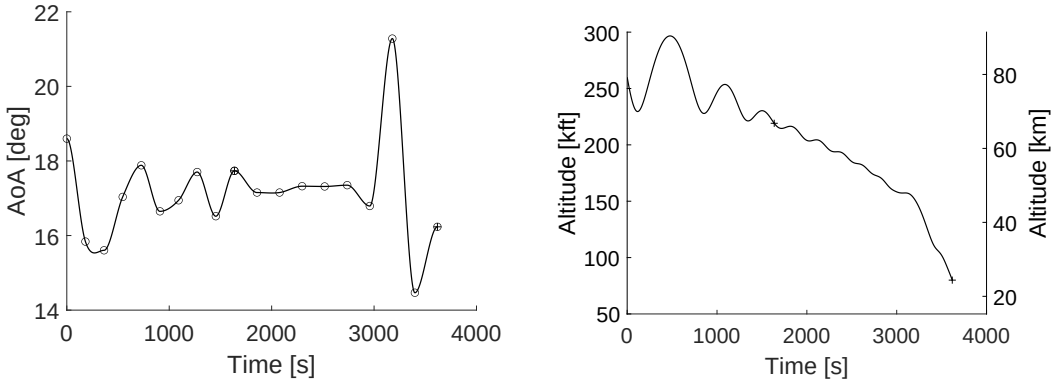

(a) Time history of the angle of attack (b) Time history of the altitude

Figure 3.4: Selected plots from validation case *traj09*

The cost function at convergence is $\theta_f = 3.268\,\text{rad}$ with a flight duration of $t_f = 3\,619\,\text{s}$.

3.6.2 Shuttle Maximum Crossrange (traj21)

The second case introduces a third dimension of manoeuvre with the addition of the angle of bank control, changing the objective of the optimisation for this case and the following ones to the maximisation of the final latitude (3.7), equivalent to the maximisation of the cross-range.

$$max\lambda(t_f) \tag{3.7}$$

The problem now includes a combination of angle of attack and bank to generate aerodynamic forces to extend the range and also deviate the trajectory towards higher latitudes. The updated problem setup is listed in Table 3.3. The bank is used to perform the change of heading, as it can be observed in Figure 3.5d.

The cost function at convergence is $\lambda_f = 0.595\,63\,\text{rad}$ with a flight duration of $t_f = 2\,013\,\text{s}$.

Table 3.3: *betts21* Test case setup

Variable			Initial value	Bounds	Final value
Altitude	h	ft	260000	[0, 260000]	80000
Velocity	v	ft/s	25600	[1, 25600]	2500
FPA	γ	deg	-1	[-89, 89]	-5
Heading angle	χ	deg	90	[-pi, pi]	
Latitude	λ	rad	0	[-pi/2, pi/2]	
Longitude	θ	rad	0	[-pi, pi]	
AoA	α	deg		[-90, 90]	
AoB	β	deg		[-90, 1]	
Duration	t	s	0	[0, 2500]	

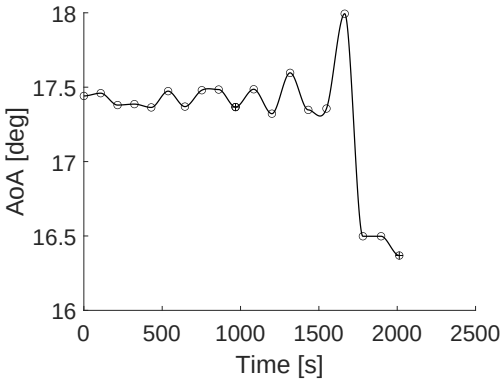

(a) Time history of the angle of attack

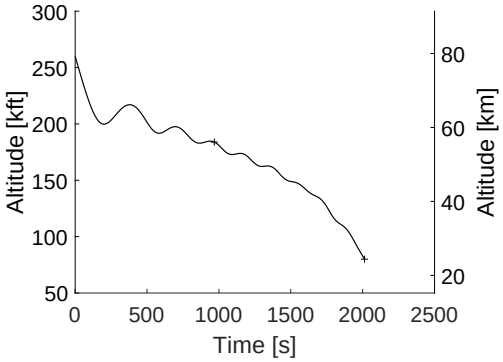

(b) Time history of the altitude

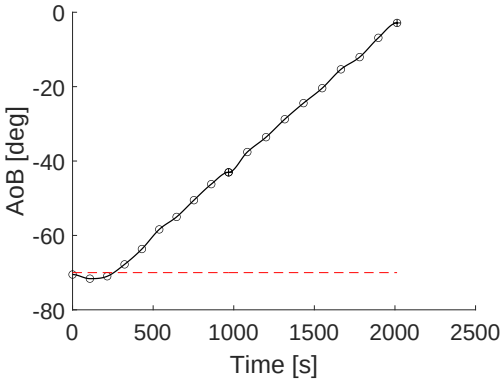

(c) Time history of the angle of bank. The dashed red line indicates the limit applied to cases *traj22* and *traj36*

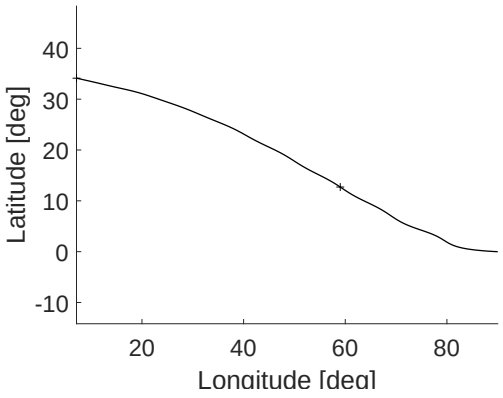

(d) Ground track of the vehicle

Figure 3.5: Selected plots from validation case *traj21*

3.6.3 Shuttle Maximum Crossrange with Control Bound (traj22)

The third case limits the maximum bank angle to a rotation of 70° with the addition of the inequality constraint (3.8), but the problem setup of the previous section 3.6.2 is not modified.

$$\beta \leq 70° \tag{3.8}$$

Given the fact that the optimal result for the second scenario was exceeding this threshold in Figure 3.5c, the value of the cost function is expected to be lower, due to the limitation on the bank angle imposed. The optimisation results correctly satisfy the bound on the angle of bank control variable, as it can be observed in Figure 3.6c.

The cost function at convergence is $\lambda_f = 0.595\,56\,\text{rad}$ with a flight duration of $t_f = 2\,035\,\text{s}$.

3.6.4 Shuttle Maximum Crossrange with Heat Limit (traj36)

The last case introduces a heat rate limit to 70 BTU/ft/s^2 with an inequality constraint (3.9), without changing the problem setup of Table 3.3.

$$q \leq 70 BTU/ft/s^2 \tag{3.9}$$

The previous case *traj22* exceeded this new thermal threshold by a factor of 2.

Figure 3.7e illustrate the results with a correct implementation of the path constraints applied to the aerodynamic heating. This major change in the problem setup results in a time history of the altitude that does not exhibit oscillations, as it can be seen in Figure 3.7b.

The cost function at convergence is $\lambda_f = 0.531\,81\,\text{rad}$ with a flight duration of $t_f = 2\,222\,\text{s}$.

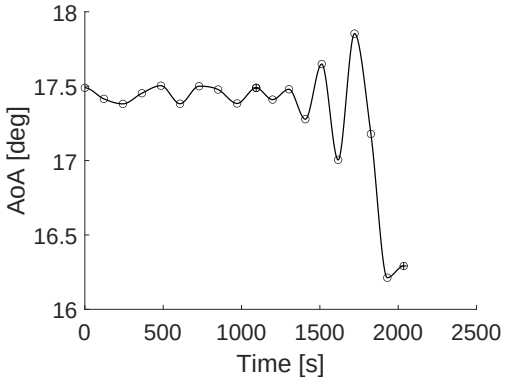

(a) Time history of the angle of attack

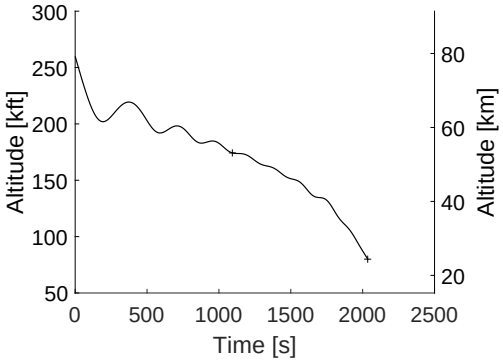

(b) Time history of the altitude

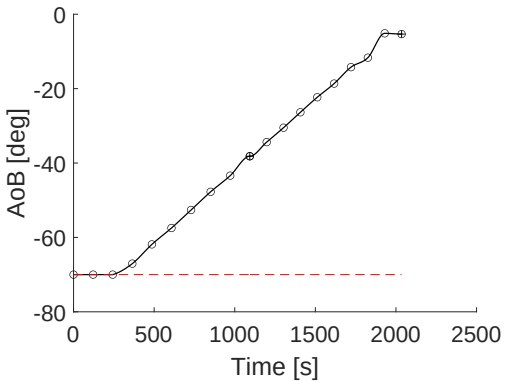

(c) Time history of the angle of bank. The dashed red line indicates the limit applied to cases *traj22* and *traj36*

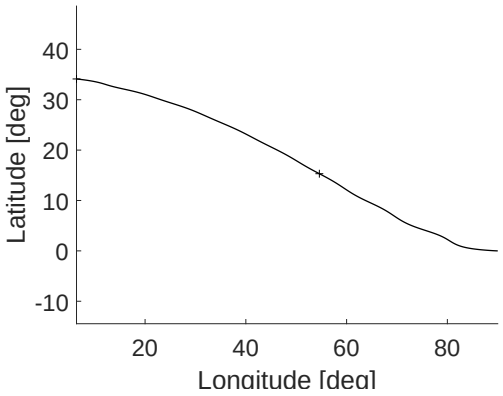

(d) Ground track of the vehicle

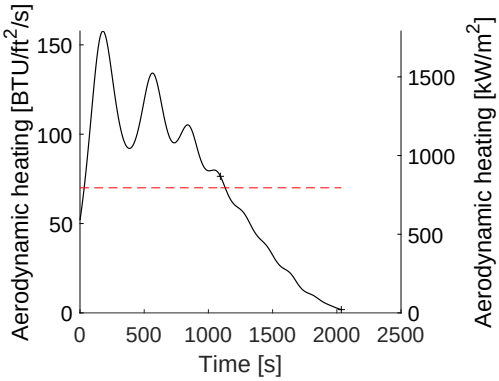

(e) Time history of the heat flux.The dashed red line indicates the limit applied to case *traj36*

Figure 3.6: Selected plots from validation case *traj22*

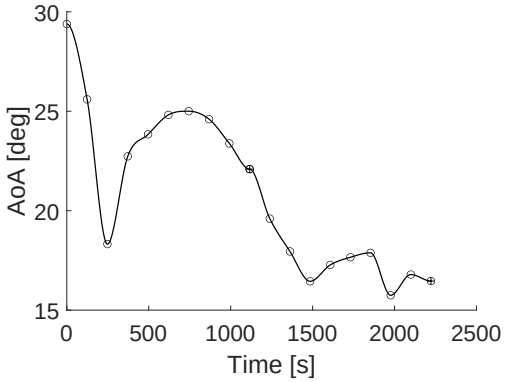

(a) Time history of the angle of attack

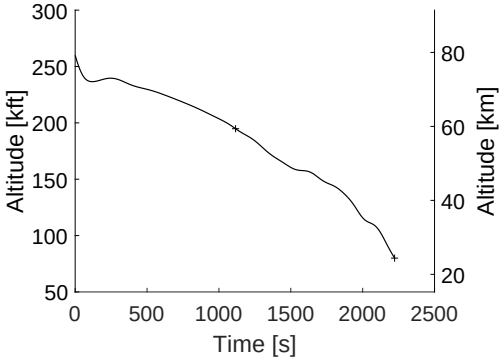

(b) Time history of the altitude

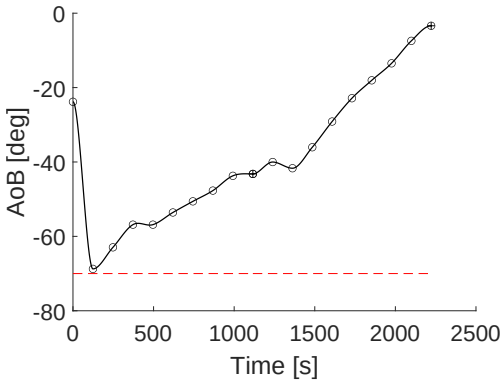

(c) Time history of the angle of bank. The dashed red line indicates the limit applied to cases *traj22* and *traj36*

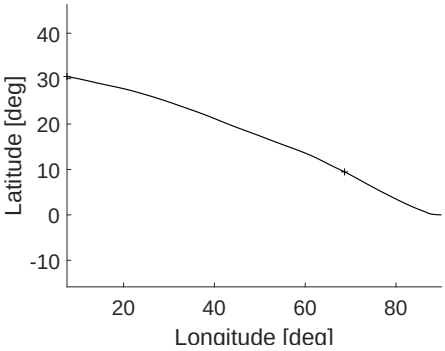

(d) Ground track of the vehicle

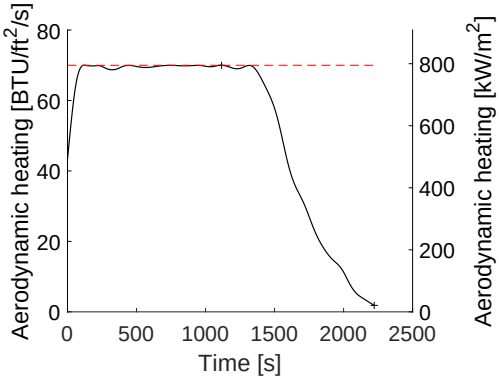

(e) Time history of the heat flux. The dashed red line indicates the limit applied to case *traj36*

Figure 3.7: Selected plots from validation case *traj36*

3.6.5 Validation summary

The application to the cases provided by Betts provide confidence in the approach of the methodology and confirm the correct implementation of the necessary bounds and constraints.

Table 3.4: Comparison with Bett's reference results.

Test cost	**Bett's cost**	**Cost ratio**
3.26802	3.2726493	0.99858
0.59563	0.59587608	0.99958
0.59556	0.59574673	0.99969
0.53181	0.53451536	0.99493

The results of the 4 test cases are reported in Table 3.4, where it can be observed that the results obtained fall within the 1% threshold expected from literature [41] comparison of indirect and direct methods.

3.7 Application cases

The following chapters present a selection of case studies encountered in academic and industrial applications, as well as new ones, demonstrating the capabilities of the methodology over a wide range of scenarios of interest.

The cases presented are:

- Ascent and separate descent of a Single Stage To Orbit (SSTO) vehicle (Chapter 4)
- Multi disciplinary sizing of a Two Stages To Orbit (TSTO) vehicle (Chapter 5)
- Performance study of a TSTO orbital insertion at different altitudes and inclinations (Chapter 5)
- Abort scenarios during the ascent of a TSTO vehicle (Chapter 6)

The different scenarios will demonstrate the flexibility of the methodology to address questions from the preliminary to the operational phases of a reusable launch system program.

Chapter 4

Ascent and descent of a Single Stage To Orbit vehicle

The first application case presented is a more complex scenario compared to the validation ones, including the analysis of both the ascent and descent performances of a spaceplane. The two analyses are performed separately.

A test mission is analysed with take-off and landing at the ESA Kourou Centre Spatial Guyanais (CSG) launch site near the equator. The vehicle will deliver a payload to a 300 km altitude circular equatorial orbit, with semi-major axis $a = R_E + 300\,\text{km}$, eccentricity $e = 0$, inclination $i = 0°$. The operational orbit segment is neglected here, with the optimisation looking at only the ascent and descent trajectories.

This test case and methodology have been previously presented at the 66th International Astronautical Congress, 2015 [88].

4.1 Vehicle design

The vehicle design of CFASTT-1 (Figure 4.1) is a conceptual construct of a lifting body SSTO spaceplane, based on the Reaction Engines Skylon [121] vehicle, with a hybrid air-breathing and rocket propulsion system, a blended wing (mainly through the additional of lateral strakes) and a V-tail configuration [89]. The total vehicle length

is 83 m, with a reference area S_{ref} of 300 m^2, a wing span of 20 m and a maximum wet mass at take-off of 250 t.

The vehicle is modelled through a set of engineering models that describe the behaviour of the subsystems via surrogate or low fidelity models that characterize the performance of the vehicle without excessively impacting on the computation time.

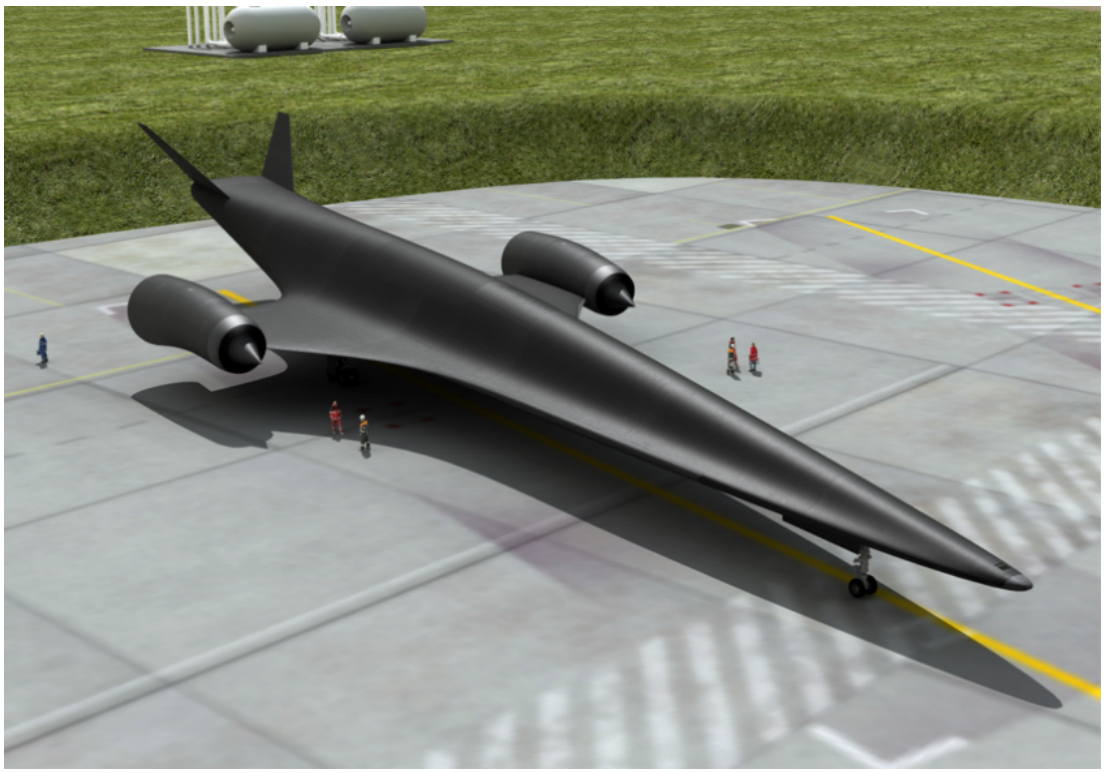

Figure 4.1: The CFASTT-1 Reusable Launch Vehicle during ground-hold operations. (Original graphic by Adrian Mann.) [122]

4.1.1 Mathematical models

The following section presents the mathematical models used to simulate the vehicle performance, specifically the vehicle structure and mass, aerothermodynamics, and propulsion system, and the trajectory dynamics and control, gravitational and atmospheric models.

Aerothermodynamics

The aerodynamics of the vehicle are modelled to predict the total coefficient of lift c_L and drag c_D as a function of the angle of attack α and Mach number M for a set of atmospheric conditions. For the test case presented here, the aerodynamics and propulsion models were both designed as surrogate models, with curve fitting based on higher fidelity simulations using CFD for the continuum regime in the lower atmosphere and Direct Simulation Monte Carlo (DSMC) based methods for the upper atmosphere with a rarefied flow regime [123]. The surrogate models were necessary to lower the computation run time compared to the higher fidelity simulations which are generally infeasible to incorporate into a complex design optimisation.

In the subsonic and supersonic regimes, the coefficient of lift is modelled based on linearised aerodynamic theory [124],

$$C_{L,ss} = C_{L_\alpha} \sin\alpha \cos\alpha \tag{4.1}$$

where $C_{L_\alpha}(M)$ is a piecewise fitted polynomial based on Mach number. The coefficient of lift within the hypersonic regime is modelled based on modified Newtonian theory,

$$C_{L,hs} = 2\sin^2\alpha \frac{S_{hs}}{S_{ref}} \cos\alpha \tag{4.2}$$

The total value for C_L over the different regimes is calculated based on a weighted function that smooths the transition between the two:

$$C_L = \frac{C_{L,ss} + C_{L,hs}}{2} + \sqrt{\left(\frac{C_{L,ss}}{2}\right)^2 + \left(\frac{C_{L,hs}}{2}\right)^2} \tag{4.3}$$

The drag coefficient is computed as the sum of a C_{D_0} term and the induced drag of lifting surfaces. The zero-lift drag term accounts for wave, base and viscous drag and is function of the Mach number. Similarly to the C_{L_α} term, C_{D_0} was approximated by a 10^{th} order polynomial derived through curve fitting to higher fidelity simulations.

$$C_D = C_{D_0}(M) + C_L \tan \alpha \tag{4.4}$$

The lift and drag forces used within the dynamic model are given by,

$$L = \frac{C_L \rho v^2 S_{ref}}{2} \qquad D = \frac{C_D \rho v^2 S_{ref}}{2} \tag{4.5}$$

where ρ is the atmospheric density, v is the relative velocity and S_{ref} is the reference area.

The thermodynamic model, used primarily in the upper phase of the re-entry, evaluates the heat flux and wall temperatures along key areas, namely the nose cone, wing leading edge and nacelle. The convective heat flux $\dot{q}_{conv}$ was modelled using the Fay-Riddell equation corrected for the hot wall temperature T_W. [125]

$$\dot{q}_{conv,nose} = K\sqrt{\frac{\rho}{r_C}}v^3 \left(1 - \frac{H_W(T_W)}{H_{ST}}\right) \tag{4.6}$$

where r_C is the local radius of curvature of the geometry, ρ is the atmospheric density, K is an empirical constant, H_W is the enthalpy on the wall as a function of the wall temperature T_W, and H_{ST} is the static enthalpy of the incoming flow.

The radiative head flux is derived using the Stefan-Boltzmann law:

$$\dot{q}_{rad} = \epsilon_T \sigma (T_W^4 - T^4) \tag{4.7}$$

where σ is the Stefan-Boltzmann constant, T is the atmospheric temperature, and ϵ_T is the emissivity of the body.

The wing leading edge and the nacelle are considered as cylindrically inclined shapes and require a correcting function $f(\theta_{sw})$ based on the sweep angle of the surface encountering the flow.

$$\dot{q}_{conv,le,n} = K\sqrt{\frac{\rho}{r_C}}v^3 \left(1 - \frac{H_W}{H_{ST}}\right) f(\theta_{sw}) \tag{4.8}$$

where θ_{sw} is the inclination angle of the geometry with respect to the incoming flow and is equal to the leading sweep angle for the wing and the angle of attack for

the nacelle. The constant K is empirically determined through CFD analyses on the vehicle.

Setting (4.7) equal to (4.6) for the nose cone and equal to (4.8) for the wing and nacelle, the resulting equations are solved numerically with Newton's method, minimising the relative error of the two heat fluxes, to obtain the wall temperature T_W at that point on the surface. The temperature initial guess is set to 500 K for the first time-step, and the solution is carried over for all the following time-steps.

Propulsion

This preliminary design study has been conducted assuming a hybrid air-breathing/ rocket propulsion system similar to SABRE [126] under development by Reaction Engines Ltd. The air-breathing propulsion system is modelled on a turbojet-ramjet configuration which has been evaluated at set points and then curve fitted as a function of angle of attack α, Mach number M, and atmospheric conditions to extrapolate a faster surrogate model for preliminary design purposes. This model gives a maximum I_{sp} of about 3 000 s.

The upper phase of the ascent trajectory is powered by two LOX/LH2 rocket engines each with an I_{sp} of 450 s, the performance metric publicly available for SABRE. For the purpose of this study, the mixture ratio is assumed constant and the two propellants are treated as a single mass flow $\dot{m}_p$.

The throttle control τ dictates the fraction of maximum thrust applied, as well as the fraction of total propellant mass flow. The maximum thrust is set at $T_{max} = 800$ kN. The mass flow is then calculated using the rocket equation [127], with g_0 being Earth's standard gravity.

$$F_T = \tau T_{max} \tag{4.9}$$

$$\dot{m}_p = \frac{F_T + p\, A_e}{g_0 I_{sp}} \tag{4.10}$$

A penalty proportional to atmospheric pressure p and nozzle exit area A_e is introduced to account for the effect of incorrect nozzle expansion when not in a vacuum.

4.1.2 Operating environment

The Earth is modelled as a perfect sphere with a radius $R_E = 6\,375\,253\,\mathrm{m}$ and angular velocity $\omega_E = 7.292\,115 \times 10^{-5}\,\mathrm{rad\,s^{-1}}$. The Earth's gravitational acceleration is a function of altitude h above the surface,

$$g = \mu_E r^{-2} = \mu_E (h + R_E)^{-2} \tag{4.11}$$

where $\mu_E = 398\,600.441\,8\,\mathrm{km^3\,s^{-2}}$.

The International Standard Atmosphere [128] (ISA) was used to model the atmospheric characteristics: Given the altitude h, the model computes the values of atmospheric pressure p and temperature T, which are then used to determine the air density ρ.

4.1.3 Trajectory dynamics

The dynamics for the transatmospheric flight, described in the previous chapter, are the same for ascent and descent. The spaceplane is considered as a point with a time-varying mass centred on the Centre-of-Mass of the vehicle. The set of equations of motion are calculated within a geocentric rotating reference frame using spherical coordinates.

A standard two-body system is used for the orbital dynamics, based on a closed orbit around a central body with a gravitational field. An elliptical transfer trajectory is found by numerically solving Lambert's problem. The solution is the Keplerian orbit connecting the starting and ending position vectors, in Earth Centred Inertial (ECI) coordinates, and a total time-of-flight. Battin's formulation [129] iteratively computes the solution with the Newthon-Raphson method. The initial guess for the first iteration is determined by the eccentricity anomaly of the target point, following Shen's approach [130].

The state vector $\mathbf{x}^{\mathcal{F}}$ was transformed into the ECI reference frame via the Earth Centered Earth Fixed (ECEF) frame using the conversions defined by the IAU Resolutions [108].

4.2 Optimisation

4.2.1 Optimal control problem

For the given problem, path constraints on axial and normal accelerations have been included in the optimization problem formulation. Additional equality constraints are set on the final orbit, in the case of the ascent 4.12, while maximum temperatures and final landing coordinates are limited in the case of descent 4.13.

$$a(t_{f,a}) = r_E + 300\,\mathrm{km} \tag{4.12a}$$

$$e(t_{f,a}) = 0 \tag{4.12b}$$

$$acc_x \leq 3g_0 \tag{4.12c}$$

$$acc_z \leq 2g_0 \tag{4.12d}$$

$$T_{\mathrm{nosecap}} \leq 2\,000\,\mathrm{K} \tag{4.13a}$$

$$T_{\mathrm{wing}} \leq 2\,000\,\mathrm{K} \tag{4.13b}$$

$$T_{\mathrm{nacelle}} \leq 1\,050\,\mathrm{K} \tag{4.13c}$$

$$acc_z \leq 1.5g_0 \tag{4.13d}$$

$$\lambda(t_{f,d}) = 5.237\,2^\circ \tag{4.13e}$$

$$\theta(t_{f,d}) = -52.760\,6^\circ \tag{4.13f}$$

4.2.2 First guess

Different strategies to provide a good first guess to the optimiser were used. This further showcases the modularity of the approach presented.

For the descent, a single integration of the trajectory from a given initial state is used (i.e., single shooting). The trajectory is integrated from given initial conditions and constant controls till the reaching of the final orbit or the landing site altitude. The

final trajectory is subdivided into the n segments of the multiple shooting transcription method used. The state variables $\mathbf{x}_i$ in the multiple shooting nodes are initialized with the corresponding state value of the reference trajectory and the control are kept constant, $\mathbf{u}_j^i = U$ for all $i = 0, ..., n-1$ and for all $j = 0, ..., n_c$. The multiple shooting time length t_i is initialized to zero.

The quick run of the stochastic global search is the first guess strategy used in the case of the ascent. This is largely due to the shorter time of flight required for the ascent trajectory, requiring less multiple shooting segments. The resulting optimization problem has a smaller number of equality constraints so it can be more easily solved with a global stochastic strategy that includes the constraints in the objective function as penalty parameters. The MATLAB genetic algorithm `ga` was used in the test case here. The solution obtained is then used to warm start the constrained optimisation problem.

4.2.3 Optimization algorithm

The NLP problem is solved using the Sequential Quadratic Programming (SQP) algorithm with `fmincon` in MATLAB subject to a number of equality and inequality constraints. The SQP algorithms employs Newton-like methods to directly solve the necessary conditions for optimality (KKT conditions) of the original NLP problem. The problem to be solved is transformed into the minimization of a quadratic approximation of the Lagrangian function subject to a linear approximation of the constraints. A sequence of quadratic problems need to be solved in order to converge to the local optimum.

4.2.4 Ascent

The control vector for ascent trajectory problem is $\mathbf{c}_1 = [t, \alpha, \mu, \tau]$ where t is the time coordinates of each control node within a phase. As the control law is discrete and characterized by a vector of 8 equally spaced points for each shooting phase, the evaluation of each of the parameters – the angle of attack α, bank angle μ and throttle τ – is linearly interpolated. The search space D is constrained by the domain of the

aero-propulsive models within the bounds listed in Table 4.1. The initial states are limited within the expected region of flight for the outlined mission. The total flight duration for each shooting phase between 30 s and 190 s, with the initial guess set in between those bounds to 110 s. There are 5 shooting phases, with the entire trajectory constrained between 150 s and 850 s.

Table 4.1: Bounds for the ascent problem

Variable		Bounds
Altitude	km	$[0.1, 1000]$
Velocity	$\mathrm{km\,s^{-1}}$	$[0.1, 10]$
Flight Path Angle	deg	$[-90, 90]$
Heading	deg	$[-180, 180]$
Latitude	deg	$[-90, 90]$
Longitude	deg	$[-180, 180]$
Angle of Attack	deg	$[-10, 30]$
Bank	deg	$[-30, 30]$
Throttle		$[0, 1]$
Time of Flight	s	$[150, 850]$

The objective of the optimisation is to maximise the payload mass that can be injected into the target 300 km circular orbit. If the structural dry mass of the vehicle at take-off is fixed, along with a known maximum wet mass including payload, then the two free variables are the total mass of on-board propellant, and the payload mass. The objective function is therefore,

$$\min_{\mathbf{c}_1 \in D} m(t = t_f) = \min_{\mathbf{c}_1 \in D} \int_0^{t_f} \dot{m}\, dt \tag{4.14}$$

where $\dot{m} = -\dot{m}_p$, and the total time of flight is t_f.

The initial state vector parameters for the ascent are:

$$h(t_{0,d}) = 10\,\mathrm{km}$$

$$v(t_{0,d}) = 0.4\,\mathrm{km/s}$$

$$\gamma(t_{0,d}) = \chi(t_0) = 0^\circ$$

with the latitude and longitude of Kourou CSG located at latitude $\lambda = 5.237\,2°$ N and longitude $\theta = 52.760\,6°$ W.

Additional constraints are imposed on the problem by the maximum acceleration along the longitudinal axis $a_x \leq 29.42\,\mathrm{m/s^2}$ and normal axis $a_z \leq 19.61\,\mathrm{m/s^2}$, equivalent respectively to 3 and 2 times the value of g_0.

4.2.5 Descent

The descent trajectory is divided into 3 segments: a powered de-orbit, an unpowered re-entry through the upper atmosphere, and an unpowered glide phase in the lower atmosphere.

The de-orbit phase is defined for the purpose of this problem as the trajectory above an altitude of 120 km, where aerodynamic effects have a negligible effect on the considered transfer arc [131]. While the ascent case uses the rocket engines to reach the desired orbit, for the descent, an elliptical transfer trajectory was used instead. The trajectory assumed two impulsive ΔV, one to change from the orbit to the transfer trajectory, and a second to re-align the velocity vector at the start of the re-entry. The maximum allowed ΔV was constrained to the maximum value of 500 m/s.

The control variables for the de-orbit are $\mathbf{c}_2 = [\theta_0,\, tof,\, \mathbf{x}(t_{0,d})]$, where θ_0 is the departure true anomaly of the orbit, and tof is the total time of flight of the transfer. The values of the state vector $\mathbf{x}_{re}$, specifically the velocity, flight path angle, heading angle, longitude and latitude at the transition point between the de-orbit and re-entry is also added to the control vector, with the exception of the altitude which is fixed at 120 km. The control vector is bounded within the limits of Table 4.2, where t_{orbit} is the period of the operation orbit. The initial guess was set at $\theta = \pi/10$ rad and $tof = 0.5\,t_{orbit}$.

This re-entry and glide segments requires a different search space limitation for the attitude of the vehicle, and the total flight time is set as the from the initial guess, later optimised to match the constraints on the target landing site. The descent control law is interpolated using a piecewise cubic Hermite interpolation scheme, which offers constrained polynomial interpolation, preventing the overshoot of bounds, characteristic of

Table 4.2: Bounds for the descent problem

Variable		Bounds
Altitude	km	$[0.1, 150]$
Velocity	$\mathrm{km\,s^{-1}}$	$[0.1, 10]$
Flight Path Angle	deg	$[-90, 90]$
Heading	deg	$[-180, 180]$
Latitude	deg	$[-90, 90]$
Longitude	deg	$[-180, 180]$
Angle of Attack	deg	$[-5, 90]$
Bank	deg	$[-90, 90]$
θ	deg	$[0, 360]$
tof	s	$[0, 2\,t_{orbit}]$

classic polynomial methods, and further illustrates the modularity of the methodology. The state vector limits are the same listed in Table 4.2.

The first guess for the initial state of the re-entry/glide is given as:

$$v(t_{0,d}) = 7.875\,4\,\mathrm{km/s}$$

$$\gamma(t_{0,d}) = -1.18^{\circ}$$

$$\chi(t_{0,d}) = 90^{\circ}$$

$$\lambda(t_{0,d}) = 0^{\circ}$$

$$\theta((t_{0,d})) = 0^{\circ}$$

where $t_{0,d}$ is the initial time of the descent segment.

This case requires additional constraints due to the harsh thermal environment typical of re-entry. The heat flux and heat load are evaluated using the thermal model with temperatures evaluated at three different critical points: the nosecone, the wing leading edge and the engine nacelle.

The following constraints on the temperature are considered along the whole trajectory:

$$T_{\text{nosecap}} < 2\,000\,\text{K}$$
$$T_{\text{wing}} < 2\,000\,\text{K}$$
$$T_{\text{nacelle}} < 1\,050\,\text{K}$$

Two set of trajectories have been analysed to evaluate the effect of the thermal limits. A reduced constraint on the maximum normal acceleration is imposed such that $a_z \leq 1.5 g_0$.

The objective function for the descent trajectory is the minimisation of the integral of the heat flux over the nacelle:

$$\min_{\mathbf{c}_2} \int_{t_{0,d}}^{t_f} \dot{q}(t, \mathbf{c}_2)\, dt \tag{4.15}$$

where $\mathbf{c}_2$ is the set of optimization variables described above and t_f is the optimisable time of flight.

4.2.6 Simulation results

The ascent trajectory is optimized to achieve circular orbit while satisfying all the constraints. The achieved result is on a slightly inclined plane ($i \leq 6°$) due to the space-port latitude. The ascent trajectory plots are shown in Figures 4.2 and 4.3, illustrating the evolution of the solution from the first guess that is given to the genetic algorithm and further refined with the gradient method to the end result of the optimized trajectory. The trajectory point of switch from air-breathing propulsion to rocket is highlighted with a dashed vertical line.

The control nodes are marked with circles in the AoA and throttle plots (Figure 4.2), with the crosses marking the interfaces between phases. The angle of attack profile, in plot 4.2a, follows a profile similar to the throttle of plot 4.2b, trying to maximise the lift gain in the denser part of the atmosphere.

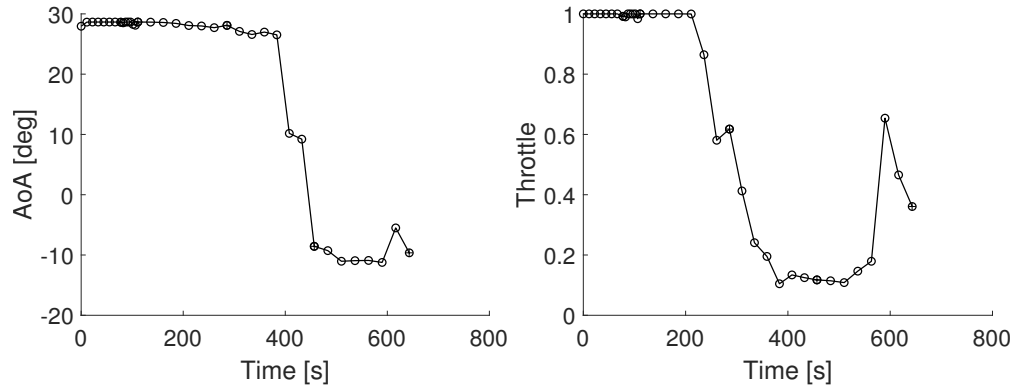

(a) Angle of attack time history (b) Throttle time history

Figure 4.2: Time history of the controls for the ascent trajectory. Engine model switch at the dashed line.

It is possible to notice how the increase in altitude (Figure 4.3a) before the engine switch corresponds to a decrease in thrust, visible in plot 4.3f, even though the throttle (Figure 4.2b) remains maxed. This matches the expectation of reduced performances of an air-breathing engine when above its operative altitude. The rocket operational mode is then used to propel the vehicle above the denser part of the atmosphere, then throttled down from $t = 300\,\mathrm{s}$ to $t = 600\,\mathrm{s}$, where the speed (Figure 4.3b) of the spaceplane increases at a lower rate, and finally fired back up for the orbit insertion manoeuvre, commonly used by orbital launch vehicles, and visible in the final peak of Figure 4.2b. The same Figure shows the effect of the acceleration limits in the constraints of the problem: when the vehicle gets lighter, the thrust of the rocket engine is excessive and it is gradually throttled down to a safe level. It is also important to highlight that the optimization algorithm develops a strategy of coasting with low thrust till the apogee to minimise the required ΔV to circularize the orbit, without prior knowledge of traditional throttling strategies. As the linear proportionality between throttle and thrust cannot be guaranteed in real-world scenarios, the applications of the chapters that follow will include a penalty factor to avoid low-throttled arcs.

The descent trajectories are shown in Figures 4.4 and 4.5, with the dashed line for the case without thermal constraints, ant the solid one for the constrained case. In the thermally unconstrained case, the nacelle and the nose reach critical temperature

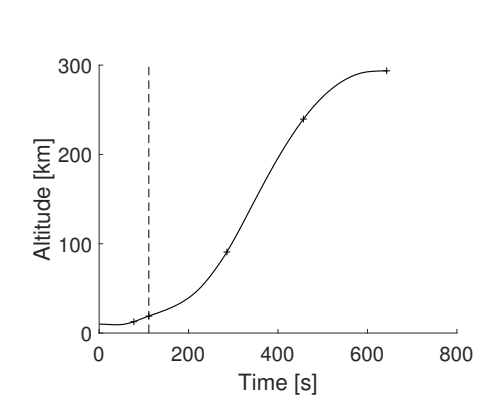

(a) Altitude time history

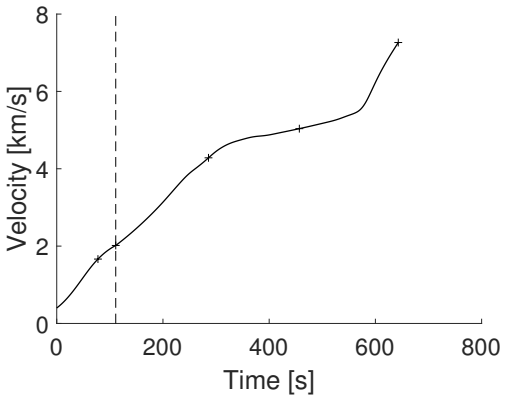

(b) Velocity time history

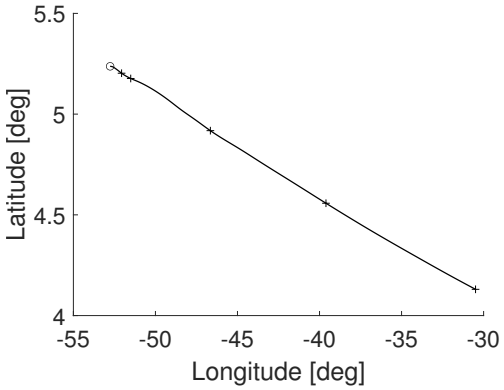

(c) Ground Track, starting from the circle marker

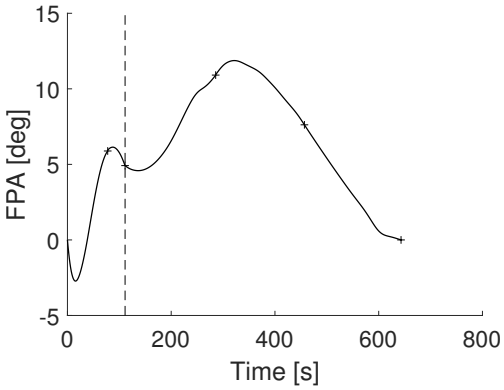

(d) Flight path angle time history

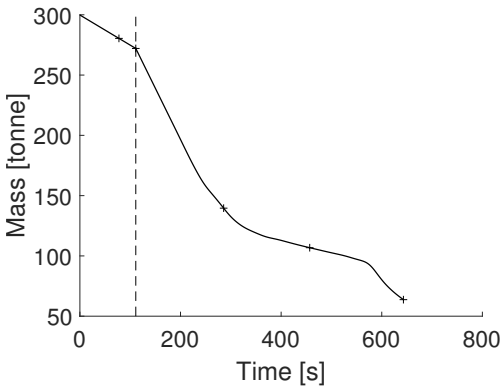

(e) Mass time history

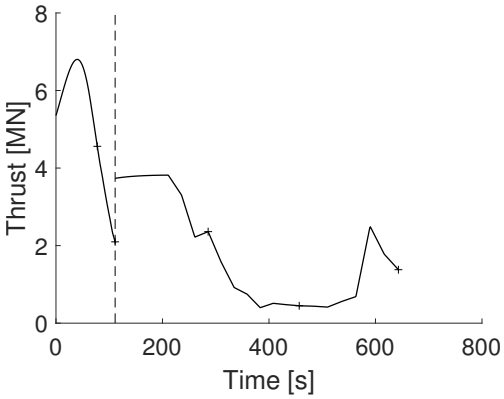

(f) Thrust time history

Figure 4.3: Time history of the states for the ascent trajectory. Engine model switch at the dashed line.

levels as can be seen in Figure 4.5b, but the introduction of the constraints stops this behaviour and modifies the descent path, slowing down the descent of the vehicle by increasing the angle of attack and therefore reducing the ballistic coefficient. This stops the occurrence of the atmospheric skipping the first 200 s (see Figure 4.4a and 4.4b) and that was causing a very steep and fast descent that was the origin of excessive heating in the unconstrained case. Both re-entry trajectories start from the same downrange distance, but the velocity profile (Figure 4.4b) of the constrained case requires additional range for the more gradual deceleration, thus inducing a turn in the final leg of the flight, as visible in Figure 4.4c, with a turn commanded by the bank profile of Figure 4.4f.

The last part of the descent is the gliding section and the obtained results are less realistic due to the fact that the aim of this analysis was to minimize the heating during re-entry, while more realistic objectives for the final flight phase are to maximise the lift to drag ratio, or correctly align the vehicle with the landing runway.

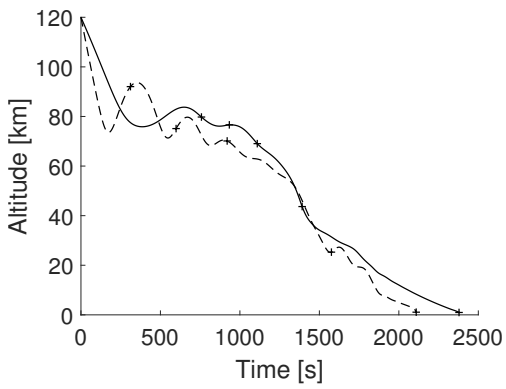

(a) Altitude time history

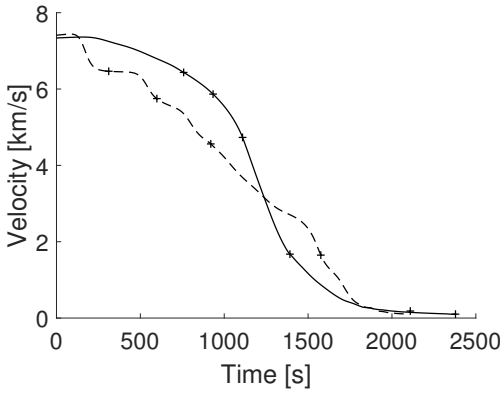

(b) Velocity time history

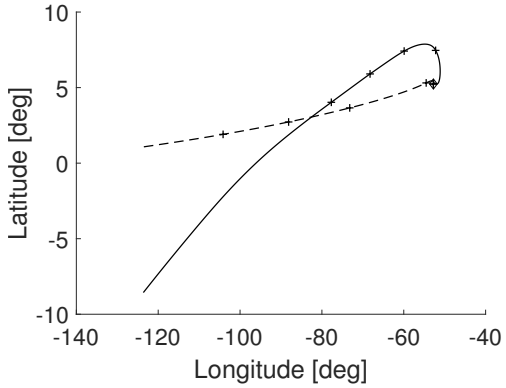

(c) Ground Track, diamond marks the target coordinates

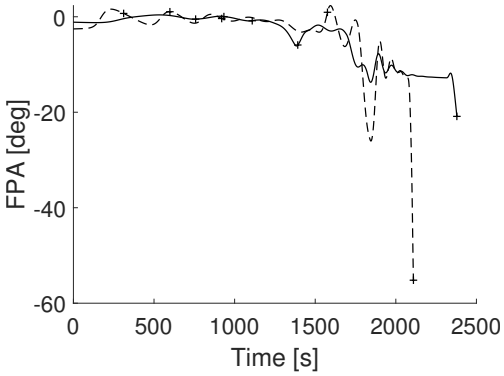

(d) Flight path angle time history

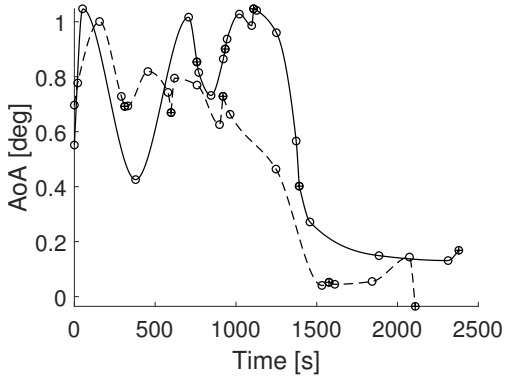

(e) Angle of attack time history

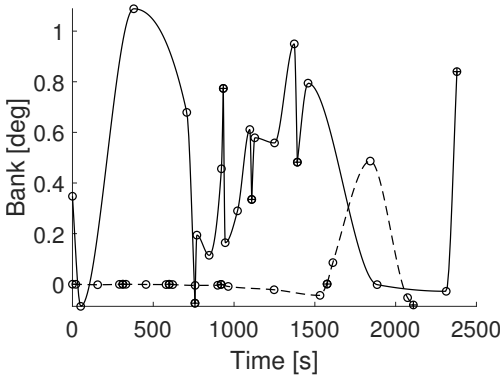

(f) Bank angle time history

Figure 4.4: Time history of the states and controls for the descent trajectories with thermal constraints (solid line), and without (dashed line).

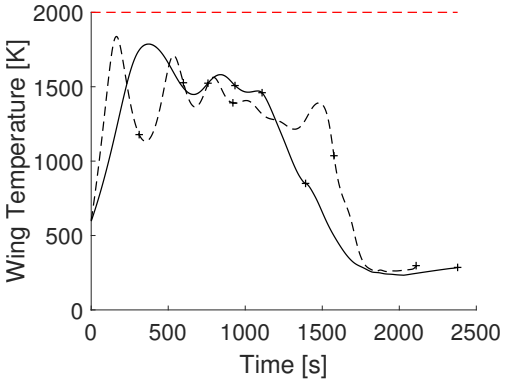

(a) Temperature of the wing leading edge time history

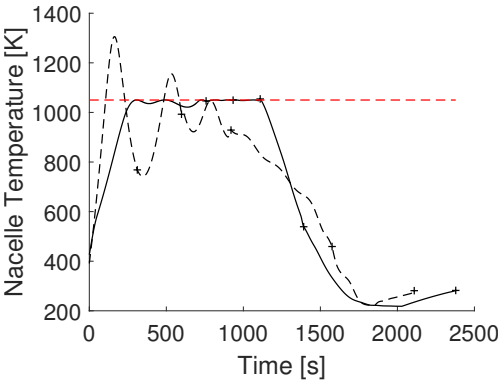

(b) Temperature of the nacelle time history

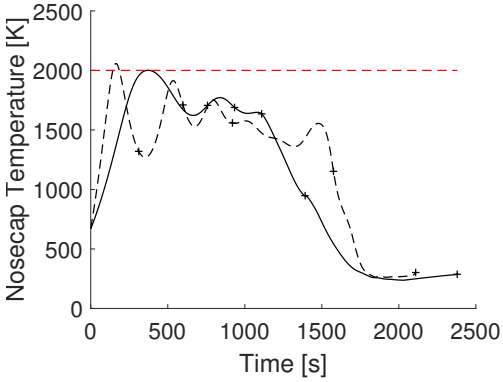

(c) Temperature of the nosecap time history

Figure 4.5: Time history of the temperatures on the vehicle surfaces during the descent for the case with thermal constraints (solid line), and without (dashed line). The temperature limits are highlighted with a dashed red line.

4.3 Summary of the chapter

This chapter has outlined the approach and the models for a preliminary design and performance evaluation of a hybrid engine SSTO vehicle. It has also presented results for the trans-atmospheric sections of a full mission test case: the ascent and descent trajectories to an equatorial 300 km circular orbit. The strategy of separating different flight phases, that would otherwise present discontinuities, is possible thanks to the modularity of the platform, leveraging the multi-shooting approach and accounting for different flight conditions. This is a further step towards an automated design platform that has modularity and flexibility at its core, allowing the solution of multiple different problems.

The next chapter will demonstrate the process of multi disciplinary system sizing in the design of a SSTO vehicle for a reference orbital mission. The performance impact of injecting the payload into non-reference orbital altitudes and inclinations will be quantified. A TSTO configuration will be introduced to enable accessing orbits characterised by higher energy than the reference mission.

Chapter 5

Vehicle sizing and performance analysis

The analysis of a spectrum of scenarios is a necessary step in the launch vehicle design to ensure that the business case is solid and the vehicle can, once in the operational phase, satisfy the projected market demand and possible evolutions. Being able to assess beforehand the payload capability, scaling over a range of diverse missions helps, not only the Launch Service Operator in targeting a specific market segment, but also the satellite and spacecraft industries to start designing payloads sized for the future launch vehicles.

This chapter present the performance analysis of a launch vehicle characterised by a reusable first stage and TSTO configuration over a range of missions from LEO to higher altitude orbits and inclinations from equatorial to retrograde orbits.

The approach proposed in this dissertation is used to study the presented problem, divided in two main activities. The first one is the MDO sizing of a launch vehicle designed around a sample mission to a 100 km circular equatorial orbit, minimising the initial gross mass. The latter investigates the performance variation when targeting different orbital conditions, maximising the final mass inserted into the target orbit.

This sizing test case and methodology have been previously presented at the 67th International Astronautical Congress, 2016 [132].

5.1 Approach

The small satellite reusable launcher is modelled as a TSTO horizontal take off and landing lifting body vehicle, with engine switching between air breathing and rocket modes to increase the I_{sp} in the lower atmosphere. The engine of the first stage can operate in a high efficiency air breathing mode in the early phases of the ascent. The switch point into rocket mode is constrained to $Mach_{switch} = 5.5$ and $h_{switch} = 28\,\text{km}$, based on the performance metrics reported in the Skylon manual [4]. The geometrical size of the main stage, propellant mass and engine scaling factor are optimisation variables.

Once all the propellant is spent, the second stage is released to perform orbital injection manoeuvres and bring the payload in the desired orbit. The second stage engine ignition happens after separation, with an initial vehicle weight of 2 500 kg, where 1 000 kg are usable fuel. This mass is included in the first stage from beginning of the trajectory to MECO (Main Engine cut-off) and separation.

The reference mission objective is to put the second stage into a 100 km circular, equatorial ($i = 0°$) orbit with a final mass of 1 500 kg. This mass includes the payload, the upper stage, and the unspent fuel. Since only 40% of the mass fraction is used during the reference second stage ascent, this leaves room to use larger amounts of propellant when targeting higher energy orbits in the second section of the analysis.

Given the second stage engine I_{sp} of 250 s, representative of common hypergolic propellants, the maximum theoretical ΔV that the upper stage can generate is 1 252 m/s, assuming no expansion or throttling losses. This is only a small fraction of the total ΔV required to reach LEO, therefore the performances of the whole system are heavily dependant on the first stage trajectory and the exploitation of the airbreathing engine.

After sizing the first stage for the reference mission, the second part of the analysis focuses on assessing the impact of delivering the payload to higher energy orbits by maximising the final mass. The range of orbits under investigation covers altitudes from 200 km to 1 200 km and inclinations from 0° to 120°.

5.2 Simulation environment

The simulation is performed with the general assumptions presented in chapter 3: the vehicles are modelled as point masses in an Earth Centered Earth Fixed reference frame with 3 degrees of freedom for all phases of the mission. The coordinates are converted into the Earth Centered Inertial frame to compute the Keplerian orbital parameters for the semimajor axis a, eccentricity e and inclination i.

The WGS84 geodetic system is used to model the Earth geometric parameters including the radius length from the centre to the Earth surface r_E as a function of latitude. The gravitational harmonics include coefficients up to the 4^{th} order.

The atmosphere is modelled using the static global International Standard Atmosphere. The model is expanded above the maximum altitude $h_{max} = 84852$ m by extending the exponential laws regulating pressure and density assuming constant temperature $T(h > h_{max}) = 186.87$ K.

The integration of the dynamic equations is performed in all cases with the Runge-Kutta 4^{th} order method on a constant timestep of 1 second for all phases unless specified otherwise. The open loop control of the throttle and vehicle attitude adjust the direction and modulus of the forces affecting the vehicle during the ascent trajectory.

5.2.1 Propulsion

Similarly to the application described in the previous chapter, the first stage propulsion system is a hydrogen fuelled motor, capable of functioning as both an air breathing engine, using atmospheric oxygen, and rocket, using the LOX stored on-board.

The implementation here presented differs from the one presented in chapter 4 by using non-proprietary models. The engine is still modelled over the SABRE concept, but it is instead based on the performance metrics reported in the Skylon user manual [4] to build a low fidelity engineering model of the engine.

The rocket maximum vacuum specific impulse is $I_{sp,max} = 450\,\text{s}$, modelled using the general rocket equation accounting for the vacuum-adapted nozzle expansion losses due to changes in atmospheric pressure with equation 5.1, with $A_{exit} = 3.4\,\text{m}^2$.

$$T_{rocket} = \dot{m}_p I_{sp,max} g_0 - A_{exit} P_{air} \tag{5.1}$$

Below a certain altitude and speed, the engine can exploit the presence of oxygen in the atmosphere and it is modelled as a modified rocket engine with variable I_{sp} directly impacting the performances depending on the flight conditions. Differently from the case presented in chapter 4, the switching conditions are constrained to the values of $h = 28\,\text{km}$ and $M = 5.5$. The equivalent specific impulse is calculated with the ratio between total pressure in flight and the sea level static one $p_{SL} = 101\,325\,\text{Pa}$ with equation:

$$I_{sp} = 4079(p_{tot}/p_{SL}) \tag{5.2}$$

The maximum equivalent specific impulse obtained from equation 5.2 is capped to the value of $I_{sp} = 4\,079\,\text{s}$ in any condition of total pressure that exceeds the sea-level static pressure. The behaviour of the model over the possible domain of air-breathing flight is plotted in Figure 5.1.

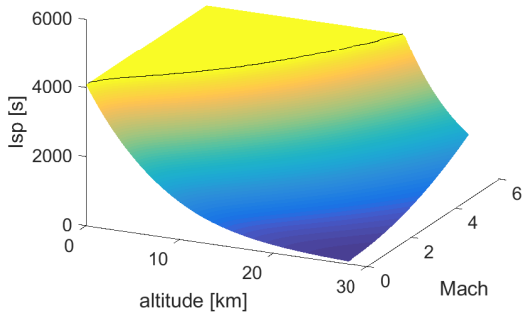

Figure 5.1: Specific impulse of the first stage motor in air breathing mode as a function of Mach and altitude

The second stage propulsion system is modelled as a thruster using a storable propellant. The maximum specific impulse is 250 s with a vacuum adapted nozzle.

Quadratic laws are employed to have peak efficiency value at 100% throttle to discourage throttled oversized engines in all stages and all operating modes. The throttle

further reduces the specific impulse with equation 5.3 and the thrust is computed with the equation 5.4.

$$I_{sp} = I_{sp}(h, M) * (1 - (\tau - 1)^2) \tag{5.3}$$

$$T = \tau n_{eng} m_p g_0 I_{sp} \tag{5.4}$$

The gravitational acceleration parameter has a constant value of $g_0 = 9.806\,65\,\mathrm{m/s^2}$ and the throttle τ multiplies the nominal value of m_p by a proportional factor varying from 0 to 1.

The scaling of the engines is performed by proportionally multiplying the values of thrust and mass flow by a factor n_{eng}, leaving the specific impulse independent from the size of the engine.

5.2.2 Aerodynamics

The aerodynamics of the vehicle are computed with the same model presented in section 4.1.1 to predict the total coefficient of lift C_L and drag C_D as a function of the angle of attack α and Mach number M, based on the cFASTT-1 reference geometry. Figure 5.2 illustrates the behaviour of the aerodynamic coefficients, and highlights the discontinuity that is present at the sonic regime. The first stage aerodynamics is subdivided in subsonic and supersonic on the $M = 1$ boundary, splitting the first two phases that otherwise share all other vehicle system and environmental models. In Figure 5.2a it can be observed that the lift coefficient follows the expected linear dependence on the angle of attack, while Figure 5.2b shows the classical peak around the sonic regime, and quadratic dependence on the angle of attack.

The second stage is released at altitudes where aerodynamic forces are orders of magnitude lower than the thrust of the engine. The reference surface area is assumed $S_{ref} = 1\,\mathrm{m^2}$ and the aerodynamic coefficients $c_L = 0$ and $C_D = 1$ are constant. The angle of attack for this flight phase is constrained to $-5^\circ \leq \alpha \leq 15^\circ$ and its expected value

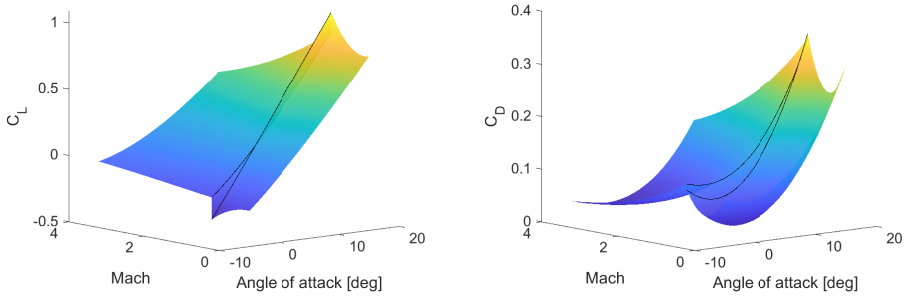

(a) Lift coefficient

(b) Drag coefficient

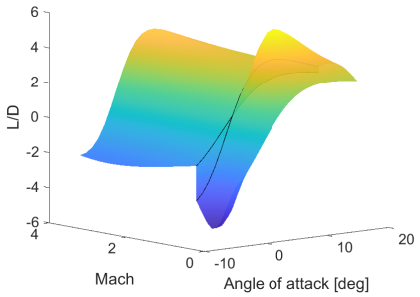

(c) Aerodynamic efficiency

Figure 5.2: Aerodynamic coefficients of the first stage in the ranges of Mach $0 \leq M \leq 4$ and angle of attack $-5° \leq \alpha \leq 15°$. Black lines highlight the discontinuity of the surrogate models at the $M = 1$ boundary.

in optimal solutions is approximately zero since the component of thrust perpendicular to the velocity vector introduces efficiency losses.

5.3 Optimisation

The optimal control problem is formulated with the direct transcription, multiple shooting method described in chapter 3.

In this analysis the Chebyshev nodes are used as grid for the control law, and the values between the nodes are computed with a Piecewise Cubic Hermite Interpolating Polynomial. Chebyshev nodes are not uniformly distributed [133], with interpolation points clustering towards the ends of the domain. This distribution would minimise the Runge's phenomenon effect on polynomial interpolation, however the specific interpolation method selected for this scenario is not affected.

Each of the multiple phases is set up with the specific set of mathematical models and numerically integrated with a 4th order fixed timestep Runge Kutta method.

The states and controls are matched with equality constraints between elements to guarantee a continuous flight. Additional equality constraints 5.5 are set on the final values of some trajectory elements to reach the desired conditions at specified events: sonic speed to switch aerodynamic model, first stage engine mode transition, and the correct combination of altitude and inclination for the target orbit. Given the non-fixed masses for the stages evolving during MDO, an equality constraint assures the mass conservation when staging.

Inequality constraints include acceleration limited to a maximum of $3g_0$ in either the X or Z axis, dynamic pressure to 200 kPa, and fuel consumption not exceeding the available propellant mass. The tolerance on all constraints is 10^{-4} and the scaling is based on the target value.

$$M_{aero,switch} = 1 \tag{5.5a}$$

$$M_{eng,switch} = 5.5 \tag{5.5b}$$

$$h_{eng,switch} = 28\,\text{km} \tag{5.5c}$$

$$a(t_f) = r_E + h_{tgt} \tag{5.5d}$$

$$i(t_f) = i_{tgt} \tag{5.5e}$$

$$e(t_f) = 0 \tag{5.5f}$$

$$acc_{x,z} \leq 3g_0 \tag{5.5g}$$

$$q_{dyn} \leq 200\,\text{kPa} \tag{5.5h}$$

The algorithm used is the single objective sequential quadratic programming. The cost functions used for the analyses are the minimisation of the vehicle starting mass for the initial sizing case, and the maximisation of the final mass inserted into orbit for the subsequent runs.

5.4 Vehicle design definition

The first part of this analysis is an optimisation of the vehicle sizing, with the objective of minimising the initial mass of the vehicle.

A nominal test case is defined to perform initial sizing of the vehicle. The starting conditions are arbitrarily chosen as representative of an equatorial launch-site shortly after take-off during the climb phase with prograde heading, and are listed in Table 5.1.

Table 5.1: Starting conditions for the sizing trajectory

Variable		Value
Altitude	m	1000
Velocity	$\mathrm{m\,s^{-1}}$	200
Flight Path Angle	deg	10
Heading	deg	90
Latitude	deg	0
Longitude	deg	0

The gross starting mass is an optimisation variable, with bounds between 50 t and 150 t based on accrued experience on similar test cases. The dry mass of the first stage is a fraction of the gross, computed by using linear interpolation between two SSTO vehicles of recent conception: the X-33 and the Skylon space-plane, having respectively 26.3% and 18.4% dry mass fractions for 129 t and 325 t. The value is extrapolated when sampled outside of the data-points. Equation 5.6 is used to compute the final dry mass based on the initial wet mass, with all the variables expressed in metric tons.

$$m_{dry,tons} = 0.31479086734 m_{wet,tons} - 0.00040147959 m_{wet,tons}^2 \tag{5.6}$$

While the data comes from vehicles with similar CONOPS, this approach should not be confused with the definition of a methodology for the estimation of the mass break-down of a SSTO vehicle. The choice of the input data and interpolation method used for this computation is completely arbitrary, as the purpose is purely demonstrative of the application presented.

The square-cube law relating mass and surface is enforced to ensure a proper scaling of the vehicle without deformation of the geometry, and preserving a proportionate amount of lift and drag generated.

The scaling parameters of the engines are part of the optimisation vector and indirectly constrained through throttling losses and acceleration constraints (3g). Having vacuum thrust too high will require throttling early to satisfy acceleration limits, while an undersized engine may waste too much fuel trying to compensate gravity losses and not reach the desired orbit.

The mass of the vehicle at the start of the second stage flight is 2 500 kg and the final mass is constrained to 1 500 kg for the vehicle sizing activity.

The mission is divided in 4 phases, illustrated in Figure 5.3, characterised by different behaviour of the subsystems, where phases 1 and 2 share a common engine model, and phases 2 and 3 share the aerodynamics:

1. First stage subsonic acceleration with the air-breathing engine to sonic conditions.
2. First stage supersonic acceleration with the air-breathing engine to $M_{switch} = 5.5$ and $h_{switch} = 28\,\text{km}$.
3. First stage rocket burn until fuel exhaustion and separation of the second stage.
4. Second stage flight until injection into the 100 km target orbit.

All phases are characterised by 5 control nodes per element and 2 elements per phase with the exception of the first (subsonic acceleration), with a single element. State and control bounds for the sizing case are listed in Table 5.2. When upper and lower bounds have the same value, the variable is set as constant and it is not added to the optimisation vector.

The bank angle is not included in the optimisation to avoid unnecessary thrust misalignment losses, thus the aerodynamic and propulsive forces lie on the X-Z plane of the aircraft body.

The problem search space is explored with a multi-start approach, distributing the initial guess vectors with Latin hypercube sampling (LHS). This method ensures

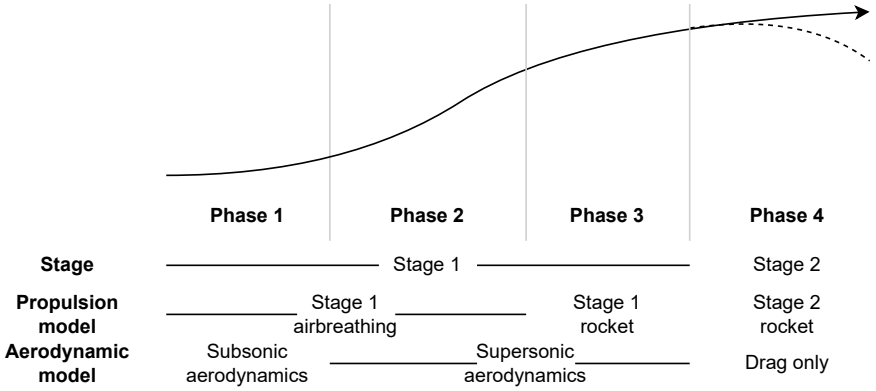

Figure 5.3: CONOPS of the reference TSTO mission

Phase			1	2	3	4
Stage			1	1	1	2
Altitude	h	km	[1, 15]	[1, 30]	[25, 100]	[50, 200]
Velocity	v	$\mathrm{m\,s^{-1}}$	[150, 500]	[250, 1800]	[250, 1800]	[5500, 8000]
FPA	γ	deg	[-90, 90]	[-90, 90]	[-90, 90]	[-90, 90]
Heading angle	χ	deg	[-90, 90]	[-90, 90]	[-90, 90]	[-90, 90]
Latitude	λ	deg	[-90, 90]	[-90, 90]	[-90, 90]	[-90, 90]
Longitude	θ	deg	[-180, 180]	[-180, 180]	[-180, 180]	[-180, 180]
Mass	m	t	[50, 150]	[50, 150]	[25, 150]	[0.25, 2.5]
AoA	α	deg	[-5, 15]	[-5, 15]	[-5, 15]	[-15, 15]
Throttle	τ	-	[1, 1]	[1, 1]	[0.5, 1]	[0, 1]
Duration	t	s	[10, 30]	[120, 300]	[120, 240]	[30, 240]
Thrust	T	MN	[1, 3]	[1, 3]	[1, 3]	[0.005, 0.025]
Surface area	S_{ref}	$\mathrm{m^2}$	[75, 225]	[75, 225]	[75, 225]	[1, 1]

Table 5.2: Bounds for the variables in the optimisation vector in the sizing case.

that the distribution of guesses occupies all portions of the sample space [134]. The 135 guesses (thus having a number of initial guesses proportional to the number of optimisation variables) are locally optimised with the algorithm described in section 3.5. When all the cases have been processed, the solution satisfying all the constraints and having the lowest value of cost function is selected as the best one found. The best case satisfies the constraints with a maximum violation of $max(c, ceq) = 3.8128e-05$ below the set tolerance $Tol_{con} = 1e-4$. This results in a vehicle with an optimised gross take off mass $m_{gtow} = 91\,561\,\text{kg}$ and first stage dry mass of $m_{dry} = 25\,457\,\text{kg}$, equal to an inert mass fraction $m_{dry}/m_{gtow} = 0.278$. The reference area that satisfies the square-cube requirement of the cfastt-1 geometry is $S_{ref} = 149.6\,\text{m}^2$. The optimised values of thrust for the first and second stage are respectively $T_{s1,max} = 1.437\,7\,\text{MN}$ and $T_{s2,max} = 23.555\,\text{kN}$.

The optimised variables relative to the gross mass, thrust and reference surface areas are extracted and fixed for the next step.

5.5 Orbit penalty computation

The cost function for all cases is the final mass that reaches the target orbit, this change removes the constraint on the mass of the second stage at the end of the ascent. The initial mass, defined in the sizing analysis, is fixed for all following runs to the value of $m_{gtow} = 91\,561\,\text{kg}$.

Having defined the vehicle configuration, it is possible to analyse its performance over a broad range of target orbits at different altitude and inclinations. The former spans from 200 km to 1 200 km with 50 km increments and the latter ranges from 0° to 120° with 10° steps, resulting in a grid of 273 cases, for 21 altitude and 13 inclination combinations.

Two additional phases are appended to the second stage flight:

1. Second stage coasting arc after its first burn.

2. Second stage circularisation burn, injecting the vehicle in the target orbit.

Phase			5	6
Stage			2	2
Altitude	h	km	[50, h_f]	[50, h_f]
Velocity	v	$\mathrm{m\,s^{-1}}$	[5500, 8000]	[5500, 8000]
FPA	γ	deg	[-90, 90]	[-90, 90]
Heading angle	χ	deg	[-90, 90]	[-90, 90]
Latitude	λ	deg	[-90, 90]	[-90, 90]
Longitude	θ	deg	[-180, 180]	[-180, 180]
Mass	m	t	[0.25, 2.5]	[0.25, 2.5]
AoA	α	deg	[-15, 15]	[-15, 15]
Throttle	τ	-	[0, 0]	[0, 1]
Duration	t	s	[30, 1000]	[30, 240]
Thrust	T	MN	[0.005, 0.025]	[0.005, 0.025]
Surface area	$\S_{ref}$	$\mathrm{m^2}$	[1, 1]	[1, 1]

Table 5.3: Bounds for the additional variables in the optimisation vector in the mission analysis cases.

As shown in Table 5.3, these new sections of flight share most settings with the preceding phase number 4 terminating at the first of the two second stage engine cut-off. They are each comprised of 1 element with 5 nodes, with different altitude bounds to match the target orbit of the case under analysis. The coasting arc is characterised by a longer time-step of 2 seconds. Having no thrust and constant aerodynamic coefficient, as described in section 5.2.2, makes it an ideal parabolic arc where the control nodes of AoA and throttle have no effect.

The same multi-start approach used in the previous sizing process is used to find the first solution. The first case selected is the one with the lowest ΔV, thus the shortest ascent duration and time required to integrate the whole trajectory, aiming to insert the payload into a 200 km circular equatorial ($i = 0°$) orbit. Once the first solution is found with multi-start, it is used as a first guess to populate the rest of the matrix, cycling between altitudes and inclinations, starting with the cases closest to the one already found.

Each of the cases is run using as a starting guess the previous solution found, regardless of the quality of the solution converged to. This leads to 209 cases violating

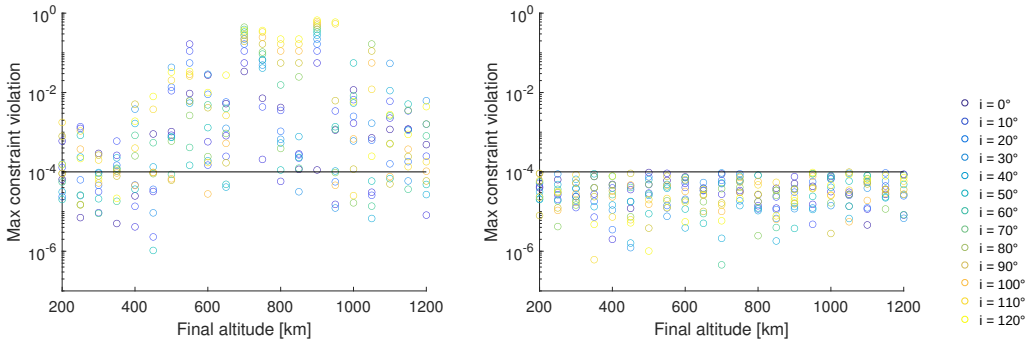

(a) Maximum constraints violation after the first optimisation pass

(b) Maximum constraints violation after refinement of the solutions

Figure 5.4: Evolution of the constraints

the tolerance of $1e{-}4$ on at least one of the equality and inequality constraints. As it can be observed in Figure 5.4a, these are mainly clustered in mid-altitude, high-inclination orbits where non-converged solutions were used as first guesses and propagated the problem.

To reduce the constraint violations, all cases that exceed the set tolerance are re-run, giving priority of execution from the constraint violation with highest value to the smallest. The neighbouring solutions are used as a first guess, but in the rare cases where none of the warm-starts produces an improvement on the case under analysis, random guesses are generated until a reduction in constraints violation.

Once all cases satisfy the constraint tolerance, an additional iteration is performed to improve the quality of the results. It is expected that both increasing the altitude and inclination of the orbit would require more fuel and reduce the final mass; therefore, any result that does not exhibit this trend, is further refined. The strategy used is the same one implemented to reduce the constraints below the desired tolerance, selecting neighbouring solutions as warm-starts. Priority is given to the cases with lowest performances when compared to the trend lines. The deployed mass performances after the smoothing process are presented in Figure 5.5.

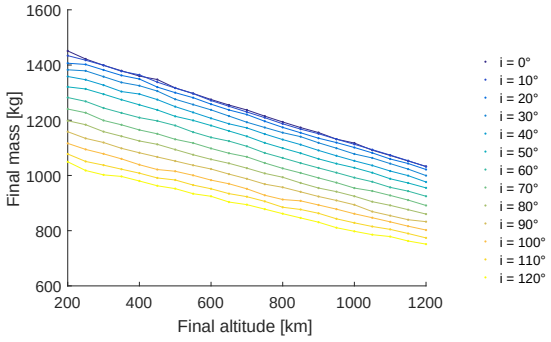

Figure 5.5: Performance curves of deployed mass into the target orbits for different combinations of altitudes and inclinations

5.6 Analysis of the results

As expected, a decreasing trend in the final mass values is detected in the direction of increasing orbit altitude and inclination, as shown in Figure 5.5

It is possible to further elaborate this connection by finding the correlations between the orbital parameters and the final mass. The lowest order polynomial with $R^2 > 0.99$ approximating this dataset is the 4th order polynomial of equation 5.7 with correlation coefficient $R^2 = 0.99943$.

$$m_f = 1528 - 0.4154h_f - 23.44i + 0.03898h_f i - 179.8i^2 + 0.01101h_f i^2 + 43.69i^3 \quad (5.7)$$

This shows linear dependency with the final altitude h_f, expressed in km, that could be a local effect due to the small range of altitudes analysed. The more complex third order dependence on the inclinations, expressed in rad is likely due to the misalignment of the vehicle co-rotating initial velocity and the earth's rotation towards east. Introducing trigonometric terms on the inclination component gives us equation 5.8, with a correlation coefficient $R^2 = 0.99133$.

$$m_f = 1245 - 0.3578h_f + 233.7\cos i \quad (5.8)$$

The reason for this trend can be identified with the analysis of the different energy levels from ground to orbit. By computing the specific orbital energy computed with formula 5.9 it is possible to generate the plots in Figure 5.6.

$$\epsilon = (v^2)/2 - \mu/r \tag{5.9}$$

Figure 5.6a illustrates the initial specific orbital energy of different initial headings, some of which benefit of the additional velocity imparted by the rotation of the Earth, which has maximum positive effect when aligned with the vehicle velocity. The optimised initial heading is consistent among trajectories sharing the same inclination, as it is expected. Figure 5.6b shows how both the altitude and inclination factors, characterising the final orbit, affect the injected mass with a comparable scale across the range of trajectories analysed. The difference from final to initial specific orbital energy plotted in Figure 5.6c introduces a small distortion when removing the contribution of the planet's rotation.

The staging conditions at the end of the first stage flight provide insight into the approach used to achieve the target orbit. Figure 5.7a shows trajectories towards higher orbits separating at higher altitudes; since the chemical energy stored in the first stage is constant, this approach trades kinetic energy for potential(Figure 5.7b). This effect, coupled with a higher Flight Path Angle at release (Figure 5.7c), inserts the second stage in a steeper parabolic arc, following the gravity turn targeting the correct orbit altitude. The points that lie outside of the visible trend are likely due to local optima affecting the solutions at low altitude. Figure 5.7 does not provide information to compare the different approaches and determine the better one, as even the outliers do follow the performance trend observable in Figure 5.6c.

The optimal trajectories generated can be collectively analysed to determine the envelope within which the vehicle is expected to fly. This process provides bounds to the conditions that the vehicle stages and the payload will experience throughout the ascent. Furthermore, it can potentially be used for safety or performance checks in real-time during flight.

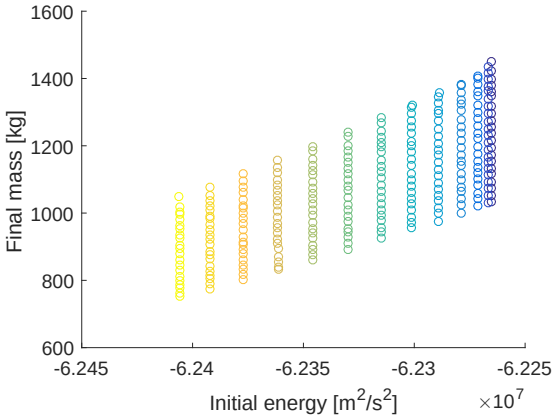

(a) Specific orbital energy at the start of the trajectories

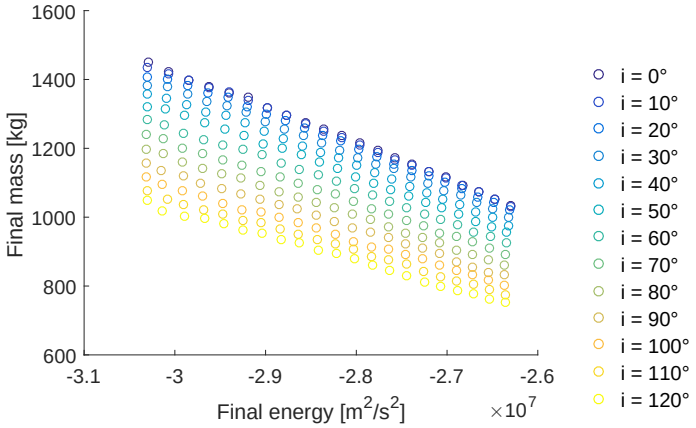

(b) Specific orbital energy at orbital insertion

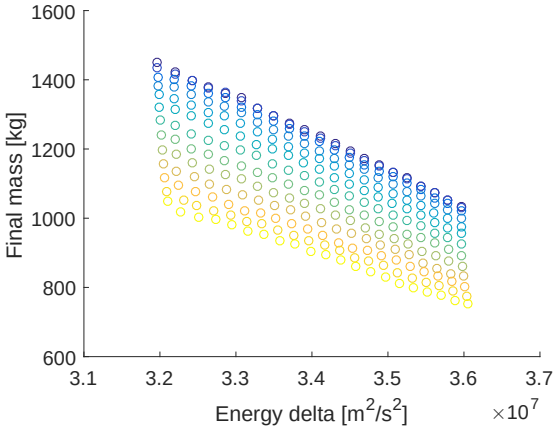

(c) Difference of specific orbital energy from final to initial conditions

Figure 5.6: Specific orbital energy for all the cases in the altitude-inclination grid

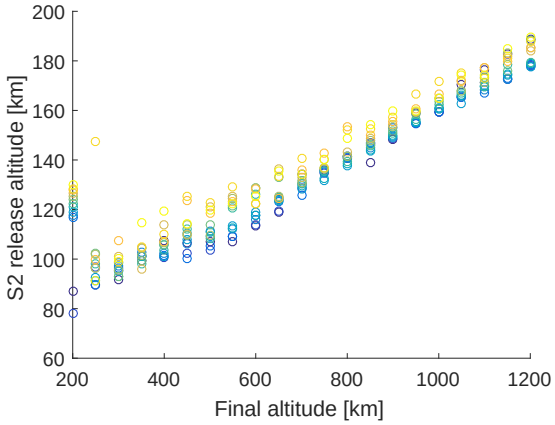

(a) Staging altitude vs final orbit altitude

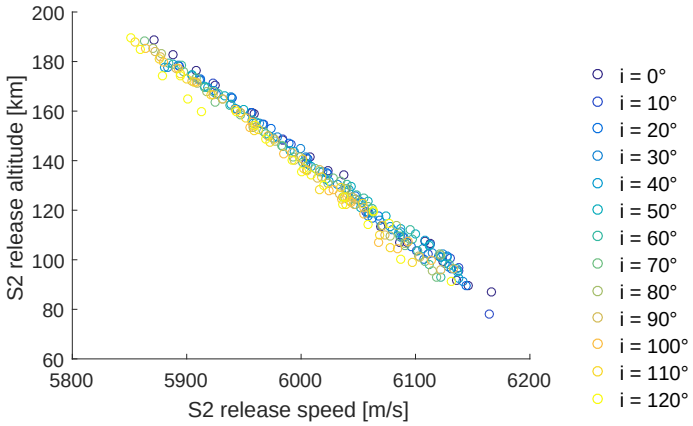

(b) Staging speed vs final orbit altitude

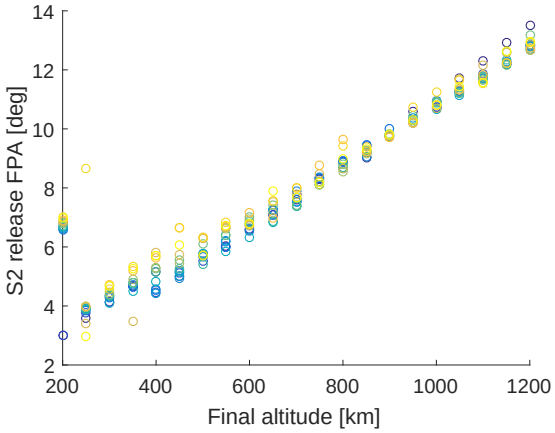

(c) Staging Flight Path Angle vs final orbit altitude

Figure 5.7: Scatter plots of the states at the staging point for different target orbits.

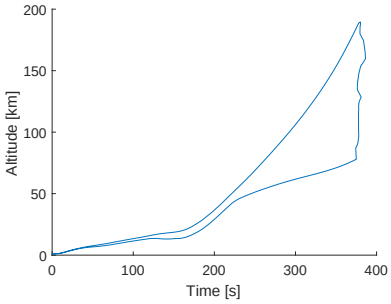

(a) Altitude envelope of the Stage 1 flight over time

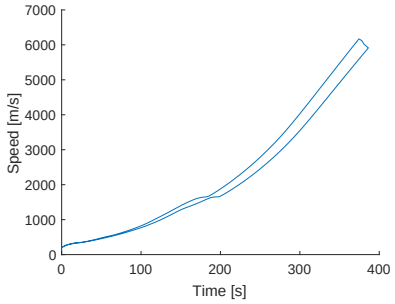

(b) Speed envelope of the Stage 1 flight over time

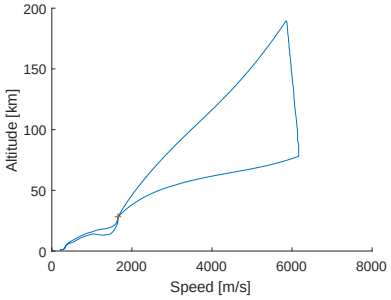

(c) Altitude and speed envelope of the Stage 1 flight

Figure 5.8: Envelope of the Stage 1 flight

It can be observed that this vehicle flies within a relatively narrow corridor during the air-breathing phase (before 200 s), in both altitude (Figure 5.8a) and speed (Figure 5.8b). The narrow operating corridor in air-breathing mode indicates that there is an optimal flight path regardless of the target orbit. This is often the case due to the interplay of aerodynamics and propulsion models. The engine switch takes place at approximately 200 s, and precisely at $Mach = 5.5$ and altitude $h = 28$ km, a condition marked with a red cross in Figure 5.8c. A similar plot, with altitude and Mach axis, is used in the field of flying qualities analysis to determine the trimline of the vehicle [135]. After the ignition of the rocket engines, the flight of the first stage follows the optimal path that injects the second stage and payload in the optimal parabolic arc as observed in Figure 5.7. This approach results in a wider range of altitudes for the rocket phase, while the speed envelope is relatively less impacted.

The controls and states of 2 trajectories from cases at the extremes of the altitude range ($h_f = 200\,\text{km}$ and $h_f = 1\,200\,\text{km}$) of analysis and no inclination ($i_f = 0°$) are shown in Figures 5.9 and 5.10. These plots present the full ascent trajectory and magnifications to highlight the stage 1 flight. Crosses and circles respectively mark the end of the multiple shooting elements and the control nodes.

Figure 5.9a presents apparently similar angle of attack profiles for both trajectories, with the second stage control law stretched in over a long flight duration to match the higher orbit. Closer inspection of the first stage flight in Figure 5.9b shows that the angle of attack profile of the launch toward the higher orbit dominates the control law of the lower orbit case.

The throttle profile exhibit comparable behaviours in Figure 5.9c, albeit with a longer burn for the second stage requiring additional ΔV. As shown in Figure 5.9d, the vehicle throttles down near the end of the stage 1 ascent to limit the acceleration below the set constraint.

The altitude (Figures 5.9f, 5.10b) and co-rotating velocity (Figure 5.10d) profiles of the first stage match the observations of the previous paragraphs on the flight corridor, with the divergence becoming more evident after engine transition. Beyond the separation point, Figures 5.9e, 5.10a and 5.10c show a bifurcation that continues increasing, until orbit insertion.

The flight path angle profile in Figure 5.10f shows a more marked dive before a consequently more pronounced pitch-up manoeuvre for the higher altitude case. This strategy is necessary to continue along the required steeper ascent of the parabolic arc until circularisation (Figure 5.10e).

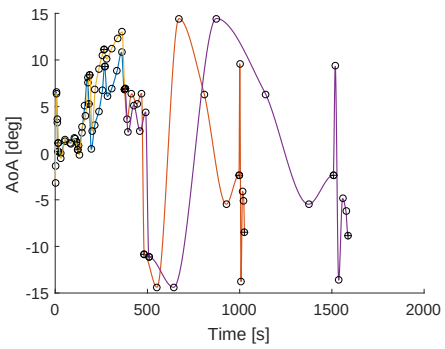

(a) Angle of attack profile, whole trajectory

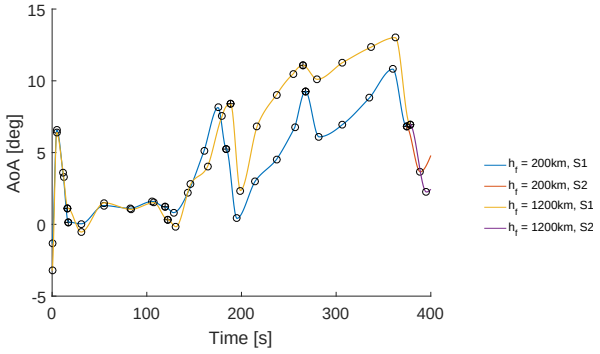

(b) Angle of attack profile, first stage flight

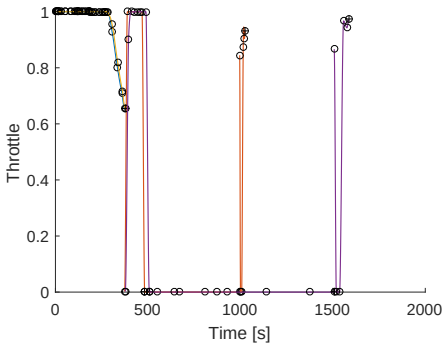

(c) Throttle profile, whole trajectory

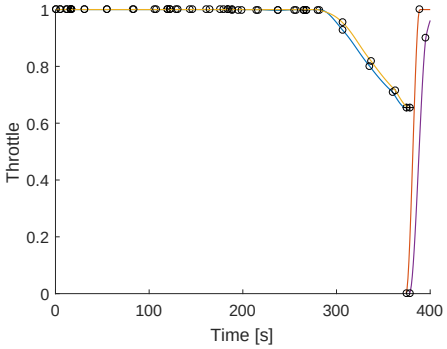

(d) Throttle profile, first stage flight

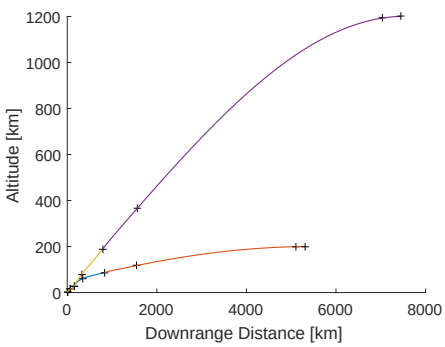

(e) Altitude vs downrange distance, whole trajectory

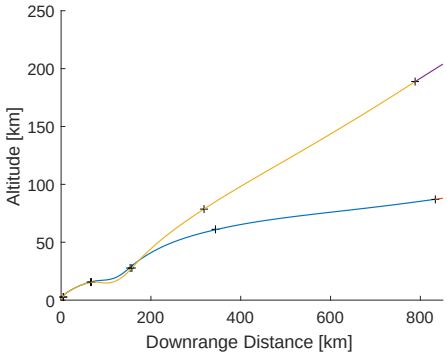

(f) Altitude vs downrange distance, first stage flight

Figure 5.9: Control and states for selected trajectories, 0° inclination, 200 km and 1 200 km - part 1/2

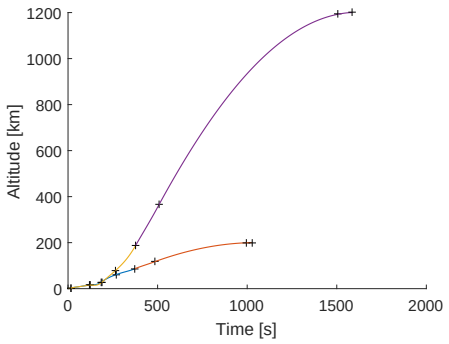

(a) Altitude time history, whole trajectory

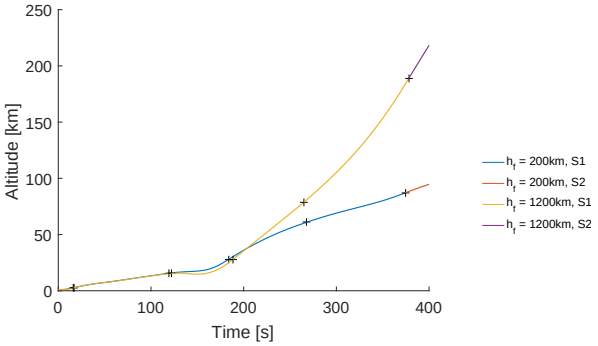

(b) Altitude time history, first stage flight

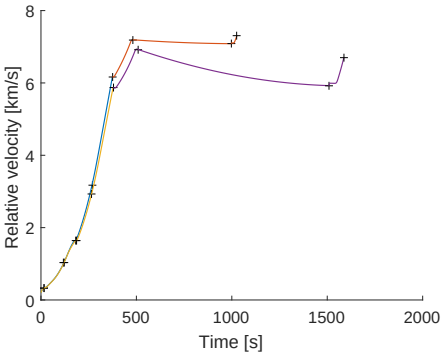

(c) Co-rotating velocity time history, whole trajectory

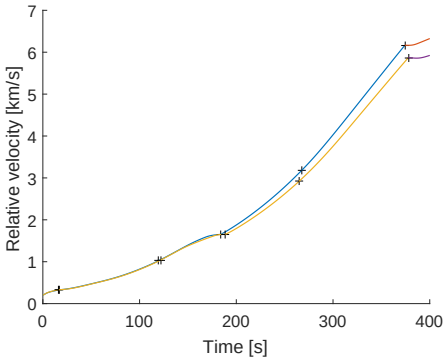

(d) Co-rotating velocity time history, first stage flight

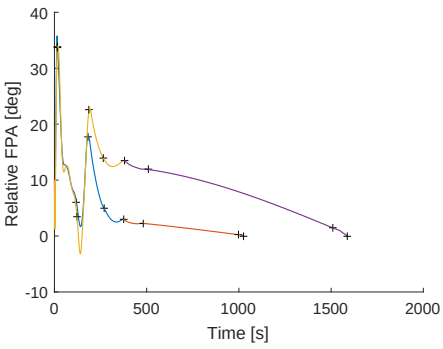

(e) Flight Path Angle time history, whole trajectory

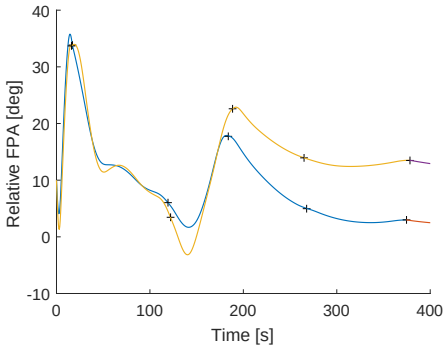

(f) Flight Path Angle time history, first stage flight

Figure 5.10: Control and states for selected trajectories, 0° inclination, 200 km and 1 200 km - part 2/2

5.7 Summary of the chapter

A modular MDO approach was used to evaluate the performance of a SSTO vehicle examining the payload mass that can be delivered against different orbits, using the vehicle mass fraction against the characteristic energy of the orbit.

A reference vehicle design was obtained for a reference orbit. This vehicle was then used to analyse the performance at higher altitude and different inclination orbits, extrapolating a set of solutions that, analysed on the payload mass - orbital energy graph, display the performance envelope of the launcher. The sharp decrease in payload capability, due to the orbital altitude increase, is mitigated by the introduction of an additional stage, drastically reducing the effect.

From these preliminary results, it is shown how designing a SSTO vehicle for a specific orbit limits the possibilities to expand the range of operations outside of the predetermined bounds and, if some effects are not taken into account, a vehicle may be unable to meet the expectations of a varied set of customers.

The next chapter will analyse the downrange and crossrange gliding capabilities of a RLV in off-nominal conditions, following an abort, with the vehicle retaining aerodynamic control, but no propulsion.

Chapter 6

Ascent abort scenarios

This chapter evaluates the flight performances during aborts occurring in the ascent of a lifting body vehicle. The case presented provides the opportunity to study the return, recovery or abort trajectories of a launcher, an increasingly important scenario in the ongoing shift towards reusability that is changing the space industry. The analysis of range capabilities is necessary to determine when the vehicle can be successfully recovered after the loss of thrust, which is historically the most common failure mode in launch vehicle operations [136].

The main sections that compose this chapter are:

1. the nominal ascent profile,
2. the abort trajectory from one of the latest states before orbit,
3. the abort trajectories for earlier onset times.

This test case and methodology have also been presented at the 21st AIAA International Space Planes and Hypersonics Technologies Conference, 2017 [137].

6.1 First guess generation

For both the baseline ascent and baseline descent mission design, a pool of starting guesses from the search space is generated with Latin Hypercube Sampling and run through the optimisation routine with the SQP solver, a simulation time-step of 3 s,

and relaxed constraints reducing the tolerance on both the equality and inequality to 10^{-3}. This approach increases the exploration speed capabilities of the algorithm. The converged solution with best cost function is refined with shorter time-step of 1 s and stricter tolerances used for the baseline data presented.

This approach to find a solution closer to the global minimum is computationally expensive and well suited only for single case analysis. In the study presented, multiple points have to be evaluated for the abort scenarios, therefore the time and resources required to complete the calculations with such approach are prohibitive. The previously converged solutions are passed as 'warm-start' initial guesses to an optimisation routine set with the correct tolerances and time-step length, starting from the highest energy abort point, and moving toward the lowest.

Choosing closely spaced abort points means that the starting conditions of consecutive cases have minor differences and the solution for the previous starting point can be used to provide the optimisation routine with a good starting guess that can quickly converge to a solution and repeat the iterative process, exploring the search space only once.

6.2 Nominal mission design

The nominal ascent mission is the deployment of $m_{payload} = 1\,000\,\text{kg}$ of payload in a 200 km circular orbit set with the equality constraints 6.1.

$$a(t_{f,a}) = r_E + 200\,\text{km} \tag{6.1a}$$

$$e(t_{f,a}) = 0 \tag{6.1b}$$

The chosen starting location for the ascent at $(0°\text{N}, 0°\text{E})$ latitude and longitude. Placing the origin of the axis in this location simplifies plotting and reference frame transformations to compute distances. The choice is arbitrary and the same approach can be applied to any other starting point; the impact of latitude of launch site and inclination of the target orbit has been documented and analysed in the past studies

[132]. In the same study, the vehicle used in this chapter is sized through the means of MDO of a TSTO configuration.

The reference vehicle, taken from the original study [137], has a gross take off mass $m_{gtow} = 90\,035\,\text{kg}$ and a dry mass of $m_{dry} = 22\,907\,\text{kg}$.

The aerodynamic model is based on experimental wind tunnel test results X-34 dataset provided by Brauckmann [138], with reference surface unchanged from the reference study $S_{ref} = 364.64\,\text{m}^2$. The data points cover a set of inputs in a range of Mach number $0.4 \leq M \leq 6$ and angle of attack $-4^\circ \leq \alpha \leq 24^\circ$. The database is used to create two functions $C_L = f(\alpha, M)$ and $C_D = f(\alpha, M)$ obtained through polynomial interpolation. The order of the polynomial is the lowest that guarantees a correlation coefficient $R^2 \geq 0.99$, assuring accurate results and fast computation.

The first stage propulsion system is based on the published performance specifications for SABRE, with the same rocket model detailed in chapter 5. At lower altitudes, the engine can exploit the presence of oxygen in the atmosphere and it is modelled as a modified rocket engine with variable I_{sp} and performance depending on the flight conditions. The maximum equivalent specific impulse is $I_{sp} = 6\,500\,\text{s}$ at sea level. Increasing altitude negatively affects this value due to the decrease of air pressure and density. Quadratic dependence on the throttle τ is included to reach the peak efficiency value at $M = 3.5$ and 100% throttle, computing the Thrust output with equations 6.2.

$$I_{sp} = 8000(p_{air}/50000)^{0.2}(-0.043M^2 + 0.3M + 0.45)(-0.2\tau^2 + 0.4\tau + 0.8) \tag{6.2a}$$

$$T = \tau m_p g_0 I_{sp} \tag{6.2b}$$

The switching point between the two engine operational modes is unconstrained and is a result of the optimisation of the ascent.

The upper stage is modelled as a small hydrazine thruster, with $I_{sp} = 250$ s, and the same formulation used for the nozzle losses of the first stage rocket, assuming 1 m diameter.

Two engine scaling parameters are added to the optimisation vector, one per stage, with a single parameter affecting both operational engine modes (air-breathing and rocket) of the first stage. The scaling parameters affect the nominal thrust level at full throttle ignoring expansion losses and are listed in the last line of table 6.2.

The starting conditions of the ascent are listed in Table 6.1 and the optimisation bounds including controls and MDO parameters are in Table 6.2. The upper stage including payload has an initial mass at separation of $m_{S2,0} = 1\,000\,\mathrm{kg}$ and its initial conditions part of the optimisation variables. The starting values of angle of attack and roll are constrained to be the same of the first stage at the instant of release, while the throttle is unconstrained.

Table 6.1: Starting conditions for the ascent trajectory

Variable		Value
Altitude	m	1000
Velocity	$\mathrm{m\,s^{-1}}$	150
Flight Path Angle	deg	0
Heading	deg	90
Latitude	deg	0
Longitude	deg	0
Mass	kg	90035

The first stage flight is divided in two phases, each consisting of $n_e = 3$ multiple shooting elements, with $n_c = 5$ control points. The second stage has the task of circularizing the orbit by raising the perigee if the first stage cannot, but its contribution is expected to be null or negligible at convergence. Thus, a reduced number of elements $n_e = 2$ is used in this phase, with $n_c = 5$ control points each.

The cost function to maximise in the ascent optimisation is the fuel mass remaining in the upper stage.

The optimisation results in a final mass $m_payload = 999.933\,\mathrm{kg}$ delivered to the target orbit, confirming the good agreement of the solution when compared to the original case [132]. The mass lost by the second stage is due to the very short circularisation

Phase			1	2	3
Stage			1	1	2
Engine			AB	Rocket	Rocket
Altitude	h	km	[1, 100]	[10, 200]	[10, 200]
Velocity	v	$\mathrm{m\,s^{-1}}$	[100, 2500]	[1000, 8000]	[1000, 8000]
FPA	γ	deg	[-60, 90]	[-60, 90]	[-60, 90]
Heading angle	χ	deg	[-180, 180]	[-180, 180]	[-180, 180]
Latitude	λ	deg	[-90, 90]	[-90, 90]	[-90, 90]
Longitude	θ	deg	[-180, 180]	[-180, 180]	[-180, 180]
Mass	m	kg	[22907, 90035]	[22907, 90035]	[100, 1000]
AoA	α	deg	[-4, 24]	[-4, 24]	[-30, 30]
Throttle	τ	-	[0, 1]	[0, 1]	[0, 1]
Duration	t	s	[60, 600]	[60, 600]	[6, 600]
Thrust	T	kN	[2500,4800]	[3200, 6000]	[0.5, 5]

Table 6.2: Bounds for the variables in the optimisation vector in the sizing case.

burn performed at the apogee. The optimised value of upper stage thrust $T_2 = 500\,\mathrm{N}$ is on the lower bound.

The reusable first stage maximum thrust values for the airbreathing and rocket mode are respectively $T_{SL,max} = 3.894\,\mathrm{MN}$ and $T_{vac,max} = 4.984\,\mathrm{MN}$. The strategy of coasting to the apogee to raise the perigee emerges by means of optimisation as can be observed at $t \approx 600\,\mathrm{s}$ in the throttle profile of Figure 6.1b .

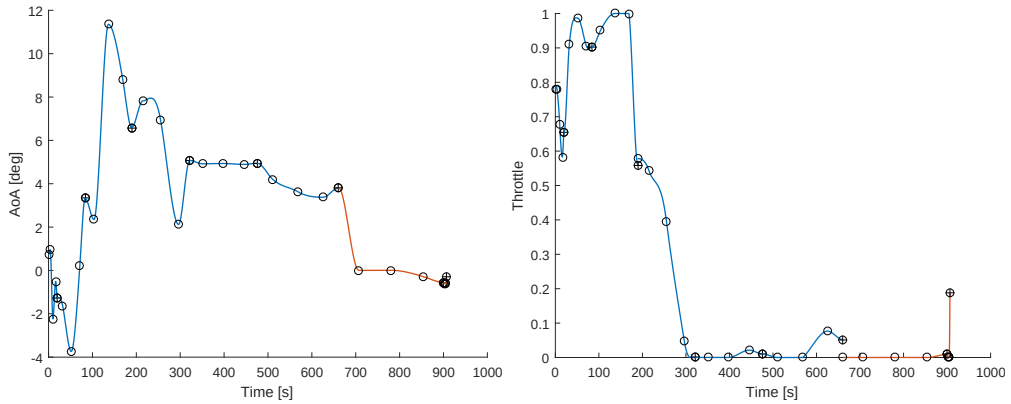

(a) Angle of attack

(b) Throttle control

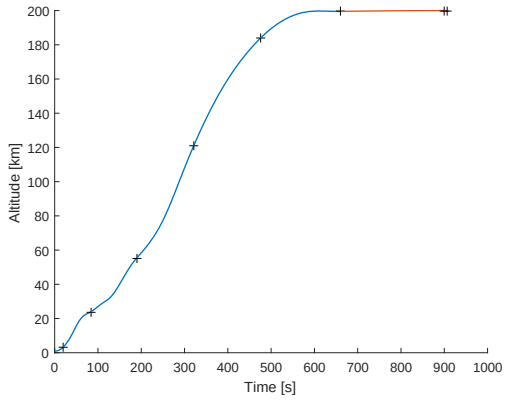

(c) Altitude

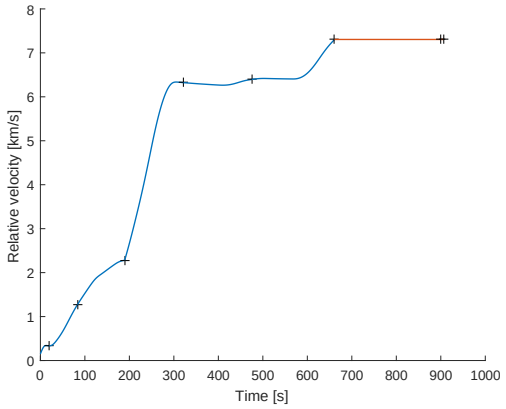

(d) Velocity

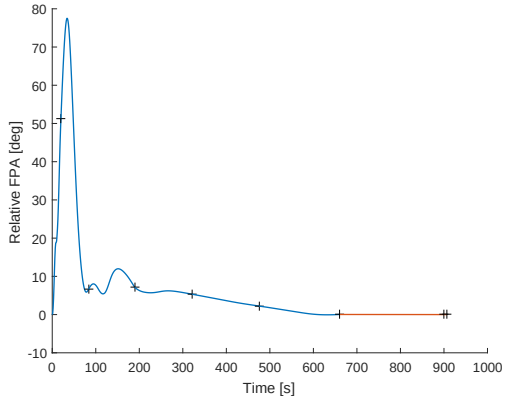

(e) Flight path angle

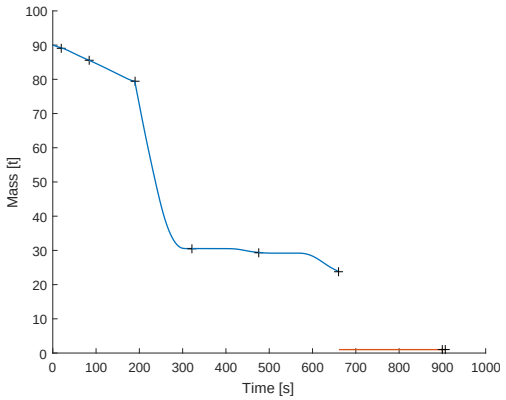

(f) Vehicle mass

Figure 6.1: Time histories for controls and states of the ascent case solution. Cross markers are placed at the element junction points. Circle markers highlight the values of control nodes. The trajectory is coloured in blue for the first stage, orange for the second one. The end of the airbreathing phase coincides with the third cross marker.

6.3 Recovery trajectories

The analysis of the abort trajectories uses the results generated from the ascent optimisation as starting point for the descent abort scenarios. The ascent throttle profile shows the separation between an initial powered phase in the air-breathing and rocket segments followed by a ballistic flight. During this phase, the vehicle will coast to the apogee of the suborbital arc, where a final boost circularizes the orbit. This phenomena simplifies the analysis of abort scenarios allowing the study of the recovery strategies in the first 4 elements of the trajectory, covering the majority of the powered ascent. After the engine cut off point, the trajectory would closely follow a nominal ballistic suborbital arc, followed by a final glide re-entry. With no thrust, no extra energy is introduced into the system, and studying any of the points after the end of the 4^{th} element would yield similar results. A set of 50 data points is selected to provide a grid of onset conditions without being too computationally intensive. Those cover a set of altitudes from 0 km to 108 km and velocities from $271\,\mathrm{m\,s^{-1}}$ to $6\,327\,\mathrm{m\,s^{-1}}$. The points are equally spaced in time every 6 seconds along the ascent trajectory. The states variables corresponding to those selected points are used as starting conditions for each of the abort scenarios.

The descent phase is constrained to achieve a final state corresponding to a landing approach with an altitude $h_f = 1\,000\,\mathrm{m}$, speed $v_f = 150\,\mathrm{m\,s^{-1}}$ and flight path angle $\gamma \leq 10°$. Given the previous assumption of equatorial ascent, it is reasonable to use only the control in the longitudinal plane of the vehicle while maximizing the descent downrange. The angle of attack of the vehicle is constrained between the limits of the aerodynamic model [138] $-4° \leq \alpha \leq 24°$, while throttle and bank angle controls are fixed to $\tau = 0$ and $\mu = 0°$.

The glide descent is composed of a single phase subdivided in $n_e = 3$ multiple shooting segments, each containing $n_c = 7$ control points following a Chebyshev nodes distribution. The values of control between the points are obtained with a piecewise cubic Hermite spline interpolation. The integration of the trajectory is performed with a 4^{th} order Runge–Kutta method with fixed timestep of 1 s. The bounds of the

optimised flight duration scale proportionally with the velocity at abort condition in each of the elements following the rule $t_{bounds} = (0.1, 2)v_{0,i}$ with SI units. Constraints 6.3 set the final state at abort completion, limit the peak accelerations acc in the x and z directions, and impose a restriction on the maximum dynamic pressure q_{dyn}.

$$h(t_{f,r}) = 1\,000\,\mathrm{m} \tag{6.3a}$$

$$v(t_{f,r}) = 150\,\mathrm{m\,s^{-1}} \tag{6.3b}$$

$$\gamma(t_{f,r}) \leq 10^{\circ} \tag{6.3c}$$

$$acc_{x,z} \leq 6g_0 \tag{6.3d}$$

$$q_{dyn} \leq 20\,\mathrm{kPa} \tag{6.3e}$$

The distance from the starting abort point is the maximised optimisation metric and it is computed with the Haversine formula (6.4), with $r = R_E$.

$$d = 2r \arcsin\left(\sqrt{\sin^2\left(\frac{\theta_2 - \theta_1}{2}\right) + \cos(\theta_1)\cos(\theta_2)\sin^2\left(\frac{\lambda_2 - \lambda_1}{2}\right)}\right) \tag{6.4}$$

A second set of analysis is subsequently performed starting from the same abort points by adding the optimisation variables for the bank angle control to identify the crossrange capabilities of the vehicle. The bank angle rotates the aerodynamic forces around the velocity axis. This analysis is separated into $n_p = 2$ phases of $n_{e,p=1} = 2$ and $n_{e,p=2} = 1$ elements with $n_c = 7$ control nodes where only the first phase includes the additional control of the bank angle. The bounds of the optimisation variables are listed in Table 6.3. The last phase, made of a single element, has only the control of the angle of attack. This choice has been made because a faulty behaviour emerged during the first trial runs: the combination of long re-entry duration from the higher starting energies and the control mesh density chosen, made the vehicle enter spirals in the final moments of flight that reduced altitude without gain in crossrange capabilities. Removing the bank control eliminates the unwanted behaviour, and does not require an increased node number, reducing the problem dimensionality when compared to intro-

Table 6.3: Upper and lower bounds for the descent downrange and crossrange analyses

Altitude	h	km	[1, 200]	
Velocity	v	$\mathrm{m\,s^{-1}}$	[150, 8000]	
FPA	γ	deg	[-60, 90]	
Heading angle	χ	deg	[-180, 180]	
Latitude	λ	deg	[-90, 90]	
Longitude	θ	deg	[-180, 180]	
Mass	m	kg	[22907, 90035]	
AoA	α	deg	[-4, 24]	
Bank	β	deg	[-80, 80]	*(crossrange only)*

ducing a constraint. In this second analysis, the optimisation metric is the maximum latitude, an approach equivalent to the maximum crossrange in the scenario with starting equatorial trajectory. The total distance is calculated with the arc length from the equator to the final latitude. The second set of results complements the first analysis, providing performance metrics on range capability in a perpendicular direction.

6.4 Results

Out of the 50 points analysed, five points are chosen as key markers of the group of solutions to help the reader interpreting the results. Four (A, B, C, and E) are selected at the end of the respective ascent trajectory elements of the multiple shooting arcs. An additional one (D) is picked in the middle of the rocket flight segment to smooth out the representation of results. Table 6.4 lists the initial state vector for each point; given the problem assumptions of section 6.2, the vehicle always starts from longitude $\theta_0 = 0°$ and eastward heading $\chi_0 = 90°$.

6.4.1 Maximum downrange

The results of the downrange analysis are shown in Figure 6.2, and display a similar oscillatory trajectory pattern to the one identified in the analysis of the range-maximal flight of a hypersonic vehicle after engine failure by Büskens and Wassel [33].

Table 6.4: Starting conditions of the selected failure onset points highlighted in the descent graphs.

Point	Altitude,[m]	Velocity,[m/s]	FPA,[rad]	Longitude,[rad]	Mass,[kg]
A	4201	339.4	1.0417	0.0009	89056
B	23879	1272.5	0.1151	0.0064	85578
C	55899	2351.5	0.1210	0.0382	78099
D	75048	4644.2	0.1039	0.0668	45531
E	107650	6327.9	0.1009	0.1142	30638

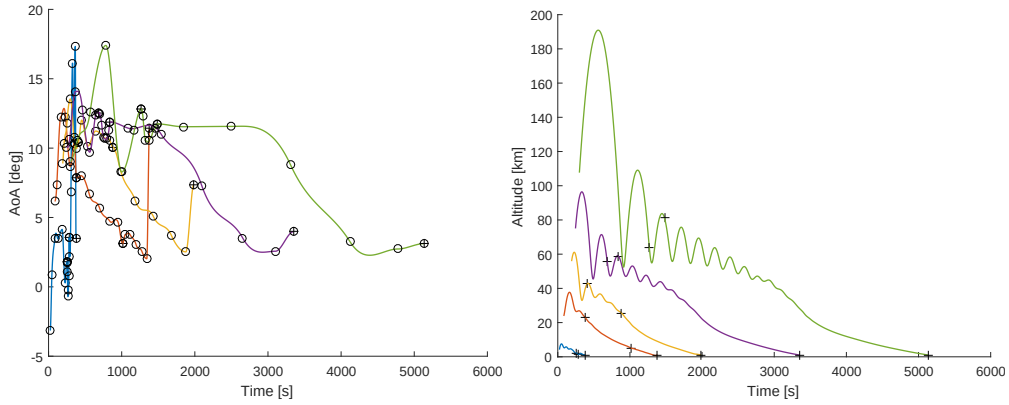

(a) Angle of attack

(b) Altitude

(c) Velocity

(d) Flight path angle

Figure 6.2: Time histories for controls and states of the descent case without bank. Cross markers are placed at the element junction points. Circle markers highlight the values of control nodes. Colours identify the 5 reference recovery cases :A-blue, B-red, C-yellow, D-purple, E-green.

The specific orbital energy plot in Figure 6.3 presents the maximum downrange distance that the suborbital flights can cover from the abort starting points. The curve

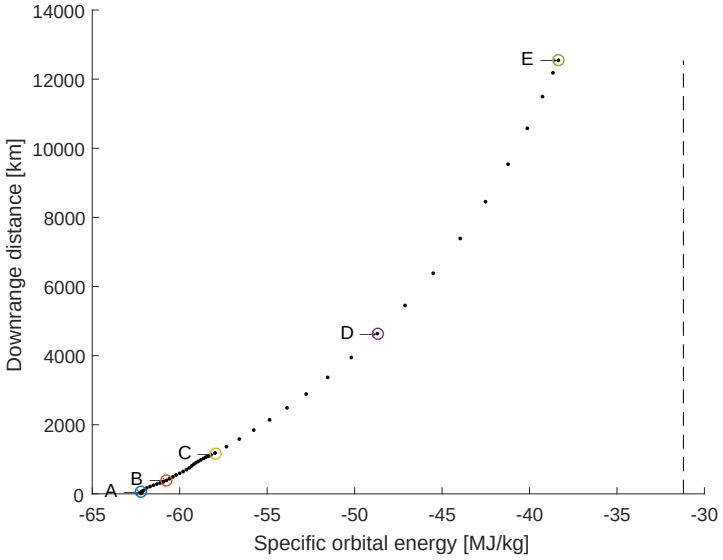

Figure 6.3: Relationship between starting specific orbital energy and downrange distance. The dashed line is the minimal energy required for a stable orbit around the Earth.

outlines the front of solutions found with the approach previously described. The small areas where the line seems to deviate from the exponential trend are due to the flight path angle change of the different abort conditions. From the same values of energy as combination of altitude and velocity, the initial angle of the velocity vector impacts the glide performances as in the problem of projectile throw.

While the skip re-entry, explained in section 3.6.1, is a return strategy that has emerged in other re-entry analyses maximising downrange distance [33], it does present practical issues such as added stress on the structure, that may imply limitations on the lifetime of the vehicle (re-usuability), onboard control and stability, etc. The phugoids can be mitigated within the analysis through more strict accelerations/loading limits, specific constraints or post-processing of the controls, though this would represent a suboptimal result compared to the maximum possible range. The focus of this study was to evaluate the maximum capability of the vehicle under emergency situations.

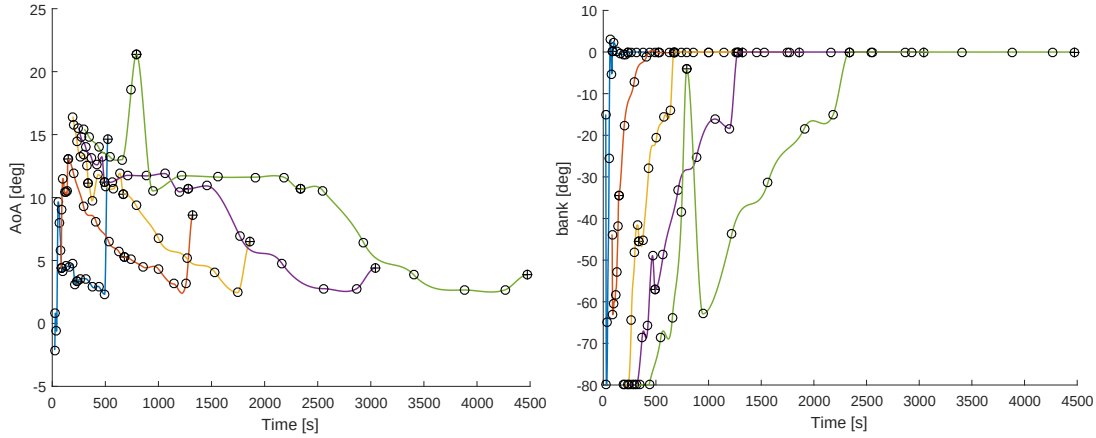

(a) Angle of attack (b) Bank angle

Figure 6.4: Time histories for the controls of the descent case with bank. Cross markers are placed at the element junction points. Circle markers highlight the values of control nodes.

6.4.2 Maximum cross-range results

Figures 6.4 and 6.5 illustrate the time histories of controls and states in the descent case. The trajectories exhibit the same skip re-entry approach observed in the maximisation of downrange. It can be observed that the cases with bank control show the expected lack of significant aerodynamic forces in the high altitude suborbital arcs. The relation between crossrange and starting energy is shown in Figure 6.6.

The combined locations of the coordinates of the final points are shown in Figure 6.7 on the latitude-longitude plane. The five sample points of Table 6.4 are highlighted to show the distribution of solutions and therefore maximum glide range of the vehicle.

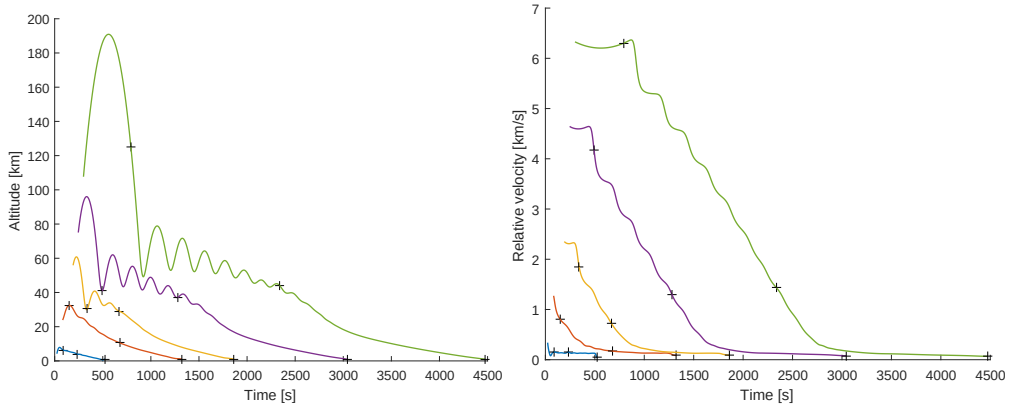

(a) Altitude

(b) Velocity

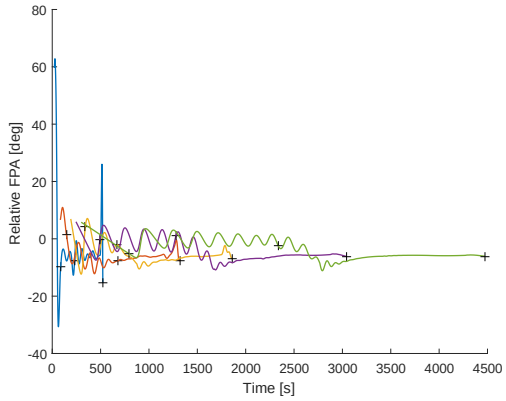

(c) Flight path angle

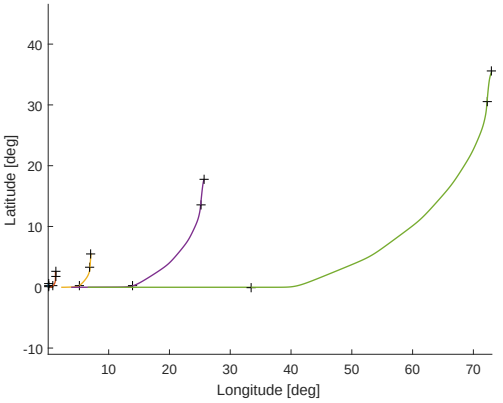

(d) Latitude

Figure 6.5: Time histories for the states of the descent case with bank. Cross markers are placed at the element junction points. Circle markers highlight the values of control nodes.

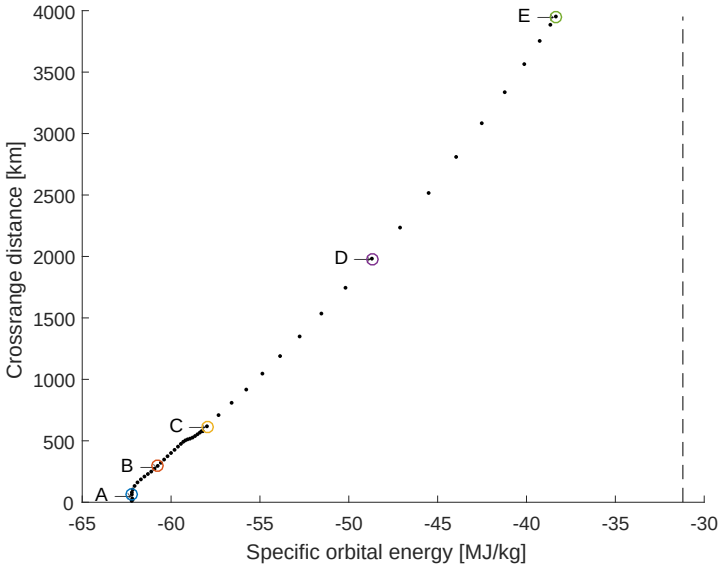

Figure 6.6: Relationship between starting specific orbital energy and crossrange distance. The dashed line is is the minimal energy required for a stable orbit around the Earth.

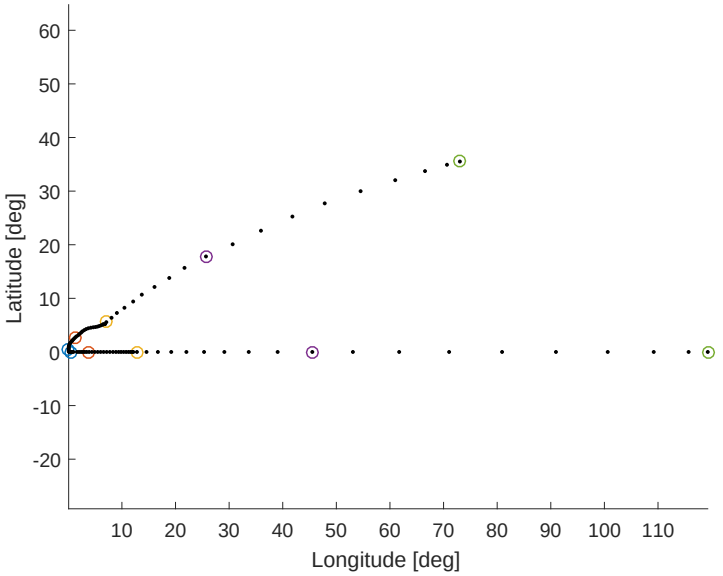

Figure 6.7: Latitude-Longitude distribution of the final points of descents for the analyses with and without bank.

6.5 Summary of the chapter

The downrange and cross-range distance performances in case of abort events during the ascent of a spaceplane have been studied. The approach and results obtained can be applied to the study of the abort procedures from any launch site, and can provide performance metrics required to satisfy regulatory or technological constraints.

The first guess creation through multi-start analysis of the nominal mission, and the successive iterative approach with warm-start has succeeded in providing results for all the abort points analysed from the powered flight of the reusable stage until MECO. This technique reached convergence in all cases, eliminating the need of repeated explorative analysis, reducing computational time. The energy-distance plots can be a useful tool to study trade-offs between vehicles, launch locations, abort procedures and risk assessment.

Chapter 7

Conclusions

The aim of this thesis was to develop a methodology to design launch vehicle trajectories to support the early phases of mission analysis, providing insights to minimise the risk associated with early concept definition decisions. The objectives of this work, first listed in section 1.1 were:

1. Devise a modular methodology to address a wide ranging multitude of cases, drawing from past research, methods and applications in the field, with a forward looking approach to the trend of future computational capabilities.

2. Develop a modular trajectory optimisation framework to be used for launch vehicle analysis, with particular attention to multidisciplinarity, computational efficiency and accessibility.

3. Demonstrate its application in a multitude of scenarios proving the capabilities for the missions and vehicles under consideration, verifying in the process that the results obtained do respect the expectations.

The research on the existing methodologies, and published applications, summarised in chapter 2, has provided a background to identify the most appropriate approach to perform mission analysis for reusable lifting body vehicles for access to space, achieving the first objective. The selected methodology, detailed in chapter 3, based on the direct multiple shooting formulation, has been used to generate results for the different application cases presented in this work.

The methodology has been implemented in a modular MATLAB framework, achieving the second objective, leveraging the opportunity of frequent interactions with industry and academia partners during the research for this work. The successful collaborations have resulted in the papers and publications listed in the opening sections of this document.

The last objective has been addressed with selected application cases, ranging from the mission analysis in the conceptual stage and preliminary sizing of a vehicle, to the more mature phases of development. The early analyses of a program are focused on the vehicle itself, guiding the development as shown in section 5.4, where a reusable launcher is sized on a reference mission. The maturity of a project would then grow into expanding the mission envelope and verifying compliance with the constraints, including all flight phases, as demonstrated in chapter 4. A more mature program would then start facing outward, towards external stakeholders, such as regulators, or potential customers, interested in the performance curves computed in section 5.5. And finally, no vehicle can fly without a license, thus one of the steps in the safety analysis domain includes the design of recovery procedures in cases of off-nominal events, with chapter 6 demonstrating the computation of down- and cross-range capabilities of a lifting body vehicle.

The applications presented in this work thus demonstrated the successful implementation of the methodology to a wide range of scenarios and problems affecting different stages of a vehicle development program.

The recombination of existing techniques in a novel way has coalesced in a framework that has successfully been employed in the study of missions, launchers and launch-sites up to the project milestones where high fidelity Flight Safety Analysis starts.

7.1 Summary

The approach developed was described in chapter 3, starting from the physics governing the flight of space access vehicles to a degree of accuracy sufficient to characterise the phenomena under the scope of this study. The selection of a 3dof simulation provides a

sweet spot in terms of complexity and computational speed, while the use of the ECEF reference frame is necessary to provide results that are ready to be used in stakeholder engagement that are on the ground or in the lower atmosphere. The latitude-longitude framework is the default for all industries that deal in transportation, and the timely delivery of information to the affected parties within the range allows the entities and authorities to react with a comfortable time-frame, minimising the commercial impact of launch activities. The dynamic equations are driven by the variables coming either from the environment or the vehicle itself. The forces at play and the characteristics that are part of the minimum requirement for a physically realistic simulations have been listed and described, with their relative influence explored in the application chapters. The complex flight dynamics require a guidance directing the vehicle toward the desired path, and the optimal trajectory for the vehicle has to be defined to be followed by the GNC. The search-space of such problem is extremely wide, and the paths that a vehicle can follow in 3dof are virtually unlimited, but only a subset of those can successfully complete the mission objectives while satisfying the constraints. Orbital access vehicles in particular are constrained due to the amount of fuel that they can carry which leaves tight margins to be respected. The optimal control problem is thus formulated using the motion dynamics described, with a direct transcription, and subdividing the trajectory in multiple shooting arcs. The transcription choice provides a robust approach, allowing the solution of problems without a good starting guess and treating the problem dynamics as a black box, easily handling discontinuities that emerge when travelling at different flight regimes. The shooting strategy provides an increase in the problem stability and a lower time to solution for the same trajectory, that can be evaluated with parallel processing. The multiple shooting combines well with the choice of optimisation algorithm, the gradient based SQP method, which leverages the sparse Jacobian matrix produced. The approach has been validated with classical optimal control problems on trans-atmospheric flight trajectories from literature.

The methodology has then been applied to a selection of relevant problems of increasing architectural complexity, starting from chapter 4, where the ascent to orbit and return to base for a lifting body vehicle have been presented. The launcher is inspired

by the reusable SSTO concept Skylon, and the modelling of the subsystems affecting flight performances is described, presenting a first application within the developed framework. Simplified models describing the vehicle and the operative environment are introduced, with the optimisation settings selected. The vehicle presents a hybrid engine, operating in dual mode depending on the flight regime, air-breathing in the lower section of the atmosphere and rocket at higher altitude. The models used for aerodynamics and propulsion present discontinuities, and the mission breakdown is structured by setting phases interfaces at such points where the models can change with no impact on the optimisation problem, treated as a black-box.

The methodology is further exploited in chapter 5, where the problem is split into 2 sections: vehicle sizing and performance analysis.

In the first section the vehicle is sized on a reference mission, performing MDO in the loop with trajectory optimisation and obtaining the lightest vehicle able to complete the mission subject to the constraints set. This demonstration of capabilities beyond designing optimal trajectory for a definite vehicle has application in the early phases of launcher design, where the payload class target is known from satellite market analysis and projections, and the vehicle size has to be minimised to reduce the Operational Expenditure. The vehicle identified with the MDO approach can target an optimal configuration to minimise excess performances that have cascading effects on the project finances.

The second section of the chapter takes as an input the vehicle designed in the first part, and analyses the performance impact of injecting the payload in orbits that are different from the reference one. The performance maps at different orbit altitude and inclinations, presented as output, are a standard occurrence in the payload user guides of launchers.

Chapter 6 re-uses the same vehicle previously designed and analyses a set of figures of merit affected by the vehicle design and related to safety, re-usability and CONOPS in case of failure. The scenario under investigation is the abort during the ascent of the lifting body vehicle, with recovery of the stage under non-powered glide flight. The nominal mission profile is constructed to define a baseline mission, with abort points

distributed along the trajectory from take-off to MECO. From each of the abort points, two trajectories are optimised to evaluate the vehicle capabilities in downrange and cross-range, obtaining figures of merit that can be used to evaluate a spaceport location based on the glide distance capability from the flightpath to the possible emergency landing sites.

7.2 Future work

The interaction opportunities offered by conferences, the collaborations with peers within academia and industry, have all contributed in the maturing of external points of view on the work herein presented, with constructive feedback and questions highlighting the areas that could be improved or clarified.

The first element to address is the complexity reduction for trajectory optimisation. While major efforts have been devoted to simplify and clarify the framework as much as possible, new analysts might still require a high degree of guidance and training. This is due to the intricate nature of the problem, which lies at the intersection of the field of mathematical optimisation, system modelling and physical simulation. These macro areas tightly interact and a mistake in either of those branches can result in unreasonable or unacceptable solutions. Identifying these issues is a major part in the day to day work on applications for the analysis of space access vehicles. Ways to mitigate the issue would be to improve the documentation, provide tutorials, creating a user-friendly GUI to help new analysts less prone to coding, and speeding up the works of experienced ones. Best practices from software engineering such as unit and integration testing would provide good starting points to reduce the issues stemming from improper user code or data.

The second area of improvement is the expansion of modelling approaches that could be employed to fit additional scenarios answering new questions. While for the analysis of HTHL reusable lifting body space vehicles presented in this work the ECEF coordinate system was suitable, this might not be the case for different systems, such as a conventional vertically launched rocket system, or orbital objects. Similar considera-

tions apply to the vehicle attitude definition angles, with varying degrees of suitability in different applications and systems.

Major benefits can be obtained by software execution optimisation, developing the methodology in languages faster than MATLAB. The speed-up of the simulation core has a linear effect in the effective time required to reach the final solution. Developers must have a good understanding of the computational advances and transitions that are happening in the processing hardware, to leverage novel architectures and instruction sets.

The application cases presented in this work have mentioned and used surrogate or meta-modelling to speed up the computational time. This has been executed manually, with model fitting performed with the analyst in the loop. Trajectory optimisation should leverage the advances in the field of reduced order modelling to generate models in a more automated way, freeing up analyst time, and possibly even integrating a progressive automated increase of fidelity similar to the mesh refinements of the collocation methods.

Bibliography

[1] Akhil Rao. "The economics of orbit use: Theory, policy, and measurement". PhD thesis. 2019.

[2] Cathy W Swan and Peter A Swan. "Why we need a space elevator". In: *Space Policy* 22.2 (2006), pp. 86–91. DOI: 10.1016/j.spacepol.2006.02.008.

[3] Delma C Freeman Jr, Theodore A Talay, and R Eugene Austin. "Reusable launch vehicle technology program". In: *Acta Astronautica* 41.11 (1997), pp. 777–790. DOI: 10.1016/S0094-5765(97)00197-5.

[4] Richard Varvill and Alan Bond. "The skylon spaceplane". In: *JBIs* 57 (2004), pp. 22–32.

[5] Emmi Yonekura, Brian Dolan, Moon Kim, Krista Romita Grocholski, Raza Khan, and Yool Kim. *Commercial Space Capabilities and Market Overview*. 2022.

[6] Joseph R Kopacz, Roman Herschitz, and Jason Roney. "Small satellites an overview and assessment". In: *Acta Astronautica* 170 (2020), pp. 93–105. DOI: 10.1016/j.actaastro.2020.01.034.

[7] Weiqiang Li, Estel Cardellach, Serni Ribó, Santi Oliveras, and Antonio Rius. "Exploration of Multi-Mission Spaceborne GNSS-R Raw IF Data Sets: Processing, Data Products and Potential Applications". In: *Remote Sensing* 14.6 (2022), p. 1344. DOI: 10.3390/rs14061344.

[8] Federal Communications Commission. *WorldVu Satellites Limited, Debtor-in-Possession, Petition for Declaratory Ruling Granting Access to the U.S. Market for the OneWeb NonGeostationary Satellite Orbit Fixed-Satellite Service V-*

Band System.
https://docs.fcc.gov/public/attachments/FCC-20-117A1.pdf. Accessed: 2022-09-01. 2020.

[9] Federal Communications Commission. *Space Exploration Holdings, LLC Request for Modification of the Authorization for the SpaceX NGSO Satellite System*. https://docs.fcc.gov/public/attachments/FCC-21-48A1.pdf. Accessed: 2022-09-01. 2021.

[10] Jonathan C McDowell. "The low earth orbit satellite population and impacts of the SpaceX Starlink constellation". In: *The Astrophysical Journal Letters* 892.2 (2020), p. L36. DOI: 10.3847/2041-8213/ab8016.

[11] *PSLV-C45/EMISAT MISSION Launch Kit*. https://www.isro.gov.in/sites/default/files/pslv-c45_launch_kitv5.0_fn_23.03.19.pdf. Accessed: 2022-09-01.

[12] *Transporter-2 launch mission description and webcast recording*. https://www.spacex.com/launches/transporter-2-mission/. Accessed: 2022-09-01.

[13] *Arianespace Vega flight VV-16 launch kit*. https://www.arianespace.com/wp-content/uploads/2020/06/VV16-launchkit-EN3.pdf. Accessed: 2022-09-01.

[14] Carlos Niederstrasser. *Small Launchers in a Pandemic World-2021 Edition of the Annual Industry Survey*. 2021.

[15] W Elkman, J Trinh, P McCaughey, and W Chen. "EMI/EMC, lightning, and ESD design approach for the falcon 9 launch vehicle: Part I". In: *2011 IEEE International Symposium on Electromagnetic Compatibility*. IEEE. 2011, pp. 290–294. DOI: 10.1109/ISEMC.2011.6038324.

[16] Rocket Lab USA. *'Still Testing' press Kit - January 2018*. https://www.rocketlabusa.com/assets/Uploads/Still-Testing-Press-kit.pdf. Accessed: 2022-09-01. 2018.

[17] Parliament of the United Kingdom. *Space Industry Act 2018*. https://www.legislation.gov.uk/ukpga/2018/5. Accessed: 2022-09-01. 2018.

[18] Parliament of the United Kingdom. *Space Industry Regulations 2021*. https://www.legislation.gov.uk/uksi/2021/792. Accessed: 2022-09-01. 2021.

[19] *Rockets that return home – SpaceX pushing the boundaries*. https://www.nasaspaceflight.com/2014/04/rockets-return-home-spacex-pushing-boundaries/. Accessed: 2022-09-01.

[20] *2021-05-09 Starlink launch mission description and webcast recording*. https://www.spacex.com/launches/starlink-mission-05-09-2021/. Accessed: 2022-09-01.

[21] Matt Darley and Peter Beck. *Return to sender: Lessons learned from rocket lab's first recovery mission*. 2021.

[22] *Chinese Long March launch tests grid fins for safety, future reusability*. https://spacenews.com/chinese-long-march-launch-tests-grid-fins-for-safely-future-reusability/. Accessed: 2022-09-01.

[23] Ansgar Marwege, Josef Klevanski, Johannes Riehmer, Daniel Kirchheck, Sebastian Karl, Davide Bonetti, J Vos, Matthew Jevons, Anett Krammer, and João Carvalho. *Retro Propulsion Assisted Landing Technologies (RETALT): Current Status and Outlook of the EU Funded Project on Reusable Launch Vehicles*. 2019.

[24] Antoine Patureau de Mirand, Jean-Marc Bahu, and Olivier Gogdet. "Ariane Next, a vision for the next generation of Ariane Launchers". In: *Acta Astronautica* 170 (2020), pp. 735–749. DOI: 10.1016/j.actaastro.2020.02.003.

[25] *Terran 1 Payload User's Guide*. English. Version 2.0. Accessed: 2022-09-01. Relativity Space.

[26] Byron Blakey-Milner, Paul Gradl, Glen Snedden, Michael Brooks, Jean Pitot, Elena Lopez, Martin Leary, Filippo Berto, and Anton du Plessis. "Metal additive manufacturing in aerospace: A review". In: *Materials & Design* 209 (2021), p. 110008. DOI: 10.1016/j.matdes.2021.110008.

[27] BRA Burns. "HOTOL space transport for the twenty-first century". In: *Proceedings of the Institution of Mechanical Engineers, Part G: Journal of Aerospace Engineering* 204.2 (1990), pp. 101–110.

[28] Zachary Krevor, Russell Howard, Todd Mosher, and Karen Scott. "Dream chaser commercial crewed spacecraft overview". In: *17th AIAA International Space Planes and Hypersonic Systems and Technologies Conference*. 2011, p. 2245. DOI: 10.2514/6.2011-2245.

[29] Arthur Grantz. "X-37B orbital test vehicle and derivatives". In: *AIAA Space 2011 Conference & Exposition*. 2011, p. 7315. DOI: 10.2514/6.2011-7315.

[30] Rajkumar Roy and C Kerr. "Cost engineering". In: *International journal of Production economics* 109.1 (2007), pp. 1–1.

[31] Mathieu Balesdent, Nicolas Bérend, Philippe Dépincé, and Abdelhamid Chriette. "A survey of multidisciplinary design optimization methods in launch vehicle design". In: *Structural and Multidisciplinary optimization* 45.5 (2012), pp. 619–642. DOI: 10.1007/s00158-011-0701-4.

[32] Deimos Space UK. *SCEPTRE final report*. https://www.hie.co.uk/media/6626/sceptre-final-report-february-2017.pdf. Accessed: 2022-09-01. 2017-02-17.

[33] Giorgio Fasano and Janos Pintér. *Modeling and optimization in space engineering*. Springer, 2013.

[34] He Linshu and Mateen-ud-Din Qazi. "Nearly-orthogonal sampling and neural network metamodel driven conceptual design of multistage space launch vehicle". In: *Computer-Aided Design* 38.6 (2006), pp. 595–607. DOI: 10.1016/j.cad.2006.02.001.

[35] John T Betts. "Survey of numerical methods for trajectory optimization". In: *Journal of guidance, control, and dynamics* 21.2 (1998), pp. 193–207. DOI: 10.2514/2.4231.

[36] Suvrit Sra, Sebastian Nowozin, and Stephen J Wright. *Optimization for machine learning*. Mit Press, 2012.

[37] Mingyang Li and Anastasios I Mourikis. "Optimization-based estimator design for vision-aided inertial navigation". In: *Robotics: Science and Systems*. Berlin Germany. 2013, pp. 241–248.

[38] Annalisa Riccardi, Edmondo Minisci, Kerem Akartunali, Cristian Greco, Naomi Rutledge, Alexander Kershaw, and Aymen Hashim. "Introduction to Optimisation". In: *Optimization Under Uncertainty with Applications to Aerospace Engineering*. Springer, 2021, pp. 223–268. DOI: 10.1007/978-3-030-60166-9_7.

[39] John T Betts. *Practical methods for optimal control and estimation using nonlinear programming*. Vol. 19. Siam, 2010.

[40] Anil V Rao. "A survey of numerical methods for optimal control". In: *Advances in the Astronautical Sciences* 135.1 (2009), pp. 497–528.

[41] Oskar Von Stryk and Roland Bulirsch. "Direct and indirect methods for trajectory optimization". In: *Annals of operations research* 37.1 (1992), pp. 357–373. DOI: 10.1007/BF02071065.

[42] Rüdiger Hohmann, Nico Hagemann, and Nicolas Kaiser. "Projectile Motion–Boundary Value Problem and Optimization in Education". In: *Proceedings of the 7th EUROSIM Congress on Modelling and Simulation, Prague, Czech Republic*. 2010.

[43] Saba Akram and Quarrat Ul Ann. "Newton raphson method". In: *International Journal of Scientific & Engineering Research* 6.7 (2015), pp. 1748–1752.

[44] Paul T Boggs and Jon W Tolle. "Sequential quadratic programming". In: *Acta numerica* 4 (1995), pp. 1–51. DOI: 10.1017/S0962492900002518.

[45] Virginia Torczon. "On the convergence of pattern search algorithms". In: *SIAM Journal on optimization* 7.1 (1997), pp. 1–25. DOI: 10.1137/S1052623493250780.

[46] Christof Büskens and Dennis Wassel. "The ESA NLP Solver WORHP". In: *Modeling and Optimization in Space Engineering*. Ed. by Giorgio Fasano and János D. Pintér. Vol. 73. Springer New York, 2013, pp. 85–110. DOI: 10.1007/978-1-4614-4469-5_4.

[47] Philip E Gill, Walter Murray, and Michael A Saunders. "SNOPT: An SQP algorithm for large-scale constrained optimization". In: *SIAM review* 47.1 (2005), pp. 99–131. DOI: 10.1137/S0036144504446096.

[48] Darrell Whitley. "A genetic algorithm tutorial". In: *Statistics and computing* 4.2 (1994), pp. 65–85. DOI: 10.1007/BF00175354.

[49] James Kennedy and Russell Eberhart. "Particle swarm optimization". In: *Proceedings of ICNN'95-international conference on neural networks*. Vol. 4. IEEE. 1995, pp. 1942–1948. DOI: 10.1109/ICNN.1995.488968.

[50] Peter JM Van Laarhoven and Emile HL Aarts. "Simulated annealing". In: *Simulated annealing: Theory and applications*. Springer, 1987, pp. 7–15. DOI: 10.1007/978-94-015-7744-1_2.

[51] Swagatam Das and Ponnuthurai Nagaratnam Suganthan. "Differential evolution: A survey of the state-of-the-art". In: *IEEE transactions on evolutionary computation* 15.1 (2010), pp. 4–31. DOI: 10.1109/TEVC.2010.2059031.

[52] Ferrante Neri and Carlos Cotta. "Memetic algorithms and memetic computing optimization: A literature review". In: *Swarm and Evolutionary Computation* 2 (2012), pp. 1–14. DOI: 10.1016/j.swevo.2011.11.003.

[53] Francesco Castellini and Michele R Lavagna. "Comparative analysis of global techniques for performance and design optimization of launchers". In: *Journal of Spacecraft and Rockets* 49.2 (2012), pp. 274–285. DOI: 10.2514/1.51749.

[54] Peter F Gath, Klaus H Well, and Klaus Mehlem. "Initial guess generation for rocket ascent trajectory optimization using indirect methods". In: *Journal of spacecraft and rockets* 39.4 (2002), pp. 515–521. DOI: 10.2514/2.3864.

[55] Francesco Marchetti, Edmondo Minisci, and Annalisa Riccardi. "Single-stage to orbit ascent trajectory optimisation with reliable evolutionary initial guess". In: *Optimization and Engineering* (2021), pp. 1–26. DOI: 10.1007/s11081-021-09698-w.

[56] Federico Toso and Christie Maddock. “Initial guess generation strategies for spaceplane trajectory optimisation”. In: *Transactions of the Japan Society for Aeronautical and Space Sciences* (2017).

[57] Makoto Matsumoto and Takuji Nishimura. “Mersenne twister: a 623-dimensionally equidistributed uniform pseudo-random number generator”. In: *ACM Transactions on Modeling and Computer Simulation (TOMACS)* 8.1 (1998), pp. 3–30. DOI: 10.1145/272991.272995.

[58] *ASTOS User Manual*. English. Version 8.0.6. Accessed: 2022-01-01. Astos Solutions. 2015.

[59] Peter Friedrich Gath. “CAMTOS-a software suite combining direct and indirect trajectory optimization methods”. PhD thesis. 2002. DOI: 10.18419/opus-3669.

[60] Michael A Patterson and Anil V Rao. “GPOPS-II: A MATLAB software for solving multiple-phase optimal control problems using hp-adaptive Gaussian quadrature collocation methods and sparse nonlinear programming”. In: *ACM Transactions on Mathematical Software (TOMS)* 41.1 (2014), pp. 1–37. DOI: 10.1145/2558904.

[61] Kathryn F Graham and Anil V Rao. “Minimum-time trajectory optimization of multiple revolution low-thrust earth-orbit transfers”. In: *Journal of spacecraft and rockets* 52.3 (2015), pp. 711–727. DOI: 10.2514/1.A33187.

[62] Yongjun Moon and Sejin Kwon. “Lunar soft landing with minimum-mass propulsion system using H2O2/kerosene bipropellant rocket system”. In: *Acta Astronautica* 99 (2014), pp. 153–157. DOI: 10.1016/j.actaastro.2014.02.003.

[63] David JN Limebeer, Giacomo Perantoni, and Anil V Rao. “Optimal control of formula one car energy recovery systems”. In: *International Journal of Control* 87.10 (2014), pp. 2065–2080. DOI: 10.1080/00207179.2014.900705.

[64] Thorsten Dahmen and D Saupeand. “Optimal pacing strategy for a race of two competing cyclists”. In: *Journal of science and cycling* 3.2 (2014), p. 12.

[65] Matthew J Weinstein, Michael A Patterson, and Anil V Rao. "Utilizing the algorithmic differentiation package adigator for solving optimal control problems using direct collocation". In: *AIAA Guidance, Navigation, and Control Conference*. 2015, p. 1085. DOI: 10.2514/6.2015-1085.

[66] I Michael Ross. *A beginner's guider to DIDO: A Matlab application package for solving optimal control problem*. Elissar Global. 2007.

[67] Oskar Von Stryk. *User's Guide for DIRCOL–A Direct Collocation Method for the Numerical Solution of Optimal Control Problems*. Lehrstuhl für Höhere Mathematik und Numerische Mathematik, Technische Universität, München. 1999.

[68] Anil V Rao, David A Benson, Christopher Darby, Michael A Patterson, Camila Francolin, Ilyssa Sanders, and Geoffrey T Huntington. "Algorithm 902: Gpops, a matlab software for solving multiple-phase optimal control problems using the gauss pseudospectral method". In: *ACM Transactions on Mathematical Software (TOMS)* 37.2 (2010), pp. 1–39. DOI: 10.1145/1731022.1731032.

[69] Sholto O Forbes-Spyratos, Michael P Kearney, Michael K Smart, and Ingo H Jahn. "Trajectory design of a rocket–scramjet–rocket multistage launch system". In: *Journal of Spacecraft and Rockets* 56.1 (2019), pp. 53–67. DOI: 10.2514/1.A34107.

[70] John P Riehl, Waldy K Sjauw, Robert D Falck, and Stephen W Paris. *Trajectory Optimization: OTIS 4*. NASA Tech Brief. 2010.

[71] Rafael A Lugo, Jeremy D Shidner, Richard W Powell, Steven M Marsh, James A Hoffman, Daniel K Litton, and Terri L Schmitt. "Launch vehicle ascent trajectory simulation using the Program to Optimize Simulated Trajectories II (POST2)". In: *AAS/AIAA Space Flight Mechanics Meeting*. NF1676L-25552. 2017.

[72] E Philip, Walter Murray, Michael A Saunders, and Margaret H Wright. *User's Guide for NPSOL 5.0: A Fortran Package for Nonlinear Programming*. Technical Report SOL 86–6. 2001.

[73] A Miele and T Wang. "Multiple-subarc gradient-restoration algorithm, Part 1: Algorithm structure". In: *Journal of Optimization Theory and Applications* 116.1 (2003), pp. 1–17. DOI: 10.1023/A:1022114117273.

[74] A Miele, R Eo Pritchard, and JN Damoulakis. "Sequential gradient-restoration algorithm for optimal control problems". In: *Journal of Optimization Theory and Applications* 5.4 (1970), pp. 235–282. DOI: 10.1007/BF00927913.

[75] Rodrigo Haya-Ramos, Gonzalo Blanco, Irene Pontijas, Davide Bonetti, Jordi Freixa, Cristina Parigini, Edmondo Bassano, Riccardo Carducci, Martins Sudars, Angelo Denaro, Roberto Angelini, and Salvatore Mancuso. "The design and realisation of the IXV Mission Analysis and Flight Mechanics". In: *Acta Astronautica* 124 (2016), pp. 39–52. DOI: 10.1016/j.actaastro.2015.12.048.

[76] Richard G Brusch. "A nonlinear programming approach to space shuttle trajectory optimization". In: *Journal of Optimization Theory and Applications* 13.1 (1974), pp. 94–118. DOI: 10.1007/978-94-010-2559-1_15.

[77] G.E. Moore. "Cramming More Components Onto Integrated Circuits". In: *Proceedings of the IEEE* 86.1 (1998), pp. 82–85. DOI: 10.1109/JPROC.1998.658762.

[78] Brian Harrington, Bret Picka, and Henry Cordova. "Space shuttle day-of-launch trajectory design operations". In: *AIAA SPACE 2011 Conference & Exposition*. 2011. DOI: 10.2514/6.2011-7197.

[79] Marco Sagliano and Erwin Mooij. "Optimal drag-energy entry guidance via pseudospectral convex optimization". In: *Aerospace Science and Technology* 117 (2021), p. 106946. DOI: 10.1016/j.ast.2021.106946.

[80] Martin J Bayer. "Comparative assessment of rocket-propelled single-stage-to-orbit concepts". In: *Journal of spacecraft and rockets* 40.2 (2003), pp. 273–278. DOI: 10.2514/2.3943.

[81] J Laube. *The X-33/VentureStar Program*. NASA Tech Brief. 1998.

[82] Robert I Baumgartner. "Venturestar™ single stage to orbit reusable launch vehicle program overview". In: *AIP Conference Proceedings*. Vol. 387. 1. American Institute of Physics. 1997, pp. 1033–1040. DOI: 10.1063/1.51920.

[83] John Vinson. "X-33 Linear Aerospike Engine". In: *Aerospace America* (1998).

[84] J Dorsey, Carl Poteet, Roger Chen, and K Wurster. "Metallic thermal protection system technology development-Concepts, requirements and assessment overview". In: *40th AIAA Aerospace Sciences Meeting & Exhibit*. 2002, p. 502. DOI: 10.2514/6.2002-502.

[85] Ashley Hill, David Anderson, Dan Coughlin, and Rajiv Chowdhry. "X-33 trajectory optimization and design". In: *Guidance, Navigation, and Control Conference and Exhibit*. 1998, p. 4408. DOI: 10.2514/6.1998-4408.

[86] A Miele and S Mancuso. "Optimal ascent trajectories and feasibility of next-generation orbital spacecraft". In: *Journal of Optimization Theory and Applications* 97.3 (1998), pp. 519–550. DOI: 10.1023/A:1022633924359.

[87] Richard Varvill and Alan Bond. "A comparison of propulsion concepts for SSTO reusable launchers". In: *JOURNAL-BRITISH INTERPLANETARY SOCIETY* 56.3/4 (2003), pp. 108–117.

[88] Federico Toso, Annalisa Riccardi, Edmondo Minisci, and Christie Alisa Maddock. "Optimisation of ascent and descent trajectories for lifting body space access vehicles". In: *66th International Astronautical Congress, IAC2015*. 2015, pp. 1–12.

[89] Romain Wuilbercq, Abdul Ahmad, Thomas Scanlon, and ER Brown. "Towards Robust Aero-Thermodynamic Predictions for Re-Usable Single-Stage to Orbit Vehicles". In: *18th AIAA/3AF International Space Planes and Hypersonic Systems and Technologies Conference. Tours, France*. 2012. DOI: 10.2514/6.2012-5803.

[90] Romain Wuilbercq. "Multi-disciplinary modelling of future space-access vehicles". PhD thesis. 2015. DOI: 10.48730/xcne-2n25.

[91] Viola Renato. "Multi-dimensional thermal response & permeability characterization for porous ablative materials". PhD thesis. 2018. DOI: 10.48730/wjg1-4n03.

[92] Javier Herrera Montojo. "Shock estimation in supersonic vehicles". PhD thesis. 2017. DOI: 10.48730/7vxs-2567.

[93] Daniel Espinoza. "An open-source hybrid CFD-DSMC solver for high-speed flows". PhD thesis. 2018. DOI: 10.48730/hm1d-mg88.

[94] Alessandro Mogavero. "Toward automated design of combined cycle propulsion". PhD thesis. 2016. DOI: 10.48730/38az-5n88.

[95] Jimmy-John O.E. Hoste. "Scramjet combustion modeling using eddy dissipation model". PhD thesis. 2018. DOI: 10.48730/jmag-cd95.

[96] Robert Garner. "Modelling launch vehicle emissions in an evolving space sector". PhD thesis. 2022. DOI: 10.48730/hp51-s325.

[97] David Young, Timothy Kokan, Christopher Tanner, Ian Clark, Christopher Tanner, and Alan Wilhite. "Lazarus: a SSTO hypersonic vehicle concept utilizing RBCC and HEDM propulsion technologies". In: *14th AIAA/AHI Space Planes and Hypersonic Systems and Technologies Conference*. 2006, p. 8099. DOI: 10.2514/6.2006-8099.

[98] David Kinney, Joseph Garcia, and Loc Huynh. "Predicted convective and radiative aerothermodynamic environments for various reentry vehicles using CBAERO". In: *44th AIAA Aerospace Sciences Meeting and Exhibit*. 2006, p. 659. DOI: 10.2514/6.2006-659.

[99] John Olds and John Bradford. "SCCREAM (Simulated Combined-Cycle Rocket Engine Analysis Module)-A conceptual RBCC engine design tool". In: *33rd Joint Propulsion Conference and Exhibit*. 1997, p. 2760. DOI: 10.2514/6.1997-2760.

[100] John R Olds. "Results of a rocket-based combined-cycle SSTO design using parametric MDO methods". In: *SAE transactions* (1994), pp. 154–173.

[101] John Olds, John Bradford, Ashraf Charania, Laura Ledsinger, David McCormick, and Kirk Sorensen. "Hyperion-An SSTO vision vehicle concept utilizing rocket-based combined cycle propulsion". In: *9th International Space Planes and Hypersonic Systems and Technologies Conference*. 1999, p. 4944. DOI: 10.2514/6.1999-4944.

[102] John Olds, Laura Ledsinger, John Bradford, Ashraf Charania, David McCormick, and D Komar. "Stargazer-A TSTO Bantam-X vehicle concept utilizing rocket-based combined-cycle propulsion". In: *9th International Space Planes and Hypersonic Systems and Technologies Conference*. 1999, p. 4888. DOI: 10.2514/6.1999-4888.

[103] *TROPICO source code*. https://github.com/federico-toso/TROPICO. Accessed: 2022-09-01.

[104] Nguyen Vinh. *Optimal Trajectories in Atmospheric Flight*. New York: Elsevier, 1981.

[105] Robert F Stengel. *Flight dynamics*. Princeton university press, 2004.

[106] PH Zipfel. *Modeling and Simulation of Aerospace Vehicle Dynamics, Second Edition*. AIAA Education Series, 2007.

[107] Davide Bonetti, Cristina Parigini, Gabriele De Zaiacomo, I Pontijas Fuentes, G Blanco Arnao, D Riley, and M Sánchez Nogales. "PETbox: Flight qualified tools for atmospheric flight". In: *6th International Conference on Astrodynamics Tools and Techniques (ICATT), Darmstadt*. 2016.

[108] George H Kaplan. *The IAU Resolutions on Astronomical Reference Systems, Time Scales, and Earth Rotation Models: Explanation and Implementation*. Circular 179. US Naval Observatory, 2005.

[109] Pedro Simplício, Andrés Marcos, and Samir Bennani. "Reusable launchers: development of a coupled flight mechanics, guidance, and control benchmark". In: *Journal of Spacecraft and Rockets* 57.1 (2020), pp. 74–89. DOI: 10.2514/1.A34429.

[110] *Pegasus Payload User's Guide*. English. Version 8.2. Accessed: 2022-09-01. Northrop Grumman.

[111] F Jivraj, A Bond, R Varvill, and G Paniagua. "The scimitar precooled Mach 5 engine". In: *Proceedings of the 2nd European Conference for Aero-Space Sciences*. 2007.

[112] Patrick Gallais. *Atmospheric re-entry vehicle mechanics*. Springer Science & Business Media, 2007.

[113] JM Picone, AE Hedin, D Pj Drob, and AC Aikin. "NRLMSISE-00 empirical model of the atmosphere: Statistical comparisons and scientific issues". In: *Journal of Geophysical Research: Space Physics* 107.A12 (2002), SIA–15. DOI: 10.1029/2002JA009430.

[114] Douglas P Drob, John T Emmert, John W Meriwether, Jonathan J Makela, Eelco Doornbos, Mark Conde, Gonzalo Hernandez, John Noto, Katherine A Zawdie, Sarah E McDonald, Joe D Huba, and Jeff H Klenzing. "An update to the Horizontal Wind Model (HWM): The quiet time thermosphere". In: *Earth and Space Science* 2.7 (2015), pp. 301–319. DOI: 10.1002/2014EA000089.

[115] Federal Aviation Administration. *Electronic Code of Federal Regulations. Title 14—Aeronautics and Space. Chapter III—Commercial Space Transportation, Federal Aviation Administration, Department of Transportation. Subchapter C—Licensing Part 417 - Launch Safety*. 2020-07-16.

[116] Jorge Nocedal and Stephen Wright. *Numerical optimization*. Springer Science & Business Media, 2006.

[117] Mathieu Balesdent, Loïc Brevault, Nathaniel B Price, Sébastien Defoort, Rodolphe Le Riche, Nam-Ho Kim, Raphael T Haftka, and Nicolas Bérend. "Advanced space vehicle design taking into account multidisciplinary couplings and mixed epistemic/aleatory uncertainties". In: *Space Engineering*. Springer, 2016, pp. 1–48. DOI: 10.1007/978-3-319-41508-6_1.

[118] Lawrence F Rowell, Robert D Braun, John R Olds, and Resit Unal. "Multidisciplinary conceptual design optimization of space transportation systems". In: *Journal of Aircraft* 36.1 (1999), pp. 218–226. DOI: 10.2514/2.2428.

[119] John T Betts. *A Collection of Optimal Control Test Problems*. Accessed: 2022-01-01. 2015.

[120] Jeng-Shing Chern and Nguyen Xuan Vinh. *Optimum reentry trajectories of a lifting vehicle*. Tech. rep. 1980.

[121] Roger Longstaff and Alan Bond. "The skylon project". In: *17th AIAA International Space Planes and Hypersonic Systems and Technologies Conference*. Vol. 2244. 2011. DOI: 10.2514/6.2011-2244.

[122] Romain Wuilbercq, Fabrizio Pescetelli, Alessandro Mogavero, Edmondo Minisci, and Richard E Brown. "Robust multidisciplinary design and optimisation of a reusable launch vehicle". In: *19th AIAA International Space Planes and Hypersonic Systems and Technologies Conference*. 2014, p. 2363. DOI: 10.2514/6.2014-2363.

[123] Abdul Ossman Ahmad, Christie Alisa Maddock, Thomas J. Scanlon, and Richard E. Brown. *Prediction of the aerodynamic performance of re-usable single stage to orbit vehicles*. 2011.

[124] JD Anderson. *Hypersonic and High-Temperature Gas Dynamics (Second Edition)*. AIAA, 2006.

[125] V Carandente, R Savino, M Iacovazzo, and C Boffa. "Aerothermal Analysis of a Sample-Return Reentry Capsule". In: *Fluid Dynamics & Materials Processing* 9.4 (2013), pp. 461–484. DOI: 10.3970/fdmp.2013.009.461.

[126] Mark Hempsell. "Progress on the SKYLON and SABRE". In: *Proceedings of the International Astronautical Congress*. Vol. 11. 2013, pp. 8427–8440.

[127] George P Sutton and Oscar Biblarz. *Rocket propulsion elements*. John Wiley & Sons, 2016.

[128] International Civil Aviation Organization. *Manual of the ICAO Standard Atmosphere: extended to 80 kilometres (262 500 feet)*. Vol. 7488. International Civil Aviation Organization, 1993.

[129] Richard H Battin. *An introduction to the mathematics and methods of astrodynamics*. AiAA, 1999.

[130] Haijun Shen and Panagiotis Tsiotras. "Using Battin's method to obtain multiple-revolution Lambert's solutions". In: *Advances in the Astronautical Sciences* 116 (2004), pp. 1–18.

[131] David Mostaza Prieto, Benjamin P Graziano, and Peter CE Roberts. "Spacecraft drag modelling". In: *Progress in Aerospace Sciences* 64 (2014), pp. 56–65. DOI: 10.1016/j.paerosci.2013.09.001.

[132] Federico Toso and Christie Alisa Maddock. "Deployed payload analysis for a single stage to orbit spaceplane". In: *67th International Astronautical Congress*. 2016.

[133] John C Mason and David C Handscomb. *Chebyshev polynomials*. Chapman and Hall/CRC, 2002.

[134] Michael D McKay, Richard J Beckman, and William J Conover. "A comparison of three methods for selecting values of input variables in the analysis of output from a computer code". In: *Technometrics* 42.1 (2000), pp. 55–61. DOI: 10.1080/00401706.2000.10485979.

[135] Davide Bonetti, Gabriele De Zaiacomo, Gonzalo Blanco Arnao, Giovanni Medici, Irene Pontijas Fuentes, and Baltazar Parreira. "Space Rider Mission Engineering". In: *Proceedings of the 8th European Conference for Aeronautics and Space Sciences (EUCASS), Madrid, Spain*. 2019.

[136] Federal Aviation Administration. *Flight Safety Analysis Handbook*. Version 1.0. 2011.

[137] Federico Toso and Christie Alisa Maddock. "Launch abort trajectory optimisation for reusable launch vehicles". In: *21st AIAA International Space Planes and Hypersonics Technologies Conference*. 2017, p. 2250. DOI: 10.2514/6.2017-2250.

[138] Gregory J Brauckmann. "X-34 vehicle aerodynamic characteristics". In: *Journal of Spacecraft and Rockets* 36.2 (1999), pp. 229–239. DOI: 10.2514/2.3453.